



Retrospective Analysis of Forest Structure Change: ALS Data Comparison and Interpretation

Final Report



Authors: Zac Coates, Garston Liang, Augustine Nguyen, Jess Grimmond, Finley Guilhaus, Scott Brown, & Johanna Voeste.

List of Acronyms

3D	three dimensions
ALS	Airborne Laser Scanning
API	Aerial Photography Interpretation
avg	average
BNA	Base Net Area
Canopy	Uppermost layer of a forest
CHM	Canopy Height Model
cov	canopy cover
CRAFTI	Comprehensive Regional Assessment Aerial Photographic Interpretation
cv	coefficient of variation
DTM	Digital Terrain Model
ESA	Environmentally Significant Area
FESM	Fire Extent and Severity Mapping
FMZ	Forest Management Zone
GEDI	Global Ecosystem Dynamics Investigation
LiDAR	Light Detection and Ranging
m	metre
MLS	Mobile Laser Scanning
NRC	Natural Resource Commission
NSW	New South Wales
p95	95th percentile
NSW	New South Wales
sd	standard deviation
se	standard error
STS	Sequential Thinning Strategy
TLS	Terrestrial Laser Scanning
TPI	Topographic Position Index
%	Percentage

Executive Summary.....	5
1. Introduction	7
1.1 Brief overview of data processing: from point clouds to ALS metrics	9
2. Longitudinal analysis	12
2.1 Canopy height analysis.....	12
2.1.1 Canopy height recovery in harvested regions	14
2.1.2 Canopy height recovery in harvested regions: comparing light and heavy harvesting practices .	17
2.1.3 Canopy height recovery in harvested regions across varied landform classes	19
2.1.4 Canopy height recovery in regions affected by fire.....	23
2.1.5 Patterns of forest height regeneration post-harvest.....	27
2.1.6 Modelling of canopy top height recovery post-harvest across landform classes, harvesting practices and FESM classes.....	35
2.2 Canopy coverage analysis	37
2.2.1 Canopy coverage recovery following harvesting activities.....	38
2.2.2 Canopy coverage recovery in harvested regions: comparing light and heavy harvesting practices	40
2.2.3 Canopy coverage across fire-impacted regions	41
2.3 Canopy foliage density analysis	43
2.3.1. Assessing change of canopy foliage density dynamics post-harvest using combined metrics: p95, p50, and canopy coverages.....	44
2.4 Skew analysis	47
2.4.1 Analysing longitudinal trends in vegetation density using skewness: impacts of harvesting and topographical landform	48
3. Recommendations	52
4. Conclusions	52
References	53
References for the Main Report and Appendix B	53
Appendix A: Supplementary figures for all ALS captures	62
Appendix B: LiDAR in forestry research: a literature review	98
1. Introduction	98
2. Methods.....	98
2.1 Search and inclusion strategies.....	98

3. Results 99

3.1 Forest sites 99

3.2 Thematic analysis 99

3.3 Primary methodologies 102

4. Discussion 112

5. Conclusions 113

Executive Summary

The NSW Natural Resources Commission (NRC) engaged with the University of Newcastle to investigate the feasibility of remote sensing technologies, particularly Airborne Laser Scanning (ALS), in monitoring forest conditions and biophysical outcomes. ALS is a form of LiDAR (Light Detection and Ranging) technology that acquires highly detailed three-dimensional data of the Earth's surface and vegetation from an aerial platform. This report covers the analyses conducted on ALS data spanning multiple captures and years within NSW State Forests, focusing on its implications for understanding various silvicultural practices. The main study objectives were to:

- **Integrating data:** Examined ALS data gathered across numerous captures and years, this will give insights into changes in forest structure, composition, and growth. By harnessing ALS technology in combination with field data, the study provides a more nuanced understanding of NSW State Forests, facilitating effective monitoring and evaluation.
- **Silvicultural Practices:** Consideration is given to the influence of various silvicultural practices, such as harvesting methods and reforestation techniques, on forest dynamics. By linking ALS data with data identifying types of silvicultural interventions used in forestry practices, this report gives insight into the effects of different practices on forest vitality, biodiversity, and adaptability.
- **Longitudinal Assessment:** Through multiple ALS captures at different time points, the report identifies trends and patterns in forest metrics over time. This longitudinal perspective aims to increase understanding of forest structure and ecosystem dynamics and may inform adaptive management strategies to foster sustainable forestry practices.
- **Recommendations:** Based on the findings, the report covers the benefits of integrating ALS analysis into monitoring and reporting frameworks for NSW State Forest management. It emphasizes the necessity for continued research and collaboration to refine remote sensing methodologies and enhance their applicability in assessing silvicultural impacts.

Within this report, we present worked examples and in-depth analysis of readily accessible remote sensing data, aimed at exploring various potential remote sensing 'indicators'. These indicators were identified and deliberated upon in earlier phases of the feasibility study. This report also highlights outputs in software and data repositories. These outputs make remote sensing data more accessible and useable for stakeholders involved in forest management. Further, these outputs can facilitate sharing knowledge for interdisciplinary collaborations, which may maximise the impact and value of utilising remote sensing technologies in monitoring and managing NSW State Forests.

At the site scale, our analysis encompasses indicators of structural complexity, including an examination of canopy gaps and harvested areas, alongside estimates of canopy foliage density. Additionally, we provide examples that examine the impacts of terrain slope data and differences across various NSW State Forest exclusion zones on forest structural attributes. Co-incident high-resolution imagery are combined with ALS data to provide metrics of the impact of fire damage from 2019/2020 wildfires.

'Key takeaways' from our analysis include:

- ALS-derived LiDAR metrics offer a means to summarise change in forest height and canopy coverage (pg. 15)

- Modelling canopy top height recovery and incorporating slope types, harvesting practices and FESM classes can describe the rate of recovery across these different factors (pg. 31)
- Canopy foliage density can be a useful means to visualise canopy characteristics using three separate, but related, LiDAR metrics: top of canopy (p95), bottom of canopy (p50) and canopy cover (pg. 40)
- Canopy top height (mean p95 heights) and canopy coverage recovers after harvest events across a range of slope classes (pg. 20 & 38)
- Despite differences in harvesting intensity, areas subjected to both light and heavy harvesting practices exhibit comparable rates of canopy regrowth over time, as evidenced by mean p95 height measurements derived from LiDAR data and similar canopy coverage recovery trends (pg. 16 & 36)
- Harvested areas exhibit similar proportions of mean p95 tree heights compared to some protected areas within state forest, highlighting potential similarities in canopy structure between areas managed for timber production and areas managed for conservation (pg. 34)
- Differences in canopy top heights due to different fire severities can be observed via LiDAR (pg. 23)
- Harvesting events in 2010 and 2015 are clearly reflected in the skewness data, with notable dips observed in skew following these events, particularly in Wauchope. However, skew returns to pre-harvest levels within a short period of time, indicating the resilience of forest ecosystems to silvicultural practices (pg. 45)
- A more nuanced understanding of forest structure over time can be obtained with more regular ALS capture data (pg. 46)

In conclusion, the integration of ALS technology may offer a promising avenue for enhancing forest monitoring and management practices in NSW State Forests. Continued research may help maximise the potential of remote sensing methodologies and ensure the sustainability of forestry practices in the region. This report recommends future research to focus on long-term monitoring with ALS captures to track changes in forest dynamics over time, as well as utilising emerging technologies, like 'Geiger-Mode LiDAR'.

1. Introduction

Airborne Laser Scanning (ALS), often referred to as LiDAR (Light Detection and Ranging), has emerged as a pivotal technology in forestry research, providing insights into forest structure and dynamics (Atkins et al., 2023). By emitting laser pulses from aircraft or ground-based platforms, ALS captures precise measurements of terrain and vegetation, offering a detailed portrayal of forest canopy height, density, and structure (Lefsky et al., 2002; Wulder et al., 2008).

In forestry applications, ALS enables comprehensive three-dimensional modelling of forests, to facilitate understanding of spatial distribution and structural variability (Atkins et al., 2023; Wulder et al., 2008). Moreover, through repeated ALS surveys over time, researchers can monitor changes in forest structures, providing valuable insights into the impacts of management practices and natural disturbances (Lefsky et al., 2002).

In the context of NSW State Forests, ALS presents a powerful tool for analysing temporal data and assessing forest disturbance and recovery dynamics (Qin et al., 2022). Following significant disturbance events such as the 2019-20 wildfires in eastern Australia, which inflicted damage on native forests (Bowman et al., 2021), understanding the patterns of recovery may be important for effective forest management and conservation efforts (Hillman et al., 2021).

In the context of analysing longitudinal data and disturbance recovery in NSW State Forests, LiDAR provides an opportunity to study the recovery trajectories of disturbed forests (Qin et al., 2022). Following the impact of the 2019-20 fires in eastern Australia, it was found that >44% of native forests suffered canopy damage (Bowman et al., 2021). Understanding recovery trajectories post disturbances like these, can inform forest management decisions and conservation efforts (Hillman et al., 2021).

This report aims to incorporate a retrospective analysis of ALS to demonstrate how this technology may be used to gain further understandings of how forest structures have evolved, and to increase our understanding of the potential interplay of a range of factors (for example topographic position and impact of disturbance) in shaping forest dynamics. The analyses presented in this report demonstrate how ALS may be beneficial in understanding and tracking different facets of forest structural change:

- **Comprehensive Change Assessment:** Building upon the insights gained from initial stages of collaboration with the Natural Resource Commission (NRC), this report is an extension of analysis across all ALS capture areas with multiple ALS capture time points (2012, 2016 & 2023). This report aims to present a comprehensive picture of longitudinal trends, shedding light on the broader patterns and drivers of forest dynamics.

This report is the second stage in the Agreement 2024-02H Retrospective LiDAR analysis of coastal NSW State Forests and further builds on work outlined in a previous report by Brown et al. (2023). The previous report presented an overview of ALS data acquired in 2022-2023, with a focus on the impact of Fire Extent and Severity (FESM) measures. This updated report extends analysis to include previous overlapping ALS data captures and analyse changes over time, demonstrating how ALS may be used to examine factors impacting forest dynamics.

This report includes information on the calculation of ALS metrics as well as worked examples of this data. The choice of analyses was guided by existing literature (see Appendix B). A comprehensive overview of processing ALS data into Canopy Height Models is provided in previous Brown et al. (2023) report.

Table 1. Overview of data processing and how these are addressed in this report.

Metric	Details	How it is addressed in this report
Canopy top height (m)	The 95 th percentile height of first returns	Section 2.1.
Canopy coverage (%)	Calculated as the number of first returns over 2m, divided by all first returns.	Section 2.2
Canopy foliage density (m)	The difference between the canopy top height (p95) and canopy median height (p50).	Section 2.3
Skew	Skewness of first returns (i.e., whether more points are in the upper strata (negative skew) or lower (positive skew))	Section 2.4
CHM p95 return height proportions	CHM p95 returns assigned one of 6 height group classes based on return height (0-2m, 2-6m, 6-12m, 12-20m, 20-35m, 35m+)	Section 2.1
Fire extent and severity mapping (FESM)	Co-incident high-resolution imagery used to classify regions subject to natural fire disturbance.	Section 2.1.2, 2.1.4, & 2.2.2

Table 2. Overview of proposed extension of analyses and how these are addressed in this report.

Proposed Extension of Analysis	How it is addressed in this report
Canopy Height Recovery Analysis after Harvesting and Fire Events.	Section 2.1.1 to 2.1.5. Impact of different harvesting types, topographical position & predictive modelling of height recovery.
Canopy Coverage Recovery Analysis after Harvesting and Fire Events.	Section 2.2.1 to 2.2.2. Impact of different harvesting types and topographical position are assessed.
Canopy foliage density Dynamics Analysis after Harvesting Events.	Section 2.3. Combination of three different metrics to assess forest density dynamics.
Skew Analysis after Harvesting and Fire Events.	Section 2.4. Analysis of skew and how this may be impacted by topographical position.

1.1 Brief overview of data processing: from point clouds to ALS metrics

ALS metrics are summary statistics derived from all points in a specified area, typically focusing on the distribution of height values.

ALS data captures consisted of roughly 10TB of LiDAR LAS data, which covered 540,000 hectares across NSW state forest. These included 27 state forests across 7 regions (Eden, Batemans Bay, Bulahdelah, Wauchope, Coffs Harbour, Styx River and Casino) across 3 separate capture years (2012, 2016 and 2023). To ensure consistency across captures, the point cloud data is first normalised to ensure that the LiDAR returns for overlapping geographical regions are equivalent. The normalised point clouds are then smoothed with a pit-free algorithm at the raw LiDAR return resolution. From the normalised point clouds, we generated a 1m x 1m resolution canopy height model for each region.

For the scope of this report, the below analyses rely upon metrics calculated at the 30m x 30m resolution. This down-sampled resolution was chosen because it equates to estimating LiDAR metrics for an ~ 0.1ha-sized pixel. The main benefit of this resolution is that it allows for meaningful comparisons across different features of forest dynamics aligned with field data such as landform, silvicultural history, and areas of environmental significance.

Down-sampling, however, can result in loss of finer details due to changes in point density. For future work, similar methods can be again utilised to examine forest mosaic at any resolution and notably at a higher point density. With the increased resolution, factors such as tree species and treetop counting become possible, albeit at a computational cost in data size and processing. Higher density point cloud analysis would allow for improved precision in the estimations of forest height, canopy cover and biomass, and in some cases be used for accurate species identification, or mapping habitats of various fauna. For future work, we provide scripts which outline processing of LiDAR data and production of TIFs which can be accessed here: <https://osf.io/jusc4/>.

Table 3. ALS metrics calculated for the analyses covered in this report.

Metric	Details	Potential limitations
Canopy top height (m)	The 95 th percentile height of first returns	May be affected by the presence of very tall structures or isolated trees, leading to an overestimation of the general canopy height. Even in the 95th percentile this could be skewed by a few extremely tall trees or structures which may not represent the overall canopy height accurately.
Canopy median height (m)	The 50 th percentile height of first returns.	The median height is dependent on both top and bottom returns within a pixel such that movement in either value is sufficient to shift the median. Smoothing of the point cloud distribution assists with this sensitivity to outliers but one should interpret the p50 with respect to other metrics for the top canopy, i.e., p95.
Canopy foliage density (m)	The difference between the canopy top height (p95) and canopy median height (p50).	Dependent on the accuracy of the p95 and p50 height measurements, which can be influenced by factors such as the density of the vegetation and the presence of gaps in the canopy.
Canopy coverage (%)	Calculated as the number of first returns over 2m, divided by all first returns.	The threshold of 2m for first returns may exclude significant understory vegetation, leading to an underestimation of overall canopy coverage . Additionally, variations environmental conditions can impact accuracy.
Skewness (m)	Skewness of first returns (i.e., whether more points are in the upper strata (negative skew) or lower (positive skew))	Skewness identifies distribution of strata but not the types of strata at each height. Therefore, skewness interpretations may be impacted by mixed strata. Mixed strata occurs where multiple layers of vegetation are present at different heights. For example, multiple canopy layers such as areas with dense upper canopy and understory with significant vegetation, gaps and openings, variation in terrain elevation or different types of vegetation (e.g., taller trees mixed in with shrubs within the same area) may all contribute to the same region of a

		distribution. Additional information about forest species and landform would be helpful for identifying the composition of the skewness distribution.
Slope	The topographical position of the analysed area. This was calculated using a topographical position index (TPI) from a digital terrain model to generate six slope classes (Valley, Lower Slope, Flat Slope, Middle Slope, Upper Slope, Ridge). Notably, the slope classes are ordinal (i.e., upper slope must be above lower slope classes). See Figure 6 for further information.	These classifications are agnostic to the aspect of slope class (i.e., the direction of the slope). That means two lower slope classifications can face in different directions, i.e., north-south vs. east-west.

2. Longitudinal analysis

In ecological research, longitudinal data analysis can play a crucial role in understanding the dynamics and recovery processes within ecosystems over time. By tracking ALS metrics across different time-points, researchers can observe patterns of forest dynamics including growth, disturbance and regeneration. The longitudinal approach enables a comprehensive examination of how forests respond to various environment factors and management interventions, providing valuable insights for conservation and sustainable practice.

In this section, changes in ALS metrics across different time-points are presented. To explore these, the subsequent sections follow a format of introduction, methods, results, and discussion. The below examples will cover the steps taken to calculate ALS metrics and utilise data to demonstrate use cases for metrics when examining forest dynamics over time.

2.1 Canopy height analysis

Introduction

Canopy height analysis plays a pivotal role in understanding forest ecosystems, particularly in assessing habitat suitability and biodiversity. Maintaining or conserving canopy height diversity is a key goal in sustainable forest management strategies. Leveraging LiDAR technology offers means to accurately capture and represent canopy structure. LiDAR data can be acquired from various platforms, including ground-based systems such as terrestrial/mobile laser scanning (TLS, MLS), aerial platforms like ALS, or even satellites such as the Global Ecosystem Dynamics Investigation (GEDI). Each platform may offer unique advantages and limitations, with a typical trade-off between detail and spatial coverage. In the following section, our focus lies on ALS data with a resolution of 30m x 30m.

The following section will cover ALS-derived metrics specifically tailored for canopy height analysis. These metrics encompass parameters such as top height, mean height, canopy cover, and skewness. While acknowledging the existence of more intricate LiDAR-derived metrics, we opt for a selection of straightforward area-based metrics that have demonstrated utility in prior studies (see Appendix B). These metrics serve not as exhaustive representations of canopy structure but rather as illustrative examples, elucidating the requisite processing procedures. It is important to note that the intricacies of forest structure may extend beyond these metrics, incorporating numerous other variables and unknowns. Despite this, the incorporated metrics still serve as valuable tools for understanding forest dynamics. While they may not capture every nuance of the forest, they offer a practical approach to categorising and studying forests, thereby contributing to our overall understanding of ecosystem dynamics, and aiding in effective forest management practices.

Methods

ALS height metrics are derived from the vertical arrangement of points within a specified spatial region. Illustrated in Figure 1 is a sample LiDAR point cloud representing a 'plot,' alongside a histogram displaying height distribution (i.e., the count of points within each height category). The summary

statistics, termed ALS metrics, can be taken from this histogram (vertical profile). These metrics include top height (p95), average height, median height, and canopy cover (the ratio of points surpassing a height threshold).

The mean top height in the 95th percentile or p95 metric was computed for each grid cell (30m x 30m pixel) within the study area and comparing these values between successive LiDAR acquisitions to examine changes in canopy height over time. This metric provides a good representation of canopy height and can account for extreme outlier values, such as bird strikes (see Figure 1).

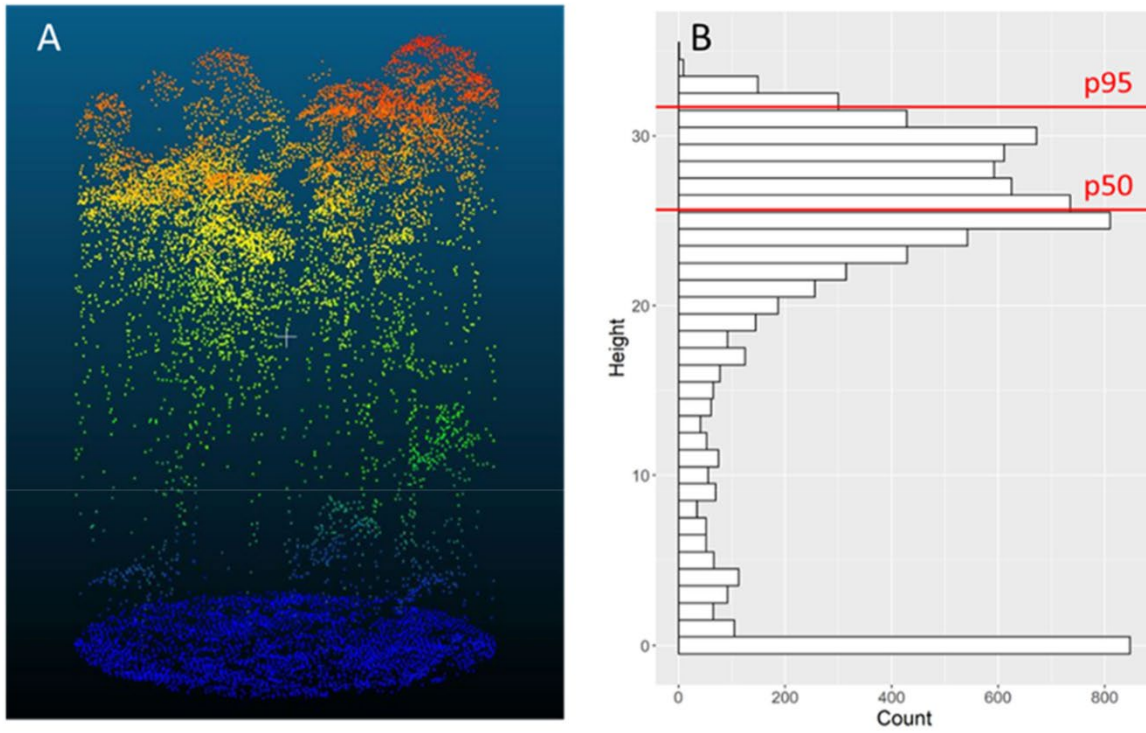


Figure 1 - Example of a 3D point cloud (left) and the corresponding distribution of height values (right), with the 50th and 95th percentiles shown in red.

ALS metrics are then projected over existing field data, commonly referred to as 'vector' data, to enable comprehensive analysis of various factors within areas of interest. The integrated approach facilitates the examination of a wide range of elements, including fires, historical harvesting activities and designated conservation zones. By overlaying ALS-derived metrics onto the vector data, researchers and forest managers can gain insight into the spatial distribution and impact of harvesting events, as well as identify areas of ecological importance for conservation efforts.

2.1.1 Canopy height recovery in harvested regions

Introduction

Understanding the dynamics of canopy recovery following forest harvesting is crucial for effective forest management and conservation efforts. This section utilises LiDAR data and accompanying field data to investigate the patterns of canopy height recovery.

While acknowledging the potential influence of multiple harvest events and natural disturbances such as bushfires, this report focuses on delineating the recovery trajectories of the upper canopy post-harvest. This report will demonstrate how ALS may be used to gain valuable insights into the resilience of forest ecosystems and examine differences in metrics, such as mean p95 heights, for management practices tailored to mitigate the impacts of human activities and environmental disturbances on canopy structure and biodiversity.

Methods

For the following analysis, LiDAR data was filtered to areas within Wauchope that were last harvested in years 2010, 2015, and 2020. For each harvest year, mean p95 heights (m) and standard errors for the same geographical regions are calculated based on ALS conducted in 2012, 2016, and 2023.

Figure 2 shows a map of analysed ALS data within Wauchope where regions that were previously harvested are shown in separate colours. As a comparison, metrics for Environmentally Significant Areas (ESA's) are averaged to provide a baseline of regions that *have not* been disturbed by silvicultural practices.

We focus on Wauchope for two reasons. First, Wauchope was measured across all three existing ALS captures (2012, 2016 and 2023). Because it contains the greatest number of ALS captures across NSW, analyses of longitudinal trends within the report are based on the Wauchope region. However, for completeness, we present the same analyses for each region separately in Appendix A.

Second, these specific regions harvested in 2010, 2015, and 2023 were chosen for their temporal proximity to the LiDAR captures. By closely following each ALS capture, we sought to demonstrate forest recovery trends prior to and following silvicultural disturbance. Regions last harvested in 2010 have had a longer period of time for recovery where all three LiDAR captures were flown after harvesting occurred. Regions last harvested in 2015 and 2020 were chosen because LiDAR captures were flown prior to and following silvicultural disturbance. We note that although regions can be harvested more than once, the most recent harvest year is used in our analyses.

Finally, when examining the impacts of fires we include Wauchope but note that the Wauchope region did not experience as extensive damage in the 2019-20 wildfires (see Figure 3). For this purpose, any analyses of fire extent and severity, indexed by FESM classifications, were conducted on the Eden region where a single ALS capture was conducted in 2023. For a description of the metric (p95) and its limitations, see Table 3.

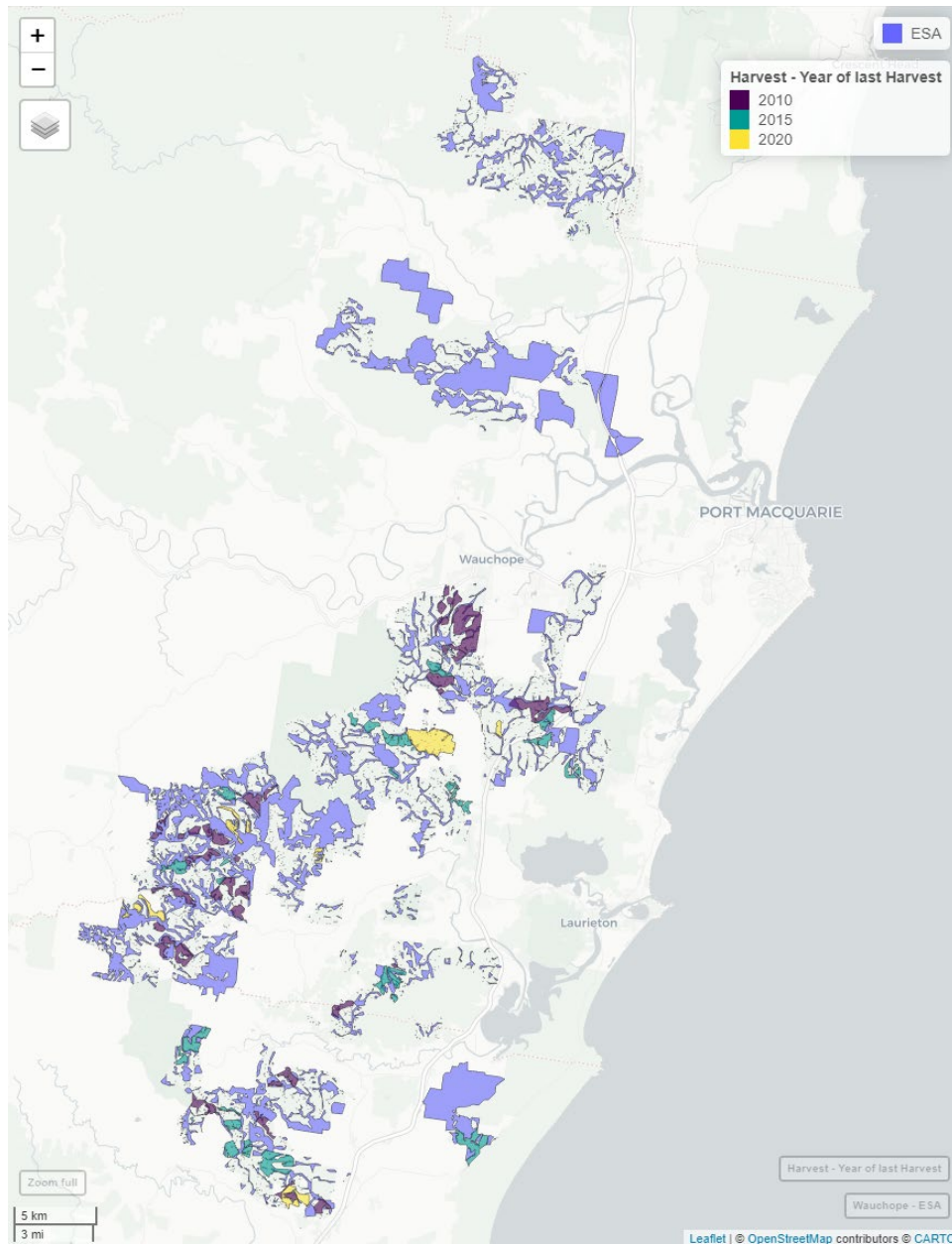


Figure 2 - Map of Wauchope identifying areas included in multiple captures analysis. Separate regions last harvested in 2010 (coloured purple), 2015 (green) and 2020 (yellow) are aggregated and compared against each other and average ESA regions (shown in blue). These regions were selected to highlight silvicultural disturbances at timepoints close to the LIDAR capture flights conducted in 2012, 2016, and 2023. ESA regions are averaged to provide a baseline comparison for regions that have not been disturbed by silvicultural practices. Click [here](#) for an interactive version of this map.

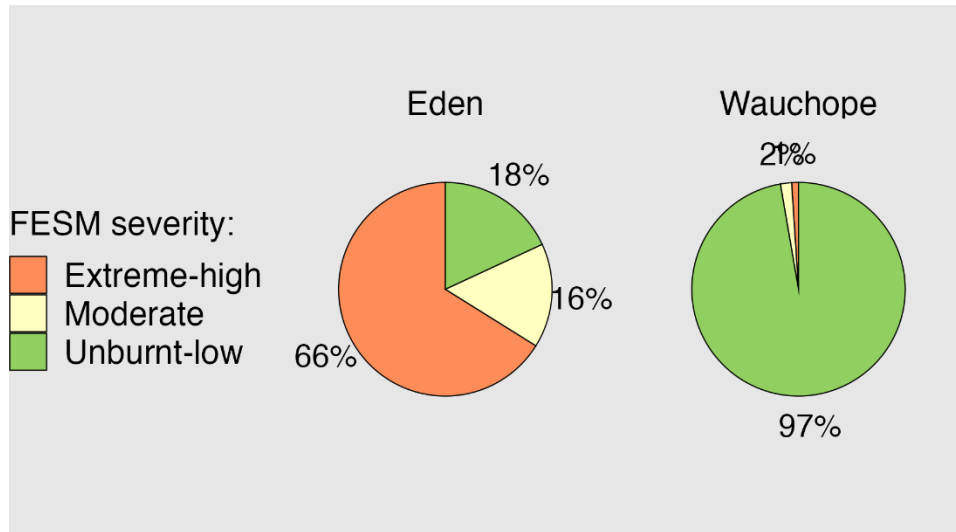


Figure 3 - Pie charts of the relative proportions of fire extent and severity mapping (FESM) ratings across Eden and Wauchope captures. In subsequent analyses of FESM, we analyse the Eden capture as to demonstrate the impacts of fire on LIDAR metrics. Of note, Eden has only a single LIDAR capture in 2023 and, so, in analyses emphasising longitudinal patterns over time, we return to analyse Wauchope where LIDAR captures were flown in 2012, 2016, and 2023. FESM ratings for other captures are available in Figure A1. Note that FESM ratings are traditionally categorised into five levels (unburnt, low severity, moderate, high, and extreme severity). For clarity, we have condensed these five levels to three where low severity is merged with unburnt, and high severity is merged with extreme.

Main results and discussion

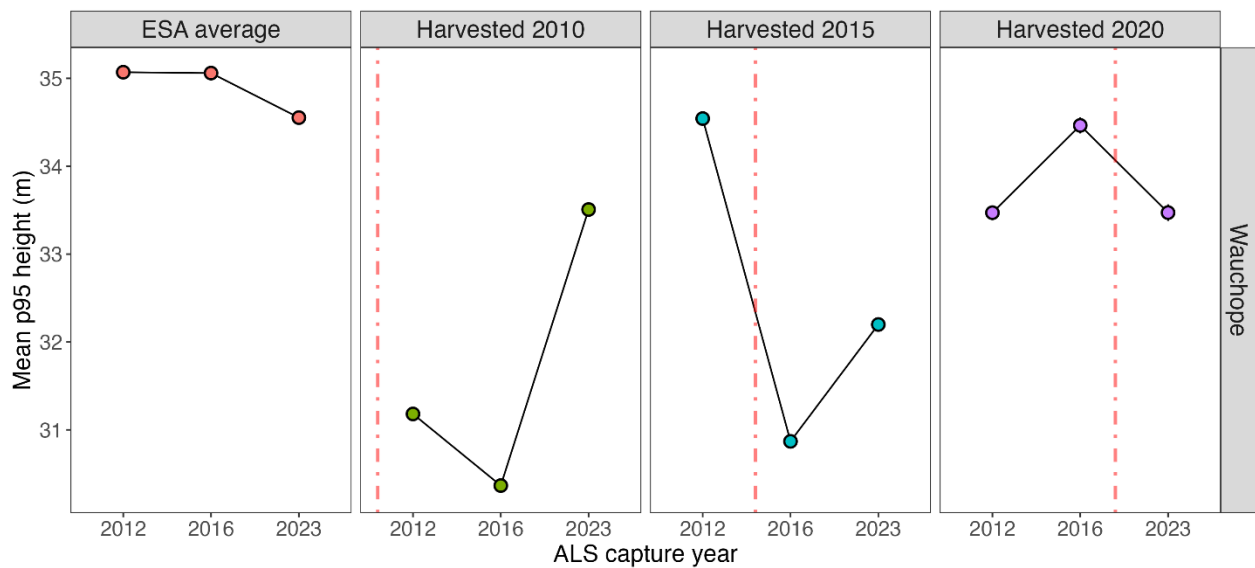


Figure 4 - Mean p95 heights for areas harvested in 2010, 2015 & 2020 with points indicating separate ALS captures. Vertical red dashed line is a visual guide of the approximate timepoint of silvicultural

disturbance, noting the change in this timepoint across regions. For all other locations see Appendix Figure A2.

Canopy top height, measured as mean p95 heights returns, can be utilised to understand recovery after harvesting events. Across panels, harvest events are signified in the time points on the dash-dotted red line. As an example, the second-from-right panel for regions harvested in 2015 exhibit top-canopy recovery as ALS captures were conducted prior to and after the harvesting event. For 2015-harvested regions, mean p95 heights returns measured in the 2016 ALS capture were 30.9m ($se = 0.09$) as compared to 34.5m ($se = 0.06$) measured in 2012 ALS capture. By 2023, the mean p95 heights returns for the same regions were recovering where mean p95 heights returns were 32.2m ($se = 0.06$). Regrowth of upper canopy also occurs post-harvest in the 2010-harvested regions albeit noting the absence of a baseline p95 CHM returns for the 2010-harvested regions. ESA average heights also decreased between 2016 (left-most panel, second point) and 2023 (left-most panel, third point) suggesting natural disturbances may have affected top canopy height across the capture.

Key Takeaways

ALS-derived LiDAR metrics offer a means to summarise change in forest height.

Canopy top height (mean p95 heights) show recovery after harvest events over the course of 11 years and across distinct regions.

For each region, p95 measurements track regrowth patterns in line with ESA averages for the same forest region.

2.1.2 Canopy height recovery in harvested regions: comparing light and heavy harvesting practices

Introduction

Forest harvesting practices encompass a spectrum of techniques, ranging from selective thinning to regeneration cuts, each tailored to achieve specific management objectives. Among these, different harvesting methods represent contrasting approaches with distinct impacts on forest ecosystems. Light harvesting, often synonymous with selective harvesting or thinning, involves the removal of a limited number of trees, typically targeting diseased or low-value specimens while preserving the overall forest canopy. In contrast, heavy harvesting involves more extensive removal of trees, aiming to regenerate forest stands or create openings for new growth. Understanding the effects of these harvesting techniques on canopy dynamics is paramount for sustainable forest management. By examining the regrowth patterns following light and heavy harvesting practices, we gain insights into the resilience of forest ecosystems and their capacity to recover from human intervention. Such analyses provide valuable guidance for policymakers, land managers, and conservationists in formulating strategies that balance timber extraction and biodiversity conservation.

Methods

For the following analysis, LiDAR data was filtered to areas within Wauchope that were last harvested in years 2010, 2015, and 2020. For each harvest-year-region, mean p95 heights (m) and standard errors are calculated based on ALS captures conducted in 2012, 2016, and 2023. Separate means were then calculated for harvest practices classified as “heavy” (e.g., STS regen or STS heavy) or “light” (e.g., STS light or “thinning”). Note that “heavy” practices were recodified in 2018 as part of a harvest practice review. The “STS-heavy” practice was discontinued, and no areas were subject to intensive harvesting following 2018. For a description of the metric (p95) and its limitations, see Table 3.

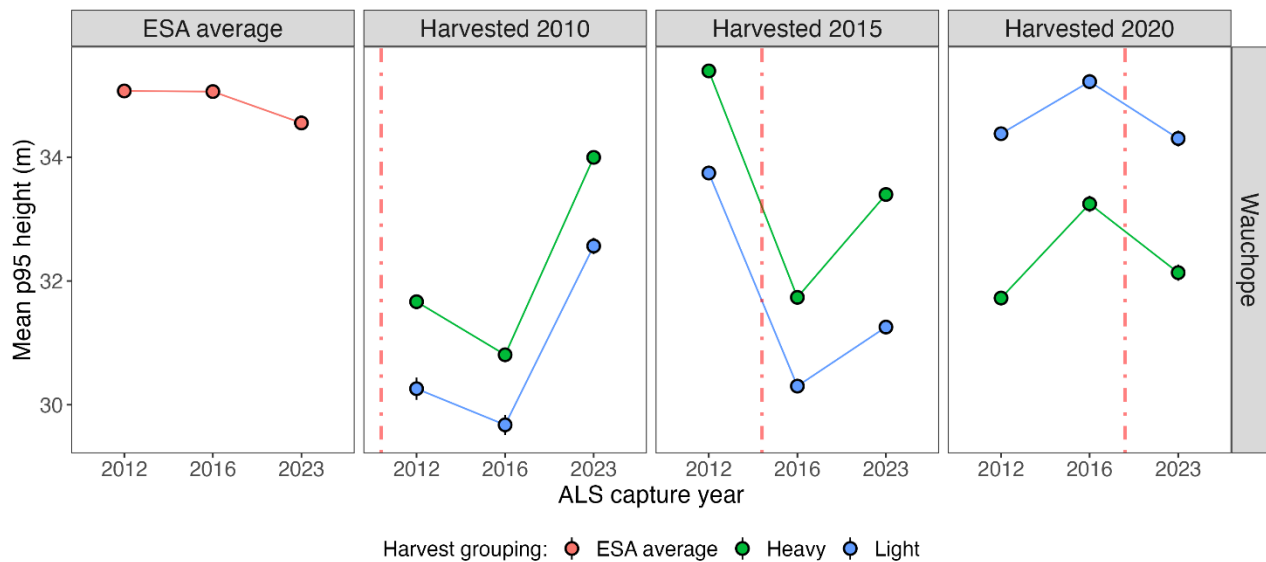


Figure 5 - Mean p95 heights for the Wauchope capture for areas harvested in 2010, 2015 & 2020 with points indicating separate ALS captures and coloured lines indicating type of silvicultural practice. Vertical red dashed line is a visual guide of the approximate timepoint of silvicultural disturbance, noting the change in this timepoint across regions. For clarity, we present only “light” (blue) and “heavy” (green) silvicultural practices in this figure, noting that other silvicultural practices, such as mixed practices or salvage harvests, are present in the data. For analyses of other capture locations areas, see Appendix Figure A3.

Main results and discussion

The analyses shown in *Figure 5* can be used to examine the impacts of different harvesting practices on mean p95 heights. Regrowth patterns for harvesting practices classified as “heavy” are shown in green points and “light” classified practices shown in blue points.

In general, regrowth patterns are similar between “heavy” and “light” practices across each of the three regions. One notable difference is that regions selected for a given silvicultural practice show a-priori differences. For example, heavy-practice harvested regions in 2010 (second-from-left panel) show

higher p95 return heights than light-practice harvested regions. However, for 2020-harvested regions this pattern is reversed where light-practice harvested regions are higher (green vs. blue points, right-most panel).

Interpretation of the long-term impacts of different harvesting practices should consider additional selection factors that affect which regions are selected for a particular silvicultural practice. Consideration of other metrics of forest regrowth such as canopy coverage (shown in Figure 18) and canopy foliage density (shown in Figure 22) are included in this report. It is worth noting that regrowth is affected by a-priori forest characteristics such as landform (e.g., valley vs. ridge areas) and species composition (e.g., eucalypt species competition).

Key Takeaways

Despite differences in harvesting intensity, regions subjected to both light and heavy harvesting practices exhibit comparable rates of canopy regrowth over time, as evidenced by mean p95 height measurements derived from LiDAR data.

2.1.3 Canopy height recovery in harvested regions across varied landform classes

Introduction

Slope position is known to influence forest type and productivity due to soil conditions, moisture availability and terrain characteristics. Due to this, different harvesting techniques may be utilised based on slope position to optimise forest productivity and regeneration. Recognising the significance of slope position in determining forest characteristics and productivity, and by adapting harvesting strategies accordingly, forest managers can enhance the sustainability of forest management practices and promote ecosystem resilience in the face of environmental challenges. This understanding underscores the importance of considering slope position as a key factor in forest management planning and decision-making processes.

Methods

Slope was identified and calculated by utilising the Digital Terrain Model (DTM). DTM's are created from ALS capture data and represent the bare earth surface without any features such as buildings or vegetation. Terrain was then classified into 6 slope categories: valley, lower slope, middle slope, flat slope, upper slope, and ridge (Figure 6).

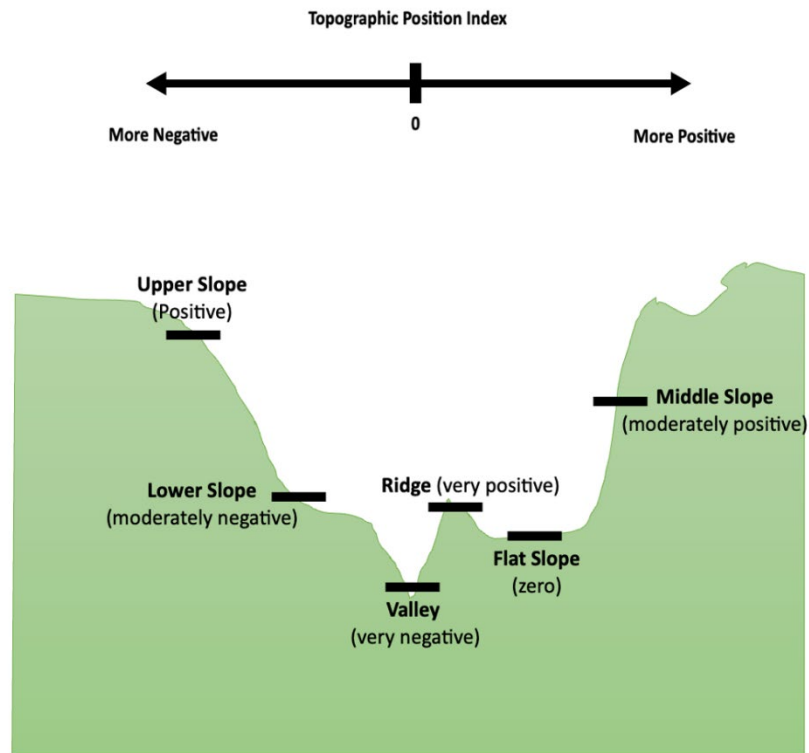


Figure 6 - Example of slope positions following the topographic position index (TPI). Adapted from Muddarisna et al. (2020) and Weiss (2001).

Weiss (2001) classifies slopes using the Topographic Position Index (TPI) these being:

- Valley: $TPI \leq -1$
- Lower Slope: $-1 < TPI \leq -0.5$
- Flat Slope: $-0.5 < TPI < 0.5$ and slope $\leq 5^\circ$
- Middle Slope: $-0.5 < TPI < 0.5$ and slope $> 5^\circ$
- Upper Slope: $0.5 < TPI \leq 1$
- Ridge: $TPI > 1$

See Figure 7, for proportions of landform classes across harvested areas in Wauchope where middle slopes are the most present landform class (70%).

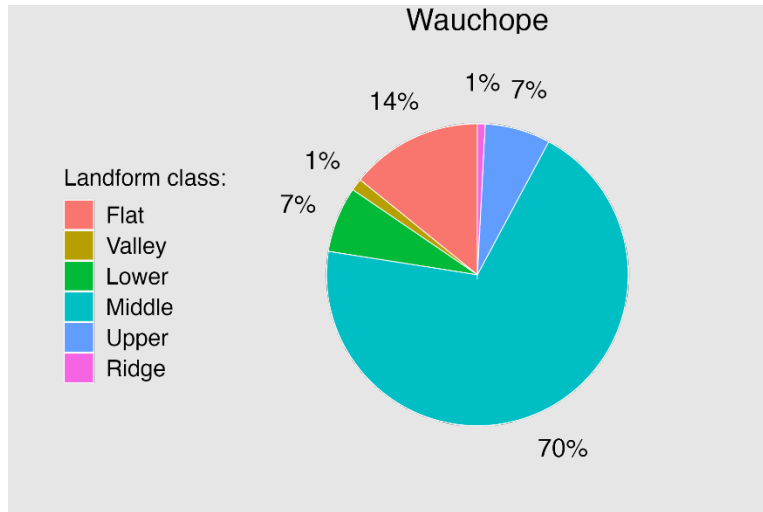


Figure 7 - Pie Chart with percentage of each slope class found in LiDAR data set within Wauchope. For all other capture regions see Appendix Figure A7.

Method

For the following analysis, LiDAR data was filtered to areas within Wauchope that were last harvested in years 2010, 2015, and 2020. For each harvest year, mean p95 heights (m) and standard errors for the same geographical regions are calculated based on ALS captures conducted in 2012, 2016, and 2023. Separate means are calculated for each slope class (e.g., Valley or Ridge) in each harvested region. Broadly, the landform composition of each region is similar where the majority of returns are from middle-slope regions (~70%) and few ridges and valleys (1% respectively). For clarity, the relative proportions of each slope class are presented in Figure 7. These proportions are to aid interpretation of Figure 8 where mean p95 heights are calculated for slope class, harvested region by year, and ALS capture. For a description of the metric (p95) and its limitations, see Table 3.

Main results and discussion

The analyses of mean p95 heights from Figure 8 are decomposed into each slope class within Wauchope. Mean p95 heights differ across slope classes (i.e., average across vertical panels). For example, returns in the “flat” class were lower than returns in the “valley” class. Mean p95 returns also differed within slope classes and across distinct regions (i.e., across horizontal panels). For example, within the “flat” class (top-most horizontal panel), mean p95 heights were higher in regions harvested in 2015 (central panel) as compared to 2012 (second-from-left panel). It is worth noting that although regions may be classed under the same slope classification, other geographical and spatial features may significantly contribute to mean p95 heights.

One notable trend is that of regions harvested in 2020 on “ridge” and “upper” slopes as compared to other slope classes (right-most column panels). Following harvest, shown in the dotted red line, mean p95 returns declined between the 2016 and 2023 ALS (x-axis) whereas in other slope classes, mean p95 returns increased between 2016 and 2023. This trend may reflect the difficulty of growth of the upper canopy on ridge and upper slopes noting similar trends in slope-matching ESA regions (left-most panels).

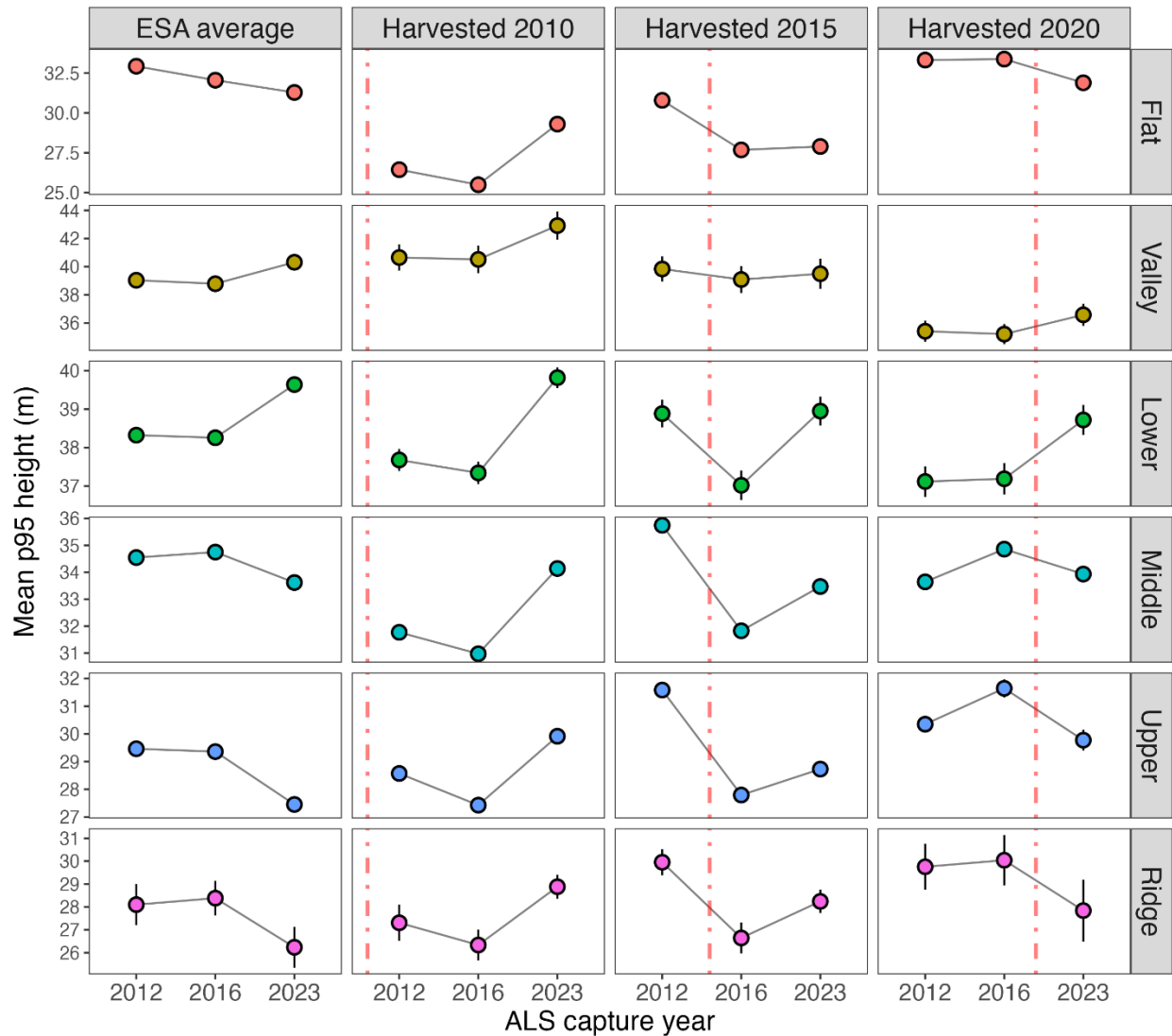


Figure 8- Mean p95 heights for the Wauchope capture for areas harvested in 2010, 2015 & 2020 with points indicating separate ALS captures and coloured lines indicating landform slope classification. Vertical red dashed line is a visual guide of the approximate timepoint of silvicultural disturbance, noting the change in this timepoint across regions. Points represent mean values and error bars represent standard error, noting that the large number of datapoints result in precise estimation of the mean values. Vertical panels indicating slope classification. Note that for clarity of the longitudinal patterns, the y-axes for each slope classification changes across vertical panels. For all other locations see Appendix Figure A6.

Key Takeaways

Canopy top height regrowth (mean p95) occurs in most regions under a range of slope classes.

2.1.4 Canopy height recovery in regions affected by fire

Introduction

Fires represent significant natural disturbance events. Certain forest regions are more at risk of fire disturbance due to a variety of factors such as geographical location, landform properties promoting or inhibiting fire spread and tree species composition, amongst other factors. The retrospective LiDAR captures includes the Eden region which was severely burnt during the 2019/20 bushfires. To measure the extent of this damage, high-resolution satellite imagery was used to generate Fire Extent and Severity Mapping (FESM) ratings that identify the fire-affected damage across a range from *unburnt* to *extreme severity*. In this section, we present canopy height metrics from the Eden capture as a function of the FESM ratings as to understand better how natural disturbances are indexed and cross-validated by LiDAR measurements.

Method

For the following analysis, LiDAR data was filtered to regions within Eden (see Figure 9). Compared to Wauchope, Eden was heavily impacted by fires in 2019 where FESM ratings show a larger proportion of extreme-high damage areas (see Figure 10). We analysed all regions in Eden and calculated mean p95 heights (m) and standard errors based on the single ALS capture conducted in 2023. Separate means are calculated for each slope class (e.g., Valley or Ridge), each FESM class (Extreme-high, Moderate, Unburnt-Low) and whether the region was in the base net area (BNA) or an environmentally significant area (ESA). For a description of the metric (p95) and its limitations, see Table 3.

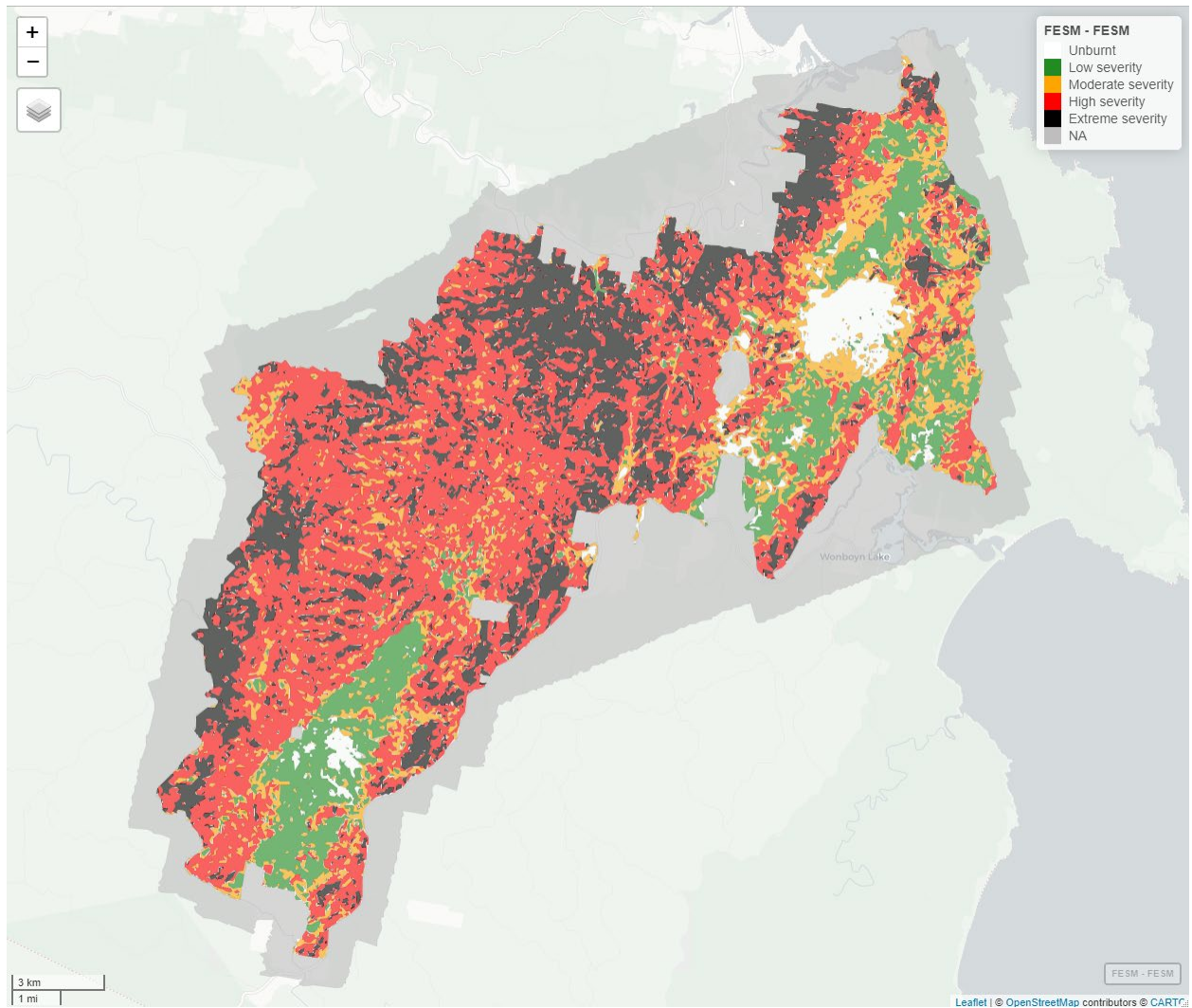


Figure 9 - Map of Eden where colours indicate fire extent & severity mapping (FESM) ratings ranging from “unburnt” in purple to “extreme” in yellow. Note that grey-shaded regions do not contain FESM rating data. Click [here](#) for an interactive version of the above map. For an interactive map showing a similar overview of the Wauchope region, click [here](#).

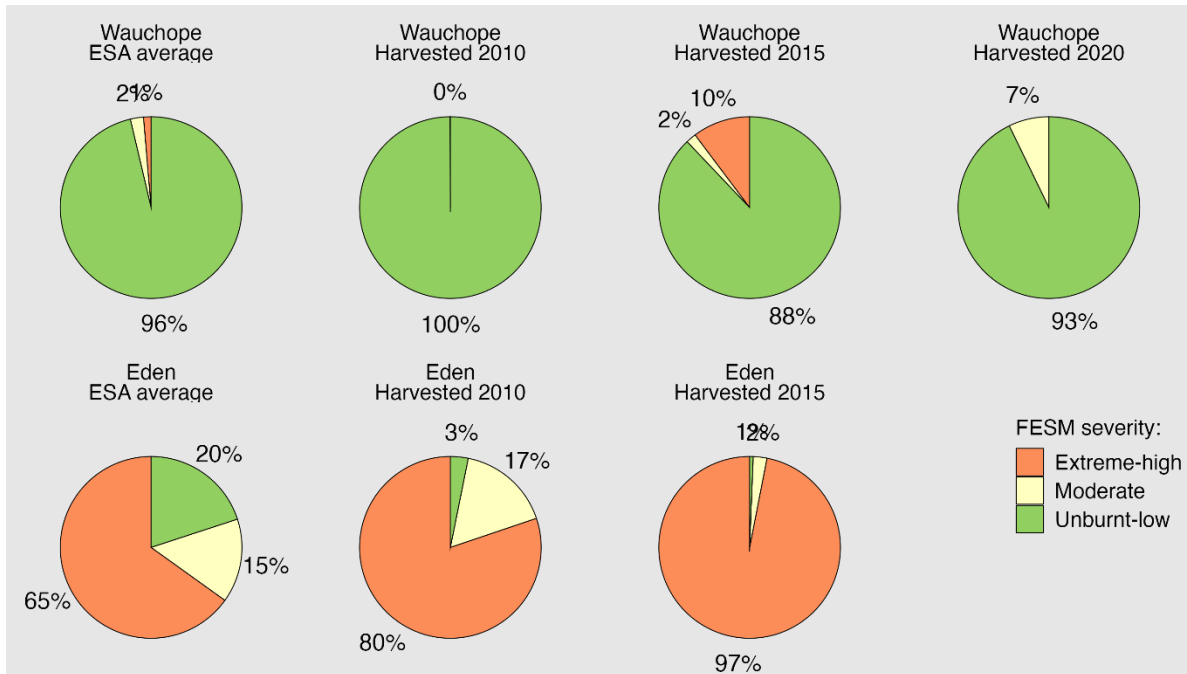


Figure 10 - Comparison of relative FESM classifications in Wauchope (top row) compared to Eden (bottom row) for select regions. Each pie chart refers to separate regions within each capture where ESA average is composed of ESA regions across the entire capture. Other regions are separated by year of last harvest from 2010 harvested areas (second column from left), 2015 harvested (third column), and 2020 harvested (right-most column) where available. Note that due to the occurrence of extensive fire damage in 2019/2020, no areas were harvested in 2020 in Eden. Figure A1 highlights significant extent of fire severity damage in Eden and the broader south coast in comparison to other forest. FESM ratings are traditionally categorised into five levels (unburnt, low severity, moderate, high, and extreme severity). For clarity, we have condensed these five levels to three where low severity is merged with unburnt, and high severity is merged with extreme.

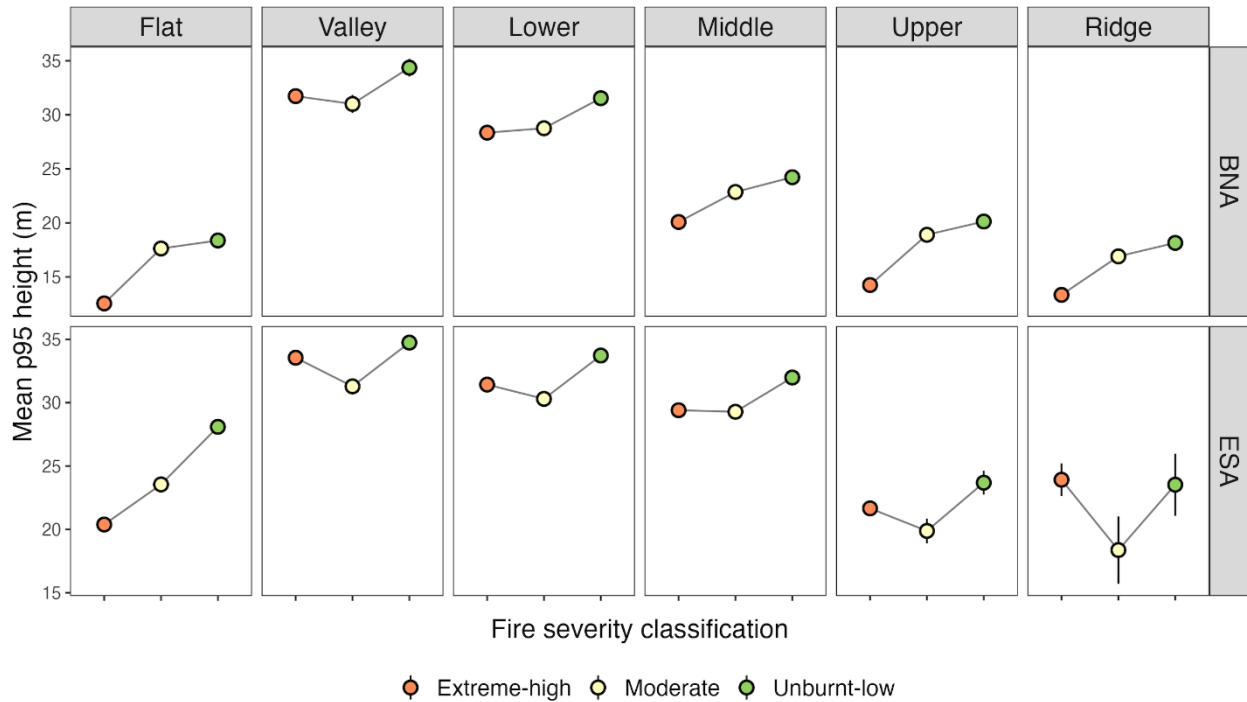


Figure 11 - Mean p95 heights of the Eden capture as a function of fire extent and severity mapping (FESM) ratings (x-axis & colours) and landform class (slope – horizontal panels). ESA and BNA regions are shown separately (vertical panels). Colours correspond to x-axis FESM ratings. Points represent mean values and error bars represent standard error, noting that the large number of datapoints result in precise estimation of the mean with small standard errors. Note that FESM ratings are traditionally categorised into five levels (unburnt, low severity, moderate, high, and extreme severity). For clarity, we have condensed these five levels to three where low severity is merged with unburnt, and high severity is merged with extreme. For all other regions in the dataset, we recreate these figures for each region separately in Appendix Figures A17 – A22.

Main results and discussion

Differences in mean canopy height can be observed across landform (horizontal panels) and fire severity ratings (colours and x-axis). In Figure 11, we primarily focus on fire severity where higher FESM ratings (orange-coloured points) were associated with lower mean p95 heights as compared to less fire-affected FESM ratings (green-coloured points). Moderate p95 returns (vanilla-coloured points) were generally in-between the higher- and lower-severity FESM classes for BNA regions. One notable exception is that in ESA regions, moderate-severity returns were lower than extreme-high severity ratings. A tentative explanation is the gradation of image colours used to generate FESM classes is less certain for moderate-range colours compared to extreme or unburnt regions. Generally, the patterns across fire severity ratings indicate that LiDAR can be used to assess natural disturbance impacts on top canopy heights.

Key Takeaways

Canopy top heights measured by p95 LiDAR returns reflect fire severity classifications generated using satellite imagery.

Analyses across landform slopes show lower top heights for regions affected more severely by fire. Expected tree growth patterns over landform, e.g., lower heights on ridges but higher in valleys, are observable using LiDAR.

2.1.5 Patterns of forest height regeneration post-harvest

Introduction

Understanding the dynamics of forest regeneration following harvesting events is crucial for effective forest management and conservation. Forests are dynamic ecosystems that undergo continuous growth, disturbance, and regeneration. By categorizing collected data into six height groups (0-2m, 2-6m, 6-12m, 12-20m, 20-35m, +35m), it is possible to capture the vertical structure of the forest canopy and assess the distribution of vegetation across different height classes.

Method

Analysis was performed on the mean p95 heights. In the context of forest analysis using LiDAR data, polygons, or multi-polygons, refer to spatial units or areas within a forest landscape that are defined by boundaries. These boundaries could be delineated based on various factors such as administrative divisions, ecological features, or research design. The below analysis focuses on multi-polygons which represent discrete forested areas or plots where LiDAR data was collected and analysed. Each multi-polygon may encompass a specific portion of the forest landscape, and consist of multiple pixels, serving as a unit for measuring canopy characteristics, such as mean p95 heights, which may be used to indicate the height of the upper canopy. By analysing data at this level, researchers can assess vegetation characteristics and regeneration patterns in different parts of the forest landscape, allowing for a more detailed understanding of forest dynamics and management needs.

Mean p95 returns of a pixel was assigned to one of 6 height groups (0-2m, 2-6m, 6-12m, 12-20m, 20-35m, +35m). Areas where harvesting is permitted but which had no record of the last harvest year were assigned the description 'Unharvested BNA'. ESAs were also included as a point of comparison. For a description of the metric (p95) and its limitations, see Table 3.

Main results and discussion

As seen in Figure 12 this analysis delves into the dynamics of regeneration and recovery within disturbed forest areas, aiming to identify the factors that contribute to regeneration. Exploring the distribution of

CHM returns by separating them into different height classes offers a nuanced perspective beyond mean p95 values alone and provides a more detailed depiction of forest structure. Refer to Appendix A for a comprehensive overview of ALS capture years across all locations.

Figure 12 shows that forests in Eden attain p95 height distributions similar to unharvested forest areas approximately a decade after harvest, with minimal alterations observed over time in Coffs Harbour. Notably, trees in ESAs (x-axis, second column from right) within Coffs Harbour exhibit a higher proportion of taller trees compared to harvested areas. It remains unclear what the cause of these differences is, and it may be the result of different forest types, silviculture histories and/or specific protection measures linked to factors coinciding with tree height, such as increased ground coverage for animals.

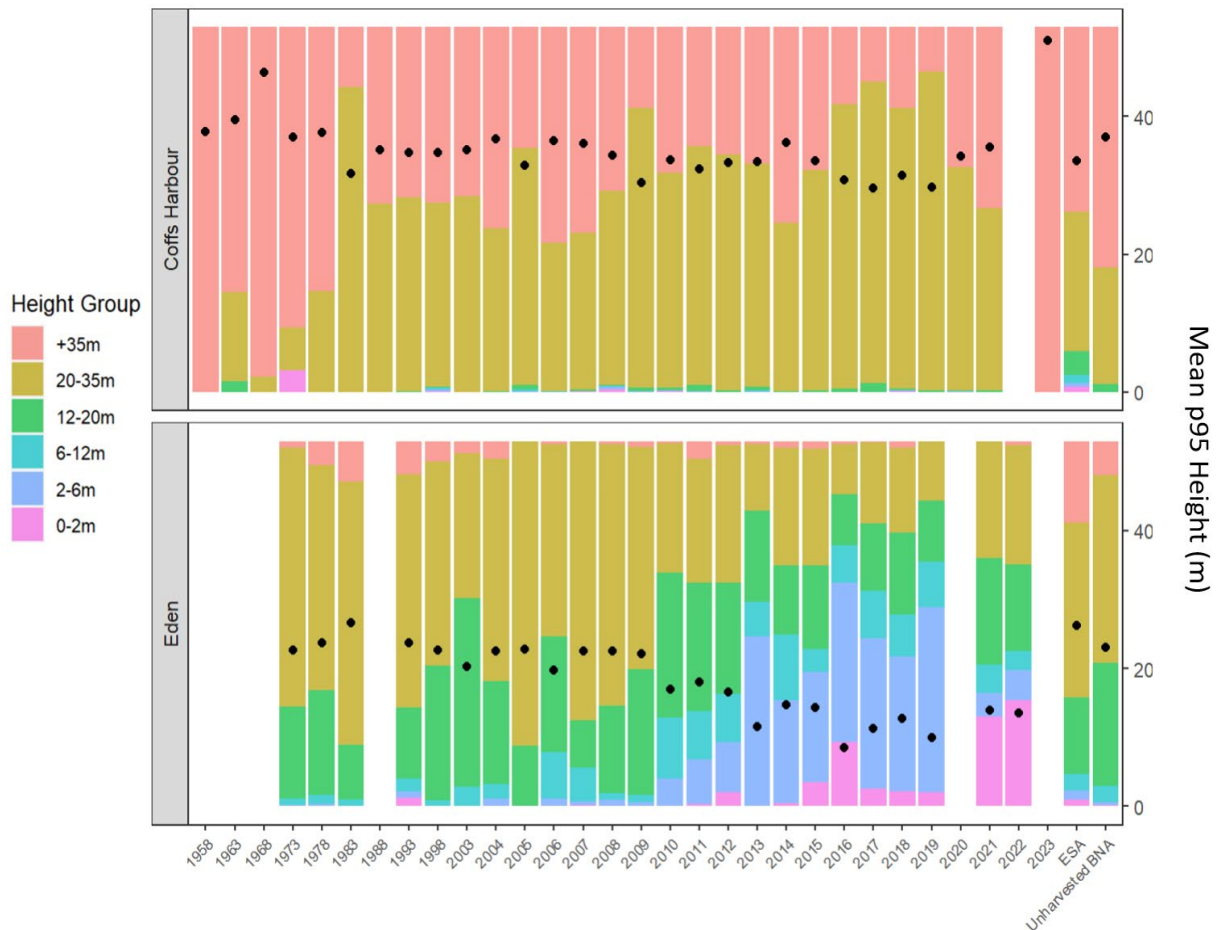


Figure 12 - Stacked bar plots showing the proportion of p95 heights (m) separated into height categories in Coffs Harbour and Eden by year of most recent harvest. This figure focuses on Coffs Harbour and Eden as these regions have the most complete data and depict growth patterns which contrast one another. For all other regions captured in 2012, 2016 and 2023 see Appendix Figure A9. The black dots show the mean p95 heights for each harvested group. Separate geographical areas of forest are shown in each bar where the x-axis marks the year of last harvest; each bar represents the regions of forest which were last harvested in the corresponding year. The columns on the far-right present data on areas available for harvest (Unharvested BNA) and environmentally significant areas (ESA) for comparison purposes. To

improve readability, the areas included on the x-axis are those last harvested every five years from 1958 to 2003 and then those last harvested within the last 20 years (each year from 2003 to 2023).

Wauchope

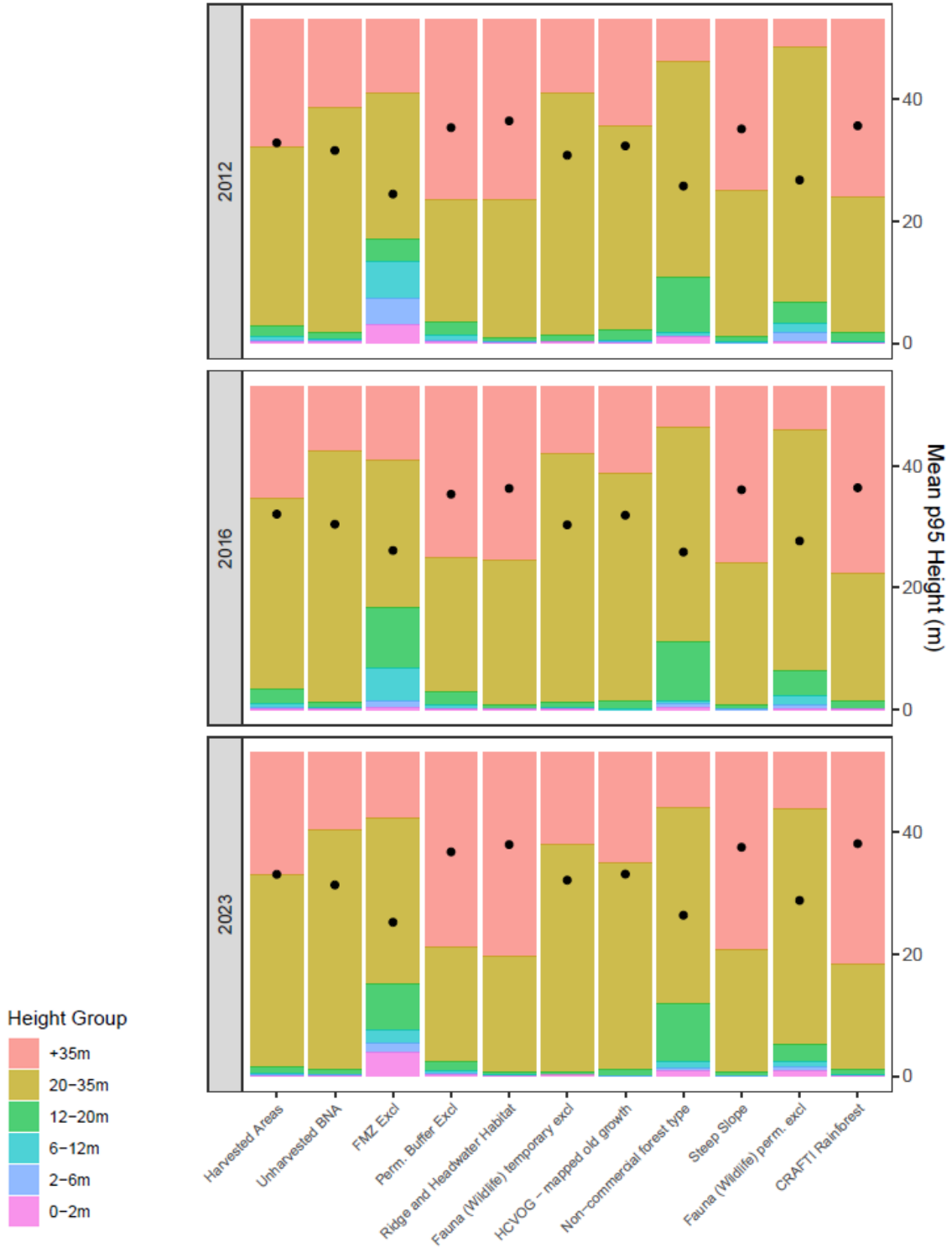


Figure 13 - This figure compares forest height groups (by p95) in different harvested and protected areas in Wauchope over ALS captures from 2012, 2016 and 2023. ESAs have been excluded from harvesting for different reasons, with areas temporarily excluded from harvesting to protect fauna showing the biggest proportion of tall trees. For all other regions in these capture years see Appendix Figure A10.

Main results and discussion

The repeated ALS captures conducted in Wauchope reveal consistent tree height proportions across various protected areas, over an 11-year period. The three captures exhibit comparable proportions across different exemption criteria, indicating a relative stability in the composition of these forest ecosystems over time. While this outcome is expected in undisturbed areas, it is noteworthy that the proportion of mean p95 tree heights in harvested regions closely resembles that found in certain protected regions.

Wauchope

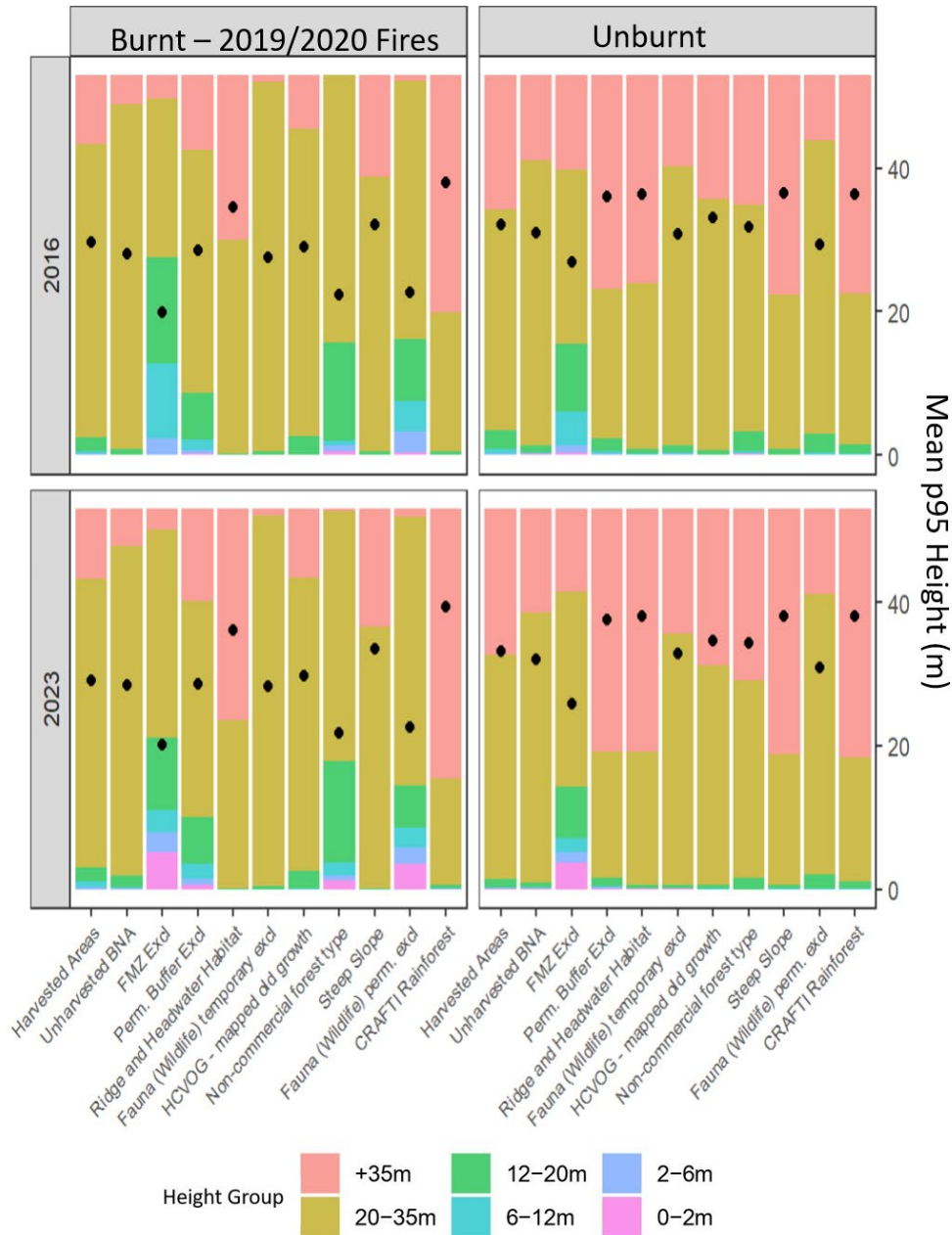


Figure 14 - This figure compares forest height groups (by p95) for burnt and unburnt areas across the ALS captures before (2016) and after (2023) FESM categorisation. The 'Burnt' areas aggregate over three different fire severity classes (Low, Moderate and Extreme) determined by satellite imagery of areas affected by the 2019/2020 bushfires. Regions marked as burnt/unburnt in the 2016 ALS capture represent a baseline measurement of regions prior to major fire disturbance. As ALS capture data is available in Wauchope for both 2016 and 2023, it provides a good example of pre-and post-FESM

categorisation data, however it should be noted that only 3% of this region was classified as 'Burnt', as shown in Figure 3.

Main results and discussion

Figure 14 shows that, overall, areas which have been affected by fire have a higher proportion of trees in the lower height classes than those which remain unburnt. The multiple ALS captures allow us to explore the impacts of fire in protected regions over time and, though there is little change for most protection classes, there is a noticeable increase in trees below 2m (pink) between the 2016 and 2023 captures for several of the harvest exclusion regions which have been burnt (FMZ exclusion zones, non-commercial forest types and fauna (wildlife) permanent exclusion zones). This indicates recent regeneration following fire damage in these areas. It should also be noted that the FMZ exclusion zone contains more small trees than any other protected region in both burnt and unburnt areas, suggesting that regions which have been excluded for this reason likely contain smaller trees in general.

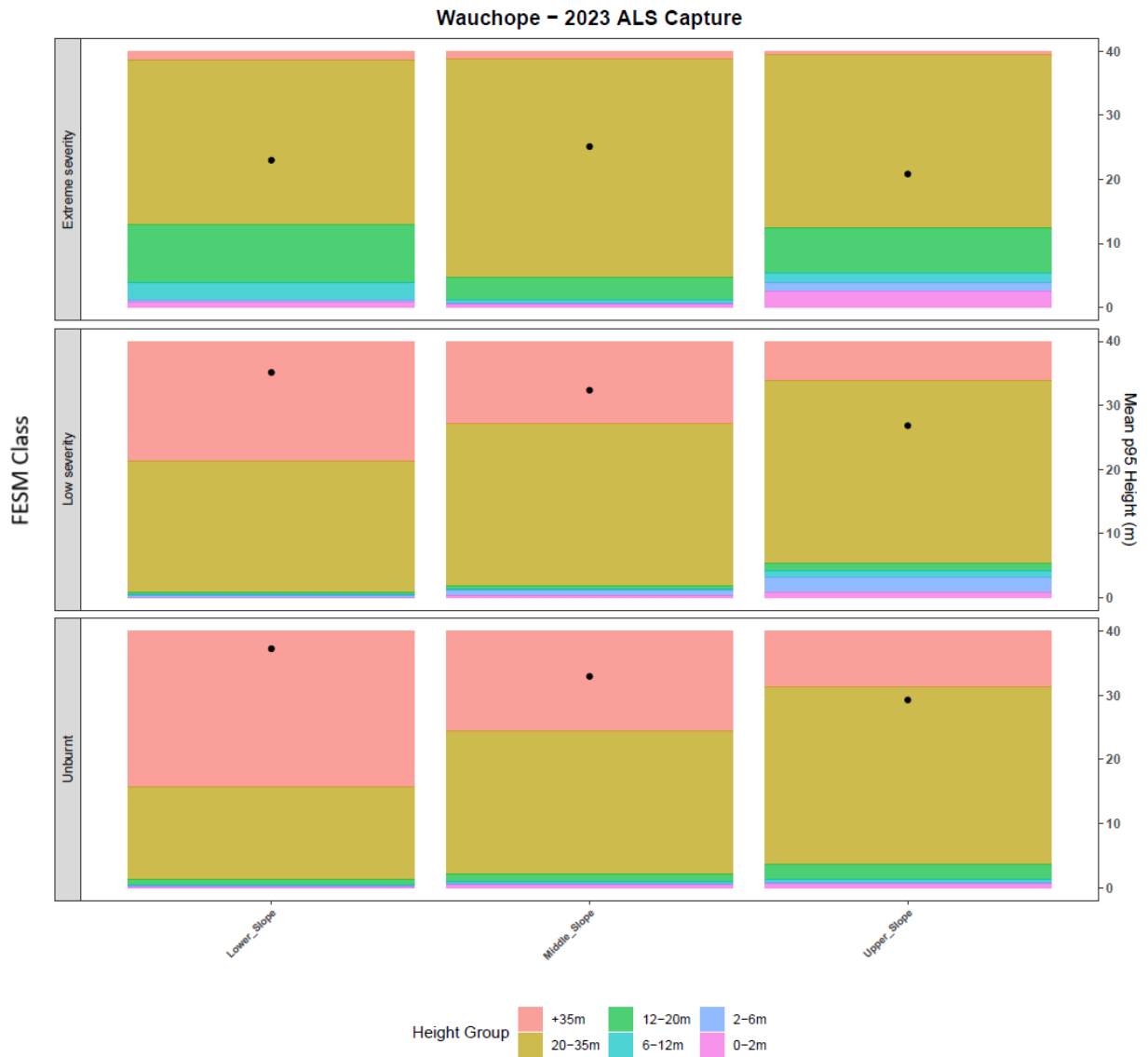


Figure 15 - Stacked bar plots showing the proportion of p95 heights (m) in Wauchope for three types of slope (Lower, Middle and Upper; x-axis) and FESM classes (Unburnt, Low Severity and Extreme Severity; y-axis). The black dots show the mean p95 heights for each harvested group.

Main results and discussion

Figure 15 explores the impact of different fire severity and slope types on forest structure in Wauchope. Importantly, Figure 15 shows little difference across the slope types when the fire severity was extreme and most trees short, but gradual decreases in height as increases across the low fire severity and unburnt regions. This interaction between fire severity and slope type is confirmed by a 3x3 ANOVA which shows the impact of fire severity is different across the slope types, $F(4, 420725) = 156.60$, $p < .001$. Additionally, there was a main effect of slope, whereby trees on lower slopes have higher mean

p95 values ($M = 36.81\text{m}$) than middle ($M = 32.80\text{m}$) and upper slopes ($M = 28.94\text{m}$), $F(2, 420725) = 7740.90$, $p < .001$, regardless of fire severity. There was also a main effect of fire such that areas which remain unburnt ($M = 33.14\text{m}$) have a marginally higher mean p95 height than those in the low fire severity category ($M = 32.26\text{m}$), which are both higher again than the areas affected by extreme fire damage ($M = 24.31\text{m}$), $F(2, 420725) = 4578.8$, $p < .001$.

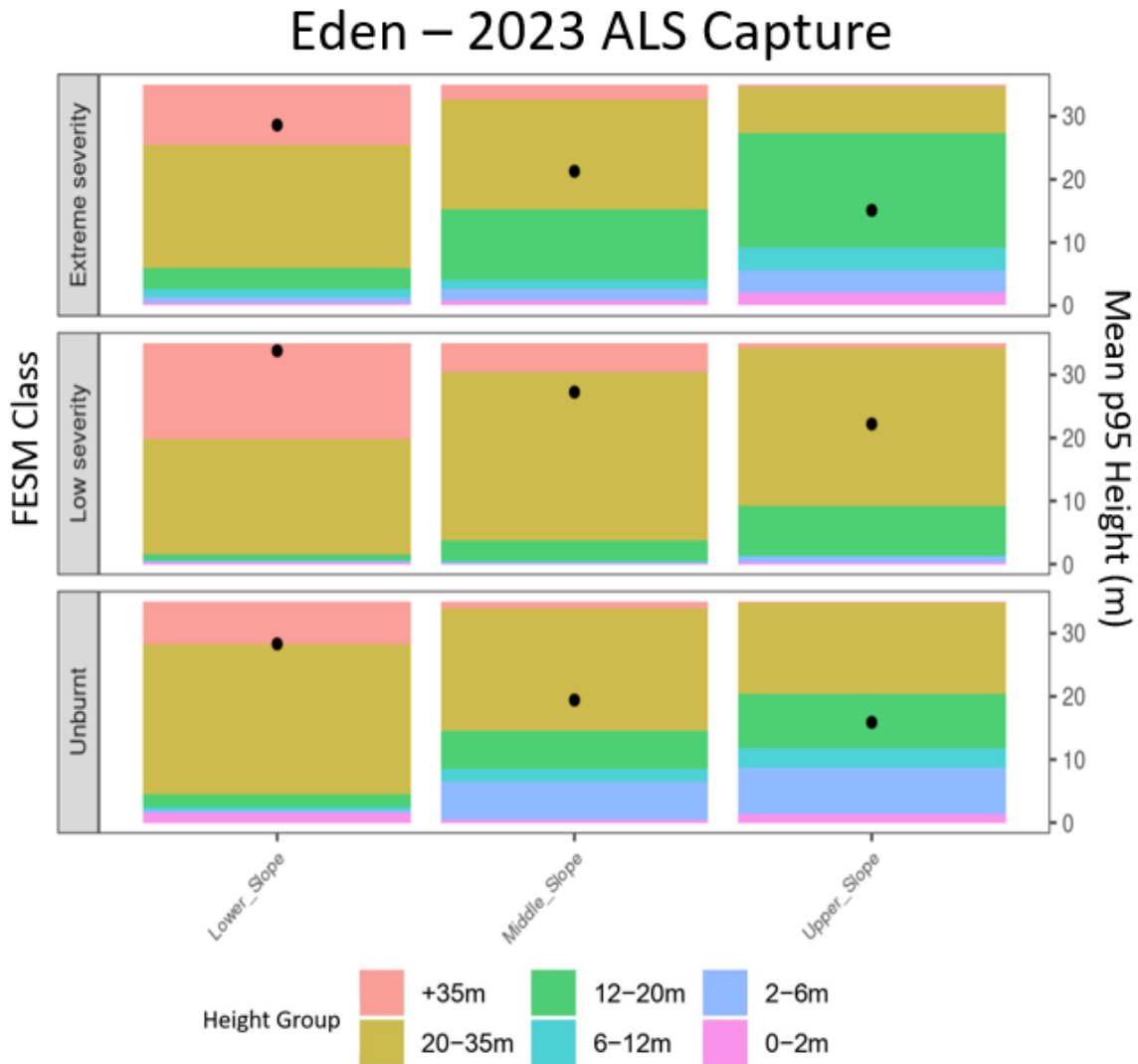


Figure 16 - Stacked bar plots showing the proportion of p95 heights (m) in Eden for three types of slope (Lower, Middle and Upper; x-axis) and FESM classes (Unburnt, Low Severity and Extreme Severity; y-axis). The black dots show the mean p95 heights for each harvested group.

Main results and discussion

While the Wauchope findings in Figure 15 are interesting, it is important to note that only 3% of Wauchope was affected by fire at the time of the FESM categorisation. Eden provides an interesting contrast as significantly more of the forest in this region (approx. 82% - see Figure 3) was affected by fire in the years preceding the 2023 ALS capture. Figure 16 shows that slope type and fire severity have a

similar impact in Eden to those demonstrated in Wauchope, whereby increases in both fire severity and slope result in lower p95 values. While the differential impact appears less noticeable in Eden (Figure 16) when compared with Wauchope (Figure 15), a 3x3 ANOVA shows the interaction between slope type and fire severity is still statistically significant, meaning the differential impact of fire across slope types is reliably observed through LiDAR data, $F(4, 247456) = 30.29, p < .001$. It should be noted, however, that the large number of data points used to run this analysis increases the likelihood of finding a statistically significant difference, even when the effect is small, and results should be interpreted with caution. With that in mind, the visual pattern shown in Figure 16 indicate that, though statistically significant, the differential impact of fire across the slope types is minimal, especially when compared to the patterns evident in Wauchope.

Key Takeaways

Looking at the proportion of trees in different height categories gives a deeper insight into forest structure than mean p95 return heights alone.

The analysis underscores the stability of tree height proportions across protected areas in Wauchope over an 11-year span, suggesting a consistent composition of forest ecosystems. Notably, harvested areas exhibit similar proportions of mean p95 tree heights compared to some protected areas within state forest, highlighting potential similarities in canopy structure between areas managed for timber production and areas managed for conservation.

The larger proportion of taller trees in regions which have been recently affected by fire and the differential impact of fire severity on forest structure across different slope types can be reliably obtained with LiDAR data.

2.1.6 Modelling of canopy top height recovery post-harvest across landform classes, harvesting practices and FESM classes

Introduction

Modelling canopy top height recovery using p95 to predict its values over specified years of growth can help us further understand forest dynamics. Moreover, integrating slope types, harvesting practices and FESM classes into the model enables a comprehensive understanding of the recovery rate across varying terrain and harvesting methodologies. This analysis can provide insight into how to optimise both harvesting and recovery.

Method

Data from the most recent ALS conducted 2023 was used for the following analysis. The data was then filtered to trees that were available for harvest. 'HarvestDetails' were grouped into light and heavy silviculture. Low frequency 'EndYears' were removed and the mean for p95 was calculated for the remaining years. To model canopy top height recovery after harvesting, the year when trees were harvested was converted to years of growth. This allows us to predict canopy top height, given how long

trees have had to grow. A multiple regression model was applied to a logistic-approach-to-asymptote transform of mean p95 (Luo, Zhang, Zhou, Chen, & Tian, 2018) for all combinations of slope type, harvest groups and FESM classes for each ALS capture. The model was used to predict values of transformed mean p95 for given years of growth. Reversing the transform yields mean p95, where the mean p95 predictions have an asymptotic value equal to the 99.9th percentile of p95.

Main results and discussion

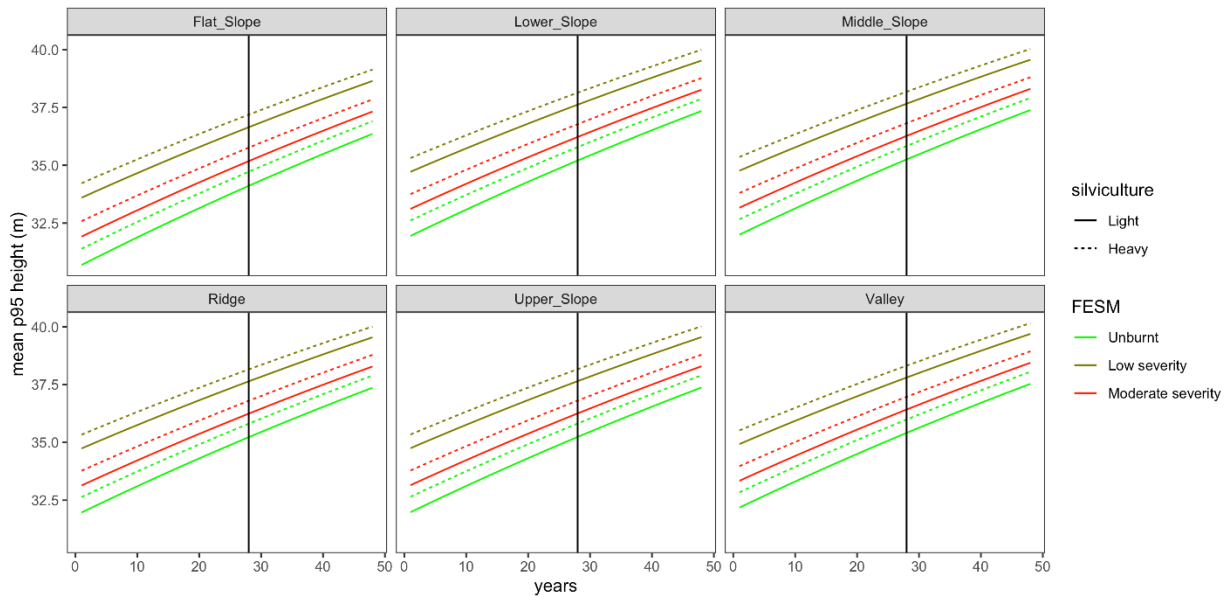


Figure 17 - This figure compares canopy top height (as measured by mean p95 height) recovery predictions for Coffs Harbour across different slope and FESM class for each harvest group. Preceding the vertical line are the model’s account of observed data and following is the model’s prediction of p95 height for given years of growth. Note that predictions appear linear because p95 does not converge on the asymptotic value equal to the 99.9th percentile of p95 height. See Appendix Figures A12-A16 for recovery predictions across other capture areas.

Table 4. Model Coefficients

	Coefficient	<i>p</i> -value
Intercept	30.55	<.001
Years	0.291	<.001
Heavy silviculture	1.509	<.001
Valley	3.214	<.001
Lower slope	2.707	<.001
Middle slope	2.824	<.001
Upper slope	2.781	<.001
Ridge	2.755	<.001
Low severity	6.266	<.001
Moderate severity	2.643	.12

A multiple regression was applied to data and the model was used to predict transformed p95. 'Light silviculture', 'flat slope' and 'unburnt' was used as reference levels for slope types and FESM classes and harvest group, respectively. Figure 17 shows the models prediction for mean p95 height recovery which incorporates slope types, FESM classes and harvest group to provide a description of the rate of recovery across these different factors. Table 4 details the model coefficients and shows that valley, lower, middle, upper and ridge slope types are associated with a significant increase in mean p95 height with reference to flat slopes. It also shows that the low severity FESM class is associated with a significant increase in mean p95 height with reference to the unburnt FESM class. Table 4 shows that the heavy silviculture grouping is correlated with an increase in p95 height compared to the light silviculture grouping. It is worth noting, however, that beyond this regression analysis there is strong evidence of selection factors for silvicultural practice (e.g., heavy vs. light comparisons in Figure 5, Section 2.1.2) whereby particular silvicultural practices are selected *because* of properties about the tree, e.g., taller, more diverse forests are selected for heavy silvicultural practices, but not smaller forests.

LiDAR data and analyses provide a rich source of data, of which the current analyses looks at a select cross section. Together, LiDAR provide an additional dataset that can inform existing growth models used by FCNSW based on long-term inventory plots.

Key Takeaways

Modelling canopy top height recovery and incorporating slope types, harvesting practices and FESM classes can provide a description of the rate of recovery across these different factors. This analysis can provide insight into how to optimise both harvesting and recovery, and provides an added source of data to inform existing growth models.

2.2 Canopy coverage analysis

Introduction

Mean canopy coverage serves as a fundamental metric in the assessment of forest ecosystems, offering valuable insights into forest health, habitat suitability, and informing future forestry management and conservation practices. This metric provides a quantitative measure of the extent and density of vegetation canopy within a given area, thus serving as a proxy for overall vegetation abundance and distribution. Canopy coverage, typically expressed as a percentage, represents the fraction of the ground area obscured by the vertical projection of vegetation. By quantifying canopy coverage, researchers and land managers can assess the state of forest ecosystems, monitor changes over time, and make informed decisions regarding conservation efforts and sustainable forest management practices.

Methods

Mean Canopy Coverage was computed for each pixel (30m x 30m) as a percentage, by calculating the number of first returns over 2m divided by all first returns. The output refers to the extent and density of vegetation canopy within the studied area. As Canopy Coverage is usually represented as a percentage – it represents the fraction of the ground area that is obscured by the vertical projection of vegetation. Higher values of mean canopy coverage denote greater vegetation density, indicating lush, densely forested areas with abundant canopy cover. Conversely, lower mean canopy coverage values signify sparser vegetation cover, suggesting either areas with less dense vegetation or more open landscapes.

2.2.1 Canopy coverage recovery following harvesting activities

Introduction

Canopy coverage, representing the proportion of ground obscured by vegetation canopy, serves as a vital indicator of forest health, habitat suitability, and ecosystem productivity. Monitoring changes in canopy coverage following harvesting activities provides valuable insights into vegetation recovery, ecosystem resilience, and the effectiveness of management interventions.

Methods

LiDAR data was filtered to regions within Wauchope that were last harvested in years 2010, 2015, and 2020. For each harvest year, mean canopy coverage (%) and standard errors for the same geographical regions are calculated based on ALS capture conducted in 2012, 2016, and 2023. Canopy coverage is calculated as the percentage of returns above 2m and designates the proportion of the ground that is obscured by the canopy foliage. Note that, although regions can be harvested more than once, the most recent harvest year is shown across the panels. For a description of the metric (canopy cover) and its limitations, see Table 3.

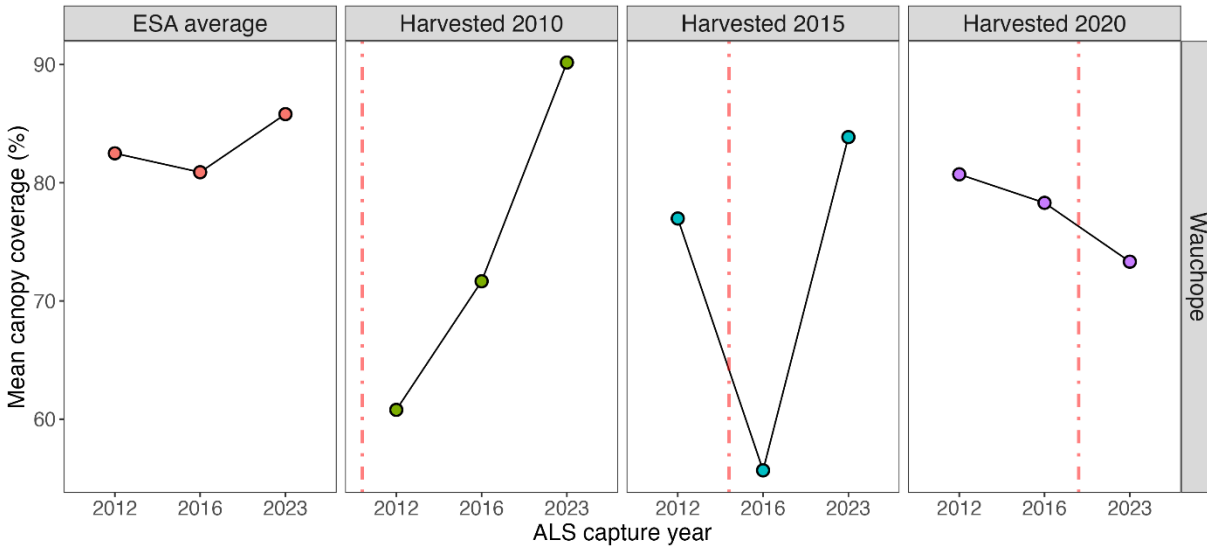


Figure 18 – Mean canopy coverage for areas in Wauchope harvested in 2010, 2015 & 2020 with points indicating separate ALS captures. Vertical red dashed line is a visual guide of the approximate timepoint of silvicultural disturbance, noting the change in this timepoint across regions. Points represent mean values, noting that the large number of datapoints result in precise estimation of the mean with negligible standard errors. See Appendix Figure A5 for mean canopy coverage across all regions.

Main results and discussion

Canopy coverage, as measured by the proportion of ground returns, shows foliage recovery after harvest. Across panels, harvest events are signified in the timepoints on the dash-dotted red line. Canopy-coverage-recovery is clearest in the third-from-left panel for regions harvested in 2015 where ALS captures were taken prior to and after the harvesting events. For these regions, mean canopy coverage measured in 2016 were 55.7% ($se = 0.16\%$) as compared to 77.0% ($se = 0.11\%$) measured in 2012. By 2023, the mean canopy coverage for the same regions had recovered beyond pre-harvest coverage to 83.9% ($se = 0.11$).

Regrowth canopy foliage also occurs following harvesting in the 2010-harvested regions but notably *not* in the 2020-harvested regions. It is unclear why mean canopy coverage decreases between the 2016 and 2023 captures; however, the following analysis of harvesting practice indicates this decline is not present for all regions. However, it is worth noting the number of recovery years between harvest and LiDAR captures was only 3 years for the 2020-harvested regions and seven years for 2015-harvested regions.

Key Takeaways

Canopy coverage recovers following harvesting practices.

2.2.2 Canopy coverage recovery in harvested regions: comparing light and heavy harvesting practices

Introduction

Within the realm of forestry management, understanding the impact of harvesting practices on canopy coverage is crucial for assessing forest regeneration and long-term sustainability. Different areas are subject to different harvesting practices. The differentiation between harvesting practices lies in their intensity and extent of tree removal, with "light" practices typically involving selective thinning and minimal disturbance to the forest canopy, while "heavy" practices encompass removal of a high proportion of non-habitat trees, which may result in more substantial alteration of canopy structure.

Method

LiDAR data filtered to regions within Wauchope that were last harvested in years 2010, 2015, and 2020. For each harvest year, mean canopy coverage (%) and standard errors for the same geographical regions are calculated based on ALS capture conducted in 2012, 2016, and 2023. Canopy cover was calculated using the first returns from the normalized point clouds from ALS data, using a grid size of 30 x 30 m. Note that, although regions can be harvested more than once, the most recent harvest year is shown across the panels. For a description of the metric (canopy cover) and its limitations, see Table 3.

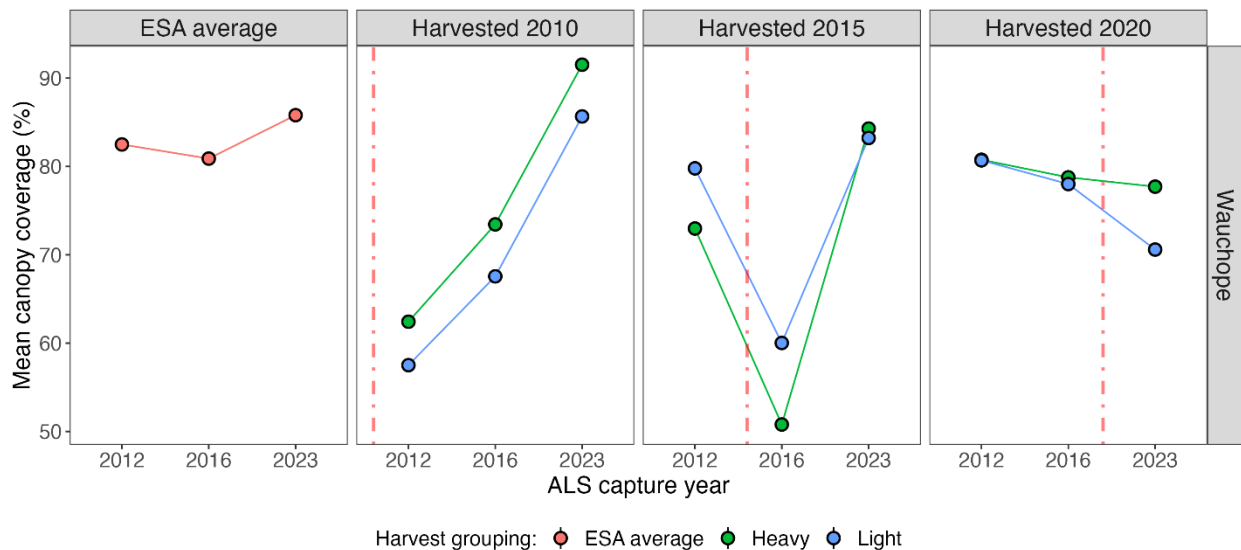


Figure 19 - Mean canopy coverage for areas in Wauchope harvested in 2010, 2015 and 2020 with points indicating separate ALS captures (x-axis) and coloured lines indicating type of silvicultural practice (heavy vs. light practices). Vertical red dashed line is a visual guide of the approximate timepoint of silvicultural disturbance, noting the change in this timepoint across regions. For clarity, we present only "light" (blue) and "heavy" (green) silvicultural practices in this figure, noting that other silvicultural practices, such as

mixed practices e.g., alternate coupe, are present in the data. For analyses of other capture locations areas see Appendix Figure A2.

Main results and discussion

Regrowth in foliage as measured by canopy coverage for harvesting practices classified as “heavy” (red points) and “light” (blue points). Broadly, canopy coverage exhibits similar regrowth patterns across heavy and light silvicultural practices. As in Figure 18, the notable exception to canopy cover recovery is for regions that were harvested in 2020 (right-most panel) where ‘light’ harvesting practices resulted in more reduction in canopy coverage. For 2020, light harvesting practices mostly consisted of STS-medium silvicultural practice (90%) and to a lesser extent, STS-light (10%). Heavy harvesting practices included STS-heavy (84%) and STS regen (16%).

Key Takeaways

In general, areas subjected to light and heavy harvesting practices show similar recovery trends as measured by canopy coverage.

2.2.3 Canopy coverage across fire-impacted regions

Introduction

To examine the impact of fires on canopy coverage, we switched our focus onto Eden where the 2023 ALS capture provides an analysis of canopy coverage after the 2019/2020 bushfires. For reference, Figure 9 provides a map of the Eden capture locations. Compared to Wauchope, Eden was heavily impacted by fires where FESM ratings show a larger proportion of extreme-high severity areas (see Figure 10).

Method

For the following analysis, LiDAR data was filtered to areas within Eden. We analysed all regions in Eden and calculated mean canopy coverage (%) and standard errors based on the single and only ALS capture conducted in 2023. Separate means are calculated for each slope class (e.g., Valley or Ridge), each FESM class (Extreme-high, Moderate, Unburnt-Low) and whether the region was in the base net area (BNA) or an environmentally significant area (ESA).

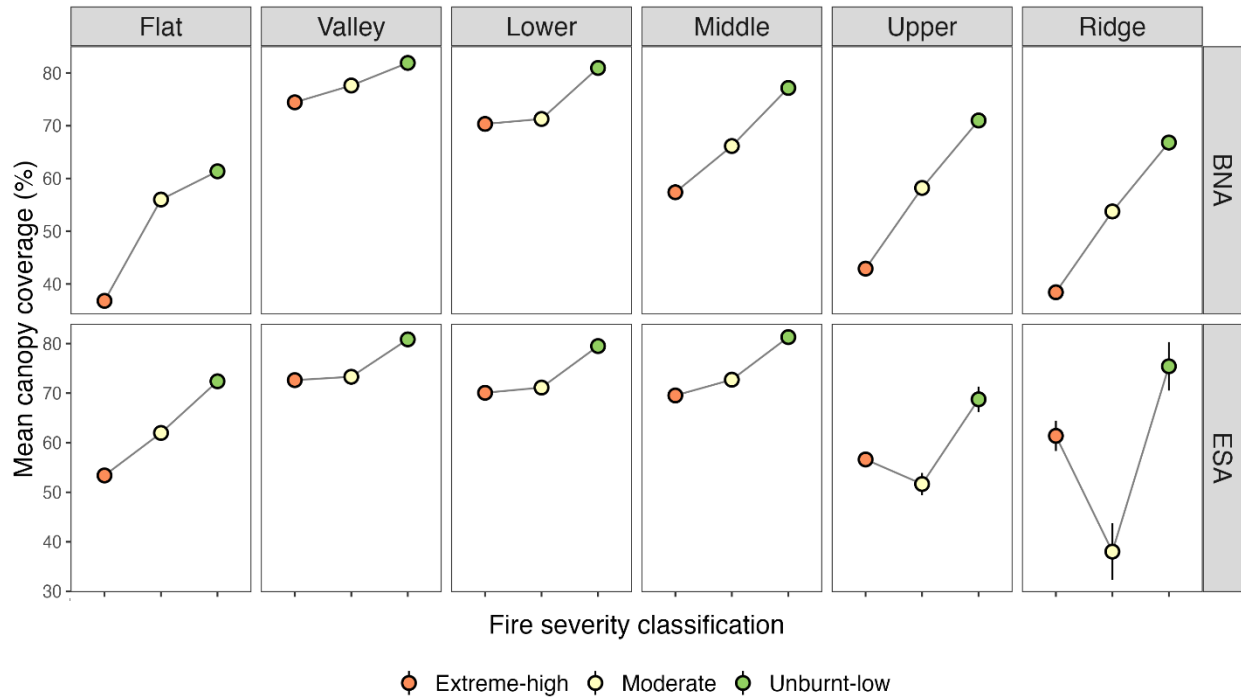


Figure 20 - Mean canopy cover of the Eden capture as a function of fire extent and severity mapping (FESM) ratings (x-axis) and landform class (slope – horizontal panels). ESA and BNA regions are shown separately (vertical panels) and colours correspond to x-axis FESM ratings. Points represent mean values and error bars represent standard error, noting that the large number of datapoints result in precise estimation of the mean with generally small standard error values. For all other regions in the dataset, we recreate these figures for each region separately in Appendix Figures A23 – A28.

Main results and discussion

Differences in mean canopy coverage can be observed across landform (horizontal panels) and fire severity ratings (colours and x-axis). In Figure 20, we primarily focus on fire severity where higher FESM ratings (orange-coloured points) were associated with lower mean canopy coverage proportions as compared to less fire-affected FESM ratings (green-coloured points). Moderate points (vanilla-coloured points) were generally in-between higher and lower FESM classes with notable exceptions in ESA with landform classes of upper (bottom-row, second-from-right panel) and ridge (bottom-row, right-most panel). In general, disturbance due to bushfires can be observed combining satellite-image based FESM ratings and LiDAR metrics.

Key Takeaways

Reductions in canopy cover due to natural disturbances can be reliably observed via LIDAR.

2.3 Canopy foliage density analysis

Introduction

Canopy foliage density serves as a fundamental indicator of forest structure, providing insights into biomass distribution, habitat suitability, and ecosystem functioning. By accurately quantifying canopy foliage density, researchers can better understand the vertical arrangement of vegetation within forested landscapes, which is essential for assessing habitat quality, species diversity, and carbon storage capacity. Additionally, canopy foliage density metrics derived from LiDAR data enable precise monitoring of changes in forest structure over time, facilitating informed forest management decisions, conservation planning, and mitigation strategies for environmental challenges such as natural disasters and habitat fragmentation.

Methods

Calculation of Canopy Foliage Density: Canopy foliage density was derived from LiDAR data by calculating the difference between the 95th percentile (p95) and 50th percentile (p50) tree-height metrics. Intuitively, this provides a measure of the “thickness” of the canopy, because the 95th percentile is close to the top of the canopy and the 50th percentile (median return) is close to the bottom of the canopy.

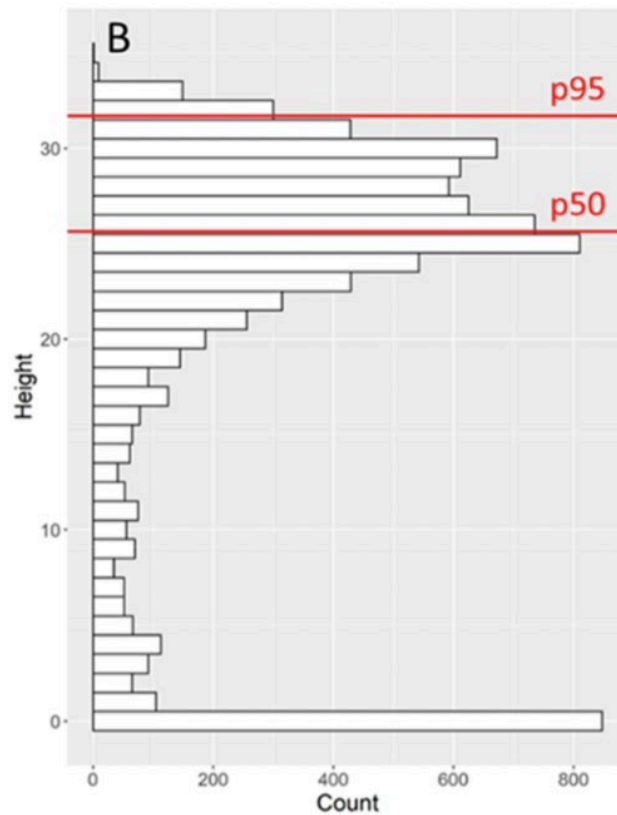


Figure 21 - Plot showing distribution of height values, with the 50th and 95th percentiles shown in red.

2.3.1. Assessing change of canopy foliage density dynamics post-harvest using combined metrics: p95, p50, and canopy coverages

Introduction

ALS is a powerful tool for understanding forestry dynamics and many metrics can be derived that characterise forest structure. In isolation, each metric is suited to understanding a different structural feature of the forest. For example, top height canopy is better understood with p95 returns whereas canopy foliage regrowth is better measured by canopy coverage. Beyond these individual metrics, however, stakeholders are often interested in commonalities across ALS measurements to understand the overarching trends across the forest.

To do so, we combine three common metrics - top canopy (p95), understory regrowth (p50), and canopy occupancy (canopy coverage %) - into a single analysis to provide a more comprehensive view of forest dynamics. This analysis was inspired by voxel-based analyses with three-dimensional data, described further in Appendix Table B4. We call this novel composite visualisation “canopy foliage density” to understand better the vertical depth (i.e., distance between p50 and p95) of canopy foliage. Together with more established indices, the main benefit of the following analyses is that it provides an overarching visualisation for characterising forest dynamics over time.

Methods

Three metrics, p95, p50, and canopy coverages, combined to illustrate canopy foliage density. Panels in Figure 22 show separate spatial locations within Wauchope that were last harvested in 2010, 2015, or 2020. Separate LiDAR captures shown on the x-axis as a rectangle. Canopy height metrics are displayed as a rectangle where the mean p95 return height (m) is shown by the upper edge of the rectangle, and mean p50 return height (m) is shown by the lower edge of the rectangle. Canopy coverage, as the proportion of area covered by the canopy, is displayed as a decimal within the rectangle. The harvesting timepoint is depicted with a red dotted line. Note that the harvesting timepoint changes across panels as each location was harvested in a different year. Harvesting timepoint and mean p95 height (m) are commensurate with Figure 3, and canopy coverage is commensurate with Figure 11. For a description of the three metrics (p95, p50, & canopy cover) and their limitations, see Table 3.

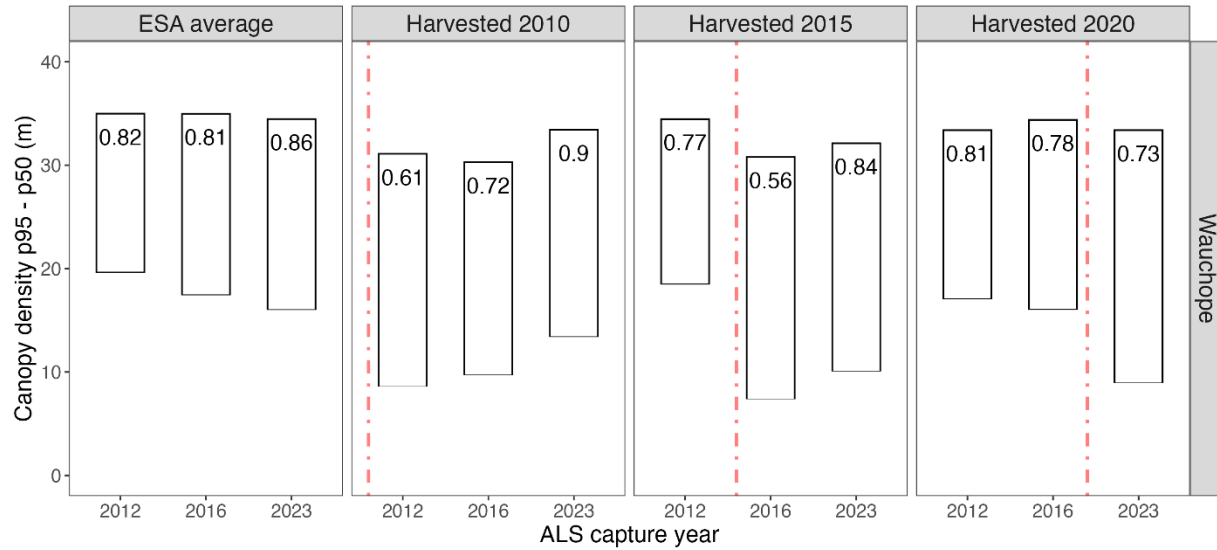


Figure 22 – Combined metrics of canopy foliage density using mean p95 heights, mean p50 heights and canopy cover. See Appendix Figure A4 for all other regions.

Main results and discussion

Figure 22 aims to combine key metrics of canopy growth. Mean p95 heights (upper edge of rectangles), p50 heights (lower edge of rectangles), and canopy coverage (decimals in rectangles) are three key datapoints to understanding canopy foliage density and recovery following harvesting events.

As an example, consider the second-from-right panel for locations harvested in 2015. Canopy foliage density is measured as the space between mean p95 height and mean p50 height shown visually by the height of the rectangle. Longer height indicates less concentrated canopy foliage density where shorter heights indicate more concentrated canopy foliage densities.

These 2015-harvest regions show declines in canopy coverage (decimals in left-2012-rectangle and central-2016-rectangles, 0.77 vs. 0.56), and top canopy p95 height (upper edge of rectangles, 34.5m vs. 30.9m) following harvesting. Canopy foliage density is also less concentrated where p50 depth is lower (lower edge of rectangles, 18.5m vs. 7.37m). Despite these changes, the 2023 ALS capture (right-most rectangle) shows recovery of canopy coverage and canopy foliage density. 2023-heights of the lower canopy depth (p50) and upper canopy height (p95) increase proportionally to 2016, shown by shifted-same height bars. Canopy coverage also increased by 2023 from 0.56 measured in 2016 to 0.84 in 2023.

Key Takeaways

Canopy foliage density can be a useful means to visualise canopy characteristics using three separate, but related, LiDAR metrics: top of canopy (p95), bottom of canopy (p50) and canopy cover.

2.4 Skew analysis

Introduction

Interpreting LiDAR-derived metrics in the context of on-ground canopy structure and management practices is essential for gaining meaningful insights into forest dynamics and informing effective management strategies. The relationship between LiDAR metrics and canopy characteristics can vary depending on location-specific factors and forest types (Haywood and Stone, 2010). For instance, positive skewness values may indicate sparse canopies, while negative values may suggest denser canopy cover. Such interpretations underscore the importance of understanding the nuances of LiDAR-derived metrics within specific ecological contexts.

Methods

To examine forest structure and density, mean skew was calculated. A forest area exhibiting a negative skew indicates most of the occupied volume towards the top, whereas a positive skew suggests more volume towards the bottom (see Figure 23). It is important to note that a higher skew does not necessarily indicate taller trees, but rather a larger concentration of volume in one tail of the distribution (see Figure 23).

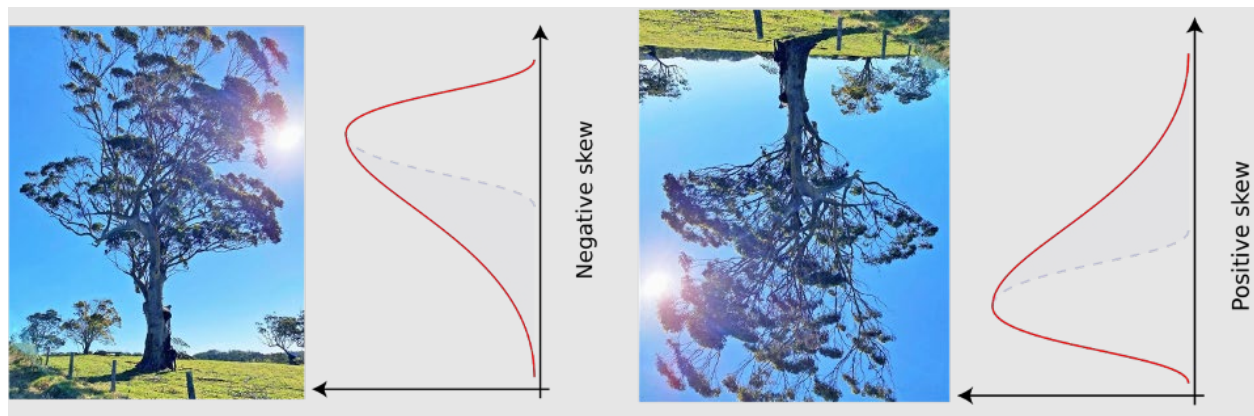


Figure 23 - Example of positive and negative skew values. Negative skew includes most of the occupied volume being concentrated towards the top, indicating taller trees or denser canopy cover at higher positions within the point cloud. As seen on the right, forest areas with positive skew indicate occupied volume concentration towards the bottom suggesting shorter trees or denser vegetation closer to the ground.

To enhance interpretability of the graphs, the axes of the skew plots of this report have been inverted, such that higher points on the plots represent denser areas.

2.4.1 Analysing longitudinal trends in vegetation density using skewness: impacts of harvesting and topographical landform

Introduction

The assessment of vegetation density, indicated by skewness values derived from LiDAR data, holds significance in understanding ecosystem dynamics across diverse landscapes. Skewness serves as a useful metric for assessing canopy structure and density and may provide information that is helpful in better understanding the distribution of biomass in the forest's vertical profile. By examining longitudinal trends in skewness across different landforms and regions we can gain a deeper understanding of forest ecosystems' resilience and inform adaptive management practices tailored to diverse landscapes.

Methods

This analysis examines pixel mean skew values as a measure of vegetation density within forested regions. Data encompassing areas last harvested in 2010, 2015, and those not yet harvested, but where harvesting is permissible ("unharvested BNA"), were included for comprehensive analysis. To aid in the interpretation of the graphs, an INVERSION OF AXES has been implemented, ensuring that denser areas which are higher from the ground are visually represented as higher points on the plots. For a description of the metric (skewness) and its limitations, see Table 3.

Main results and discussion

The following figures depict longitudinal trends in vegetation density derived from skewness measurements, highlighting variations across topographical landforms and harvested areas.

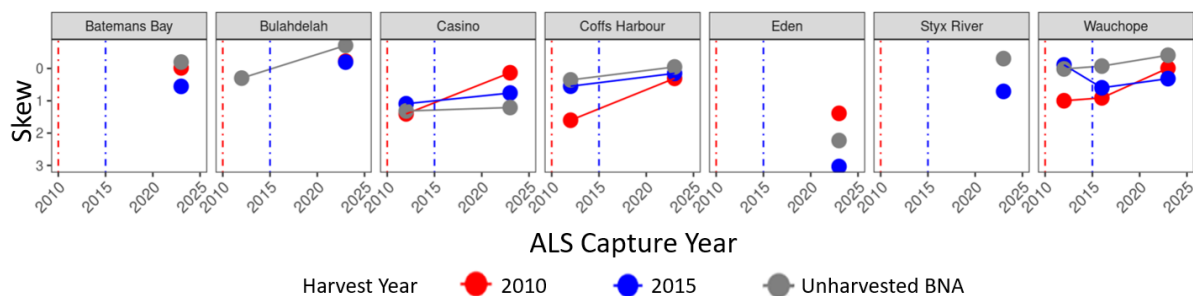


Figure 24 - Skew (y-axis) of distinct forest regions, categorized by harvesting years (2010, 2015) and unharvested areas, measured at different time points (represented on the x-axis). Forest regions are presented as separate horizontal lines, with dashed vertical lines marking harvest events in 2010 (red) and 2015 (blue). Negative skew values, representing greater density of canopy vegetation further from the ground, are visually higher on the plot, while positive skew values, indicating higher density at lower heights, appear lower. See Appendix Figure A11 for all other regions.

There is a general trend showing vegetation thickness moves further from the ground over time. In Casino and Coffs Harbour, all forest analysed (those harvested in 2010, 2015 and unharvested) show shifts in skew between the 2012 and 2023 ALS captures whereby the mass of the canopy rises, even when those regions have been harvested. In both these regions, and in Wauchope, the areas harvested in 2010 (two years prior to the first ALS capture; shown in red) show the largest decrease in skew. This may be the result of rapid regeneration in the decade following the harvest in these areas.

The 2016 ALS capture in Wauchope provides additional information about the short-term effects of harvesting on skew, beyond what can be inferred from other locations with less ALS capture data. The change in skew for the areas in Wauchope harvested one year before the 2016 capture (2015 harvested regions shown in blue) suggests there are changes in forest structure immediately following a harvest event, but this is recovered quickly. Given the 2010 harvested areas (shown in red) in Casino have regained comparable skew to those not harvested by the time of the 2012 capture, recovery from harvest may occur within as little as two years in some regions but the data from Coffs Harbour and Wauchope indicate it is likely to take a little longer in others. (approximately 10 years).

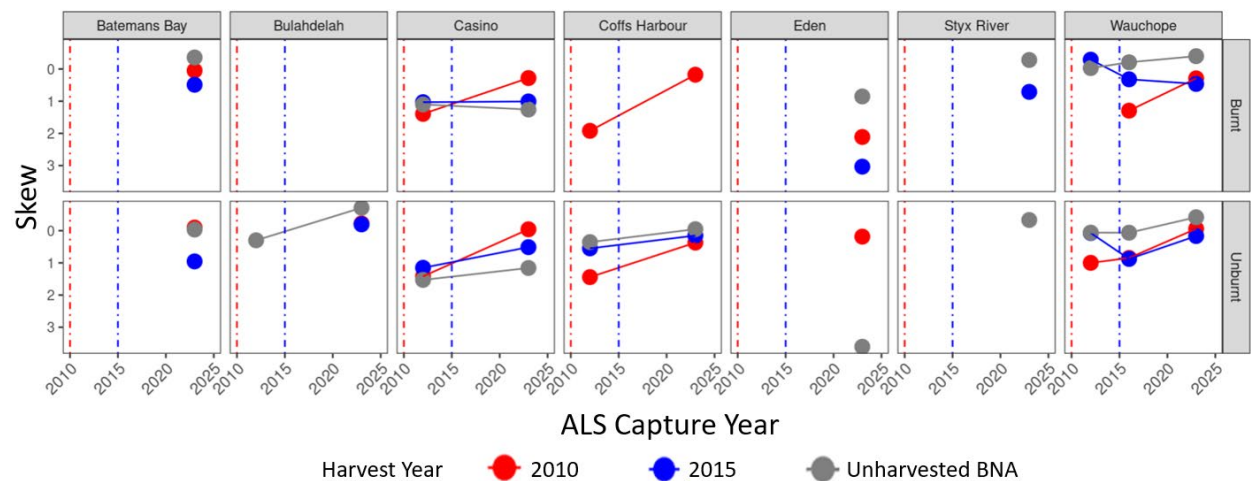


Figure 25 - Skew (y-axis) of distinct forest regions, categorized by harvesting years (2010, 2015) and unharvested areas, measured at different time points (represented on the x-axis), split by fire history status. The 'Burnt' areas aggregate over different fire severity classes.

It is important to note that other disturbance events, beyond harvesting, occur which may have a significant impact on the forest's structure. To demonstrate the influence of fire, Figure 25 splits the data shown in Figure 24 into burnt and unburnt regions. This figure shows a general reduction in the rate of skew recovery between the 2012 and 2023 captures. While the general trends are the same, where skew decreases indicating the canopy vegetation grows further from the ground over time, the rate at which this occurs is somewhat slower for the burnt (top row) regions when compared to those which have not been affected by fire (bottom row).

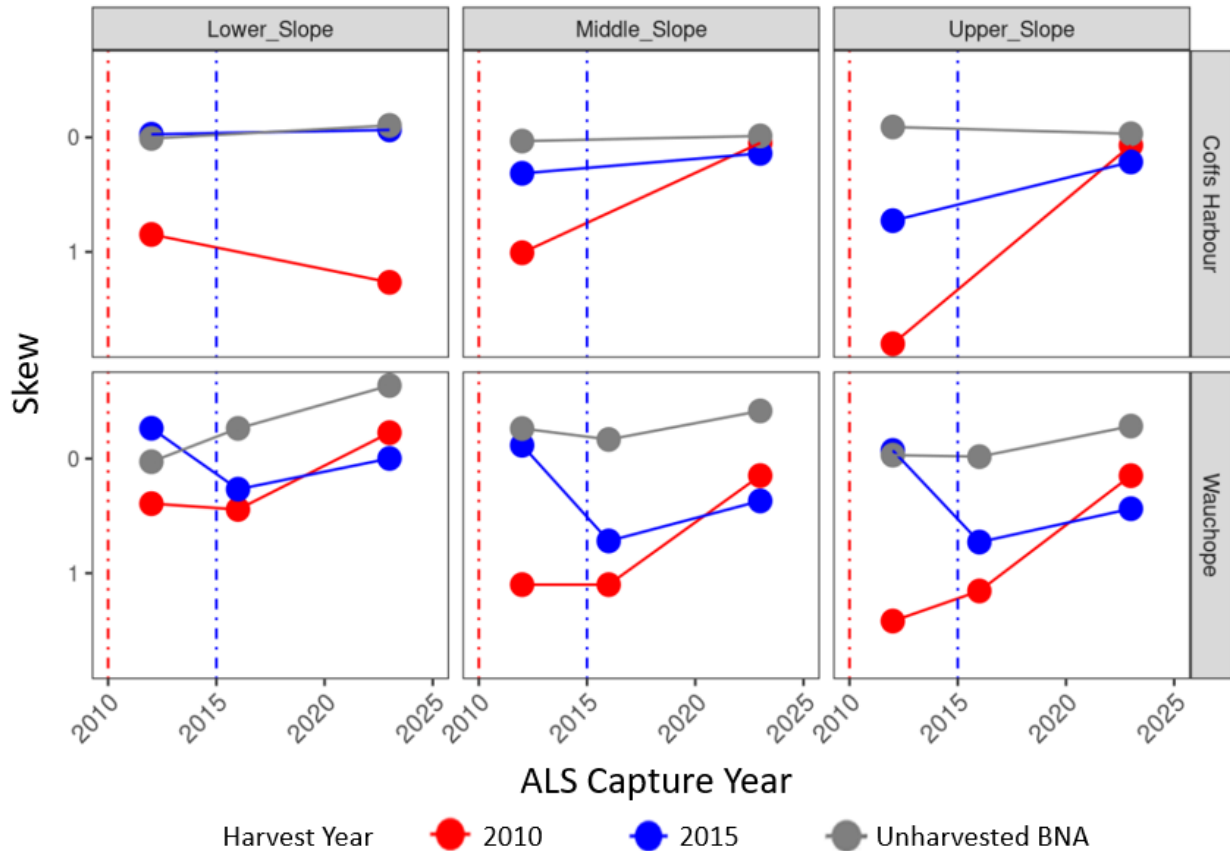


Figure 26 - Skew (y-axis) for each of the ALS captures (x-axis) for areas harvested in 2010 (red), 2015 (blue) and never harvested (grey) over selected slope types within Coffs Harbour and Wauchope. The dashed horizontal lines represent the 2012 and 2015 harvesting events, respectively. The different plots contrast the effects of the three most common slope types in Wauchope (Lower, Middle, and Upper).

To examine the impact of slope on skew over time, we focus on Lower, Middle, and Upper slope types in Wauchope and Coffs Harbour, representing areas harvested at different time points. Appendix Figure A11 contains a comprehensive depiction of all slope types and locations. Figure 26 demonstrates the influence of slope on skew trends over time in these regions. Despite similar overall trends—skew shifting away from the ground over time—different slope types exhibit varying rates of change. Notably, the 2015 harvest event (blue) results in a significant dip in skew for the 2016 capture in Wauchope, with skew showing a trend toward recovery in 2023. In contrast, skew trends for the regions harvested in 2015 in Coffs Harbour remain more stable between the 2012 and 2023 captures, likely because the forest has largely recovered in the 8 years between the harvest event and the 2023 ALS capture. These findings underscore the importance of additional ALS capture data in enhancing our understanding of the impact of silvicultural practices over time.

Figure 26 also shows the impact of slope on skew recovery following harvest. In general, the red points reflecting the areas harvested in 2010 show a steeper trend toward skew which matches those of unharvested BNA regions as slope increases. Across Coffs Harbour and Wauchope, the skew trends over time are steepest in the upper slope regions and more gradual in the lower slope areas.

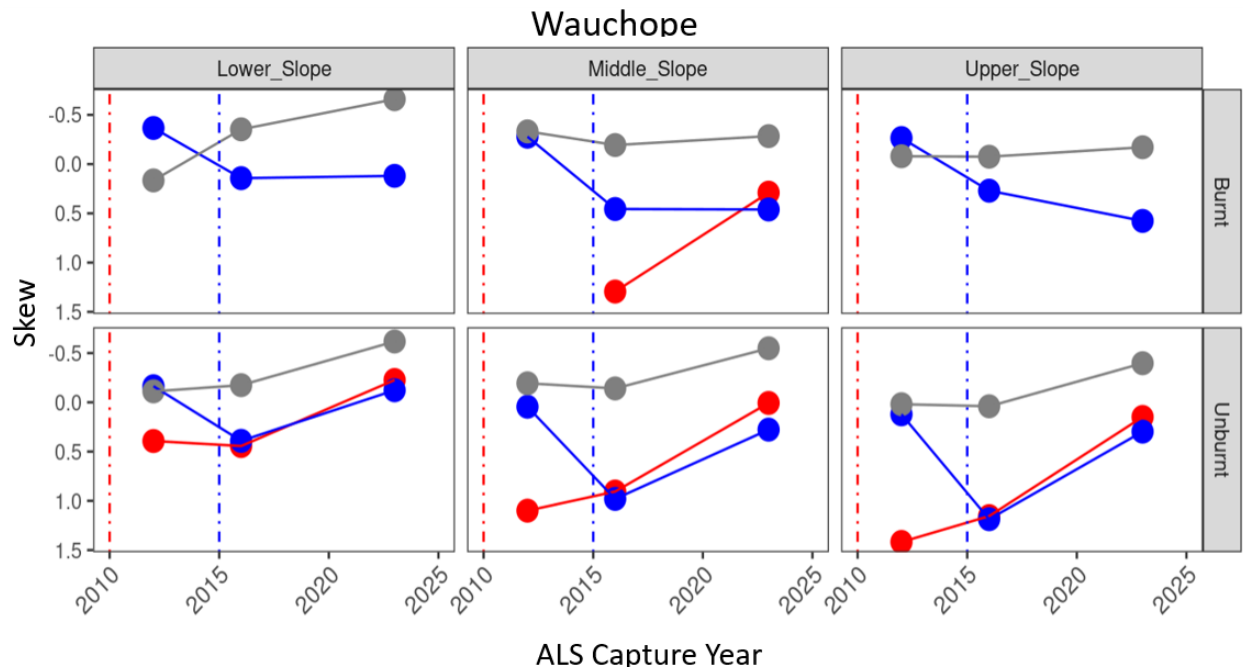


Figure 27 - Skew (y-axis) for each of the ALS captures (x-axis) for areas within Wauchope harvested in 2010 (red), 2015 (blue) and never harvested (grey) over selected slope types and fire history status.

To explore potential interactions between slope type and fire severity (which were evident in Section 2.1.4), Figure 27 shows different slope type regions in Wauchope which have been affected by fire or remain unburnt. Wauchope was chosen for this analysis because the additional temporal data in this region (2016 ALS capture) allows for a more nuanced comparison between burnt and unburnt areas. This figure shows a clear difference between the rate of skew recovery in the burnt and unburnt areas, whereby unburnt regions regain skew which is comparable to that pre-harvest within about 8 years post-harvest, but those regions affected by fire are unable to do so. These patterns appear consistent across the different slope types. It is worth noting that, while the skew of the unharvested BNAs is unchanged over time in the burnt regions, the canopy vegetation continues to trend away from the ground in regions which are not affected by fire. This means that the fire has had an impact on the forest structure of both harvested and unharvested areas.

Key Takeaways

Harvesting events in 2010 and 2015 are clearly reflected in the skewness data, with notable dips observed in skew following these events, particularly in Wauchope. However, skew returns to pre-harvest levels within a short period of time, indicating the resilience of forest ecosystems to silvicultural practices.

A more nuanced understanding of forest structure over time can be obtained with more regular ALS capture data.

3. Recommendations

1. Publicly Accessible and richly interactive data. Future reports could incorporate interactive maps to present spatial data effectively. Interactive maps offer dynamic platforms that enable users to explore geographic regions and spatial datasets in an intuitive and engaging manner. By integrating interactive mapping technologies such as web-based mapping applications, stakeholders and the public can be provided with valuable opportunities to interact with forest-related data in meaningful ways. In addition to interactive maps, ensuring the underlying data is publicly accessible and interactive, enhances the transparency and accessibility of forest-related information. By providing the raw data along with interactive visualisation tools, stakeholders and the public can gain a deeper understanding of forestry dynamics, encouraging a more engaged community. This approach not only promotes transparency in research but can also empower individual users to conduct their own analyses, contributing to collaborative efforts in forest management and conservation.

2. Long-Term Monitoring. Longitudinal studies with continuous ALS captures, over extended periods of time could be utilised to track forest dynamics and regeneration patterns more comprehensively. Long-term monitoring can provide valuable insights into the long-term effects of harvesting practices, natural disasters, and changes in climate on forest ecosystems.

3. Upcoming Technologies. For future research, it is advisable to remain aware of emerging technologies, such as 'Geiger-mode LiDAR'. Geiger-mode LiDAR can acquire data at higher altitudes and presents an opportunity to significantly increase coverage extent while maintaining, or even enhancing spatial resolution. Incorporating Geiger-mode LiDAR technology in future studies may enable more comprehensive and efficient forest assessments.

4. Conclusions

In conclusion, the comprehensive analysis presented in this report provides insights into the dynamics of forest structure, composition, and regeneration following harvesting events in NSW State Forests. By integrating ALS technology with field data and employing various analytical methods, including canopy height, canopy coverage, canopy foliage density, and skew analysis, this research offers a multifaceted understanding of forest ecosystems. The examination of mean p95 heights across different slope classes and harvested regions reveals nuanced patterns of forest regeneration and growth over time. Additionally, the predictive modelling of canopy top height recovery offers insights into the factors influencing regeneration rates across different landform classes and harvesting practices. Furthermore, the assessment of canopy coverage and density highlights the effectiveness of different harvesting practices and their impact on vegetation recovery. Overall, this report contributes to the ongoing efforts in forest management and conservation by providing a deeper understanding of changes in forest structure over time and potential relationships to disturbance events in NSW State Forests.

References

References for the Main Report and Appendix B

- Aalto, I., Aalto, J., Hancock, S., Valkonen, S., & Maeda, E. E. (2023). Quantifying the impact of management on the three-dimensional structure of boreal forests. *Forest Ecology and Management*, 535, 120885-. <https://doi.org/10.1016/j.foreco.2023.120885>
- Adhikari, A., Montes, C. R., & Peduzzi, A. (2023). A comparison of modeling methods for predicting forest attributes using LiDAR metrics. *Remote Sensing*, 15(5), 1284. <https://doi.org/10.3390/rs15051284>
- Almeida, D. R. A., S. C. Stark, R. Chazdon, B. W. Nelson, R. G. Cesar, P. Meli, E. B. Gorgens, et al. (2019). The effectiveness of lidar remote sensing for monitoring forest cover attributes and landscape restoration. *Forest Ecology and Management* 438: 34–43. <https://doi.org/10.1016/j.foreco.2019.02.002>.
- Almeida, D. R. A. de, Stark, S. C., Shao, G., Schiatti, J., Nelson, B. W., Silva, C. A., Gorgens, E. B., Valbuena, R., Papa, D. de A., & Brancalion, P. H. S. (2019). Optimizing the remote detection of tropical rainforest structure with airborne lidar: Leaf area profile sensitivity to pulse density and spatial sampling. *Remote Sensing (Basel, Switzerland)*, 11(1), 92. <https://doi.org/10.3390/rs11010092>
- Arkin, J., Coops, N. C., Daniels, L. D., & Plowright, A. (2023). Canopy and surface fuel estimations using RPAS and ground-based point clouds. *Forestry (London)*. <https://doi.org/10.1093/forestry/cpad020>
- Atkins, J. W., Bhatt, P., Carrasco, L., Francis, E., Garabedian, J. E., Hakkenberg, C. R., Hardiman, B. S., Jung, J., Koirala, A., LaRue, E. A., Oh, S., Shao, G., Shao, G., Shugart, H. H., Spiers, A., Stovall, A. E. L., Surasinghe, T. D., Tai, X., Zhai, L., ... Krause, K. (2023a). Integrating forest structural diversity measurement into ecological research. *Ecosphere (Washington, D.C)*, 14(9). <https://doi.org/10.1002/ecs2.4633>
- Atkins, J. W., Bohrer, G., Fahey, R. T., Hardiman, B. S., Morin, T. H., Stovall, A. E. L., Zimmerman, N., Gough, C. M., & Goslee, S. (2018). Quantifying vegetation and canopy structural complexity from terrestrial LiDAR data using the forest r package. *Methods in Ecology and Evolution*, 9(10), 2057–2066. <https://doi.org/10.1111/2041-210X.13061>
- Atkins, J. W., J. Costanza, K. M. Dahlin, M. P. Dannenberg, A. J. Elmore, M. C. Fitzpatrick, C. R. Hakkenberg, et al. (2023b). Scale dependency of lidar-derived forest structural diversity.” *Methods in Ecology and Evolution* 14(2): 708–723. <https://doi.org/10.1111/2041-210x.14040>.
- Bartels, S. F., Chen, H. Y. H., Wulder, M. A., & White, J. C. (2016). Trends in post-disturbance recovery rates of Canada’s forests following wildfire and harvest. *Forest Ecology and Management*, 361, 194–207. <https://doi.org/10.1016/j.foreco.2015.11.015>
- Blackburn, R. C., Buscaglia, R., & Meador, A. J. S. (2021). Mixtures of airborne lidar-based approaches improve predictions of forest structure. *Canadian Journal of Forest Research*, 51(8), 1106–1116. <https://doi.org/10.1139/cjfr-2020-0506>

- Blackman, R., & Yuan, F. (2020). Detecting long-term urban forest cover change and impacts of natural disasters using high-resolution aerial images and LiDAR data. *Remote Sensing*, 12(11), 1820.
- Bolton, D.K., Coops, N.C. & Wulder, M.A. (2015) Characterizing residual structure and forest structure following high-severity fire in the western boreal of Canada using Landsat time series and airborne LiDAR data. *Remote Sensing of Environment* 163: 48-60.
<https://doi.org/10.1016/j.rse.2015.03.004>
- Bouvier, M., Durrieu, S., Fournier, R. A., & Renaud, J. P. (2015). Generalizing predictive models of forest inventory attributes using an area-based approach with airborne LiDAR data. *Remote Sensing of Environment*, 156, 322-334. <https://doi.org/10.1016/j.rse.2014.10.004>
- Bowman, D., Williamson, G., Gibson, R., Bradstock, R., Keenan, & R. (2021). The severity and extent of the Australia 2019-20 Eucalyptus forest fires are not the legacy of forest management. *Nat Ecol Evol*, 5(7), 1003-1010. <https://doi.org/10.1038/s41559-021-01464-6>
- Brolly, G., Király, G., Lehtomäki, M., & Liang, X. (2021). Voxel-based automatic tree detection and parameter retrieval from terrestrial laser scans for plot-wise forest inventory. *Remote Sensing*, 13(4), 542. <https://doi.org/10.3390/rs13040542>
- Brown, T., Hislop, S., Wall, J., Coates, Z., Liang, G., Voeste, J., Nguyen, A., Cooper, G. (2023). Monitoring forestry outcomes in NSW native forests using airborne LiDAR, NSW Natural Resources Commission, Sydney
- Bryson, M., Wang, F., & Allworth, J. (2023). Using synthetic tree data in deep learning-based tree segmentation using LiDAR point clouds. *Remote Sensing (Basel, Switzerland)*, 15(9), 2380. <https://doi.org/10.3390/rs15092380>
- Campbell, M. J., Dennison, P. E., Hudak, A. T., Parham, L. M., & Butler, B. W. (2018). Quantifying understory vegetation density using small-footprint airborne lidar. *Remote Sensing of Environment*, 215, 330–342. <https://doi.org/10.1016/j.rse.2018.06.023>
- Carrasco, L., Giam, X., Papeş, M., & Sheldon, K. (2019). Metrics of lidar-derived 3D vegetation structure reveal contrasting effects of horizontal and vertical forest heterogeneity on bird species richness. *Remote Sensing (Basel, Switzerland)*, 11(7), 743. <https://doi.org/10.3390/rs11070743>
- Casas, Á., García, M., Siegel, R. B., Koltunov, A., Ramírez, C., & Ustin, S. (2016). Burned forest characterization at single-tree level with airborne laser scanning for assessing wildlife habitat. *Remote Sensing of Environment*, 175, 231–241. <https://doi.org/10.1016/j.rse.2015.12.044>
- Chang, L., Fan, H., Zhu, N. & Dong, Z. (2022) A two-stage approach for individual tree segmentation from TLS point clouds. *IEEE Journal of Selected Topics in Applied Earth Observation and Remote Sensing* 15: 8682 – 8693.
- Chen, Q., Baldocchi, D., Gong, P. & Kelly, M. (2006) Isolating individual trees in savanna woodland using small footprint LiDAR data. *Photogrammetric Engineering & Remote Sensing* 72: 923-932.
- Coops, N. C., Tompalski, P., Goodbody, T. R. H., Queinnec, M., Luther, J. E., Bolton, D. K., White, J. C., Wulder, M. A., van Lier, O. R., & Hermosilla, T. (2021). Modelling lidar-derived estimates of

- forest attributes over space and time: A review of approaches and future trends. *Remote Sensing of Environment*, 260, 112477. <https://doi.org/10.1016/j.rse.2021.112477>
- Cosenza, D. N., Korhonen, L., Maltamo, M., Packalen, P., Strunk, J. L., Næsset, E., ... & Tomé, M. (2021). Comparison of linear regression, k-nearest neighbour and random forest methods in airborne laser-scanning-based prediction of growing stock. *Forestry: An International Journal of Forest Research*, 94(2), 311-323. <https://doi.org/10.1093/forestry/cpaa034>
- Ehbrecht, M., Schall, P., Juchheim, J., Ammer, C., & Seidel, D. (2016). Effective number of layers: A new measure for quantifying three-dimensional stand structure based on sampling with terrestrial LiDAR. *Forest Ecology and Management*, 380, 212–223. <https://doi.org/10.1016/j.foreco.2016.09.003>
- Estrada, J. S., Fuentes, A., Reszka, P., & Auat Cheein, F. (2023). Machine learning assisted remote forestry health assessment: a comprehensive state of the art review. *Frontiers in Plant Science*, 14, 1139232–1139232. <https://doi.org/10.3389/fpls.2023.1139232>
- Ferrara, C., Puletti, N., Guasti, M., & Scotti, R. (2023). Mapping understory vegetation density in Mediterranean forests: Insights from airborne and terrestrial laser scanning integration. *Sensors (Basel, Switzerland)*, 23(1), 511. <https://doi.org/10.3390/s23010511>
- Fisher, A., Armston, J., Goodwin, N., & Scarth, P. (2020). Modelling canopy gap probability, foliage projective cover and crown projective cover from airborne lidar metrics in Australian forests and woodlands. *Remote Sensing of Environment*, 237, 111520. <https://doi.org/10.1016/j.rse.2019.111520>
- Francis, E. J., J. A. Lutz, and C. E. Farrior. (2023). Elevated mortality rates of large trees allow for increased frequency of intermediate trees: A hypothesis supported by demographic model comparison with plot and LiDAR data. *Forest Ecology and Management* 540: 121035. <https://doi.org/10.1016/j.foreco.2023.121035>
- Gelabert, P.J., Montealegre, A.L., Lamelas, M.T. & Domingo, D. (2020) Forest structural diversity characterization in Mediterranean landscapes affected by fires using Airborne Laser Scanning data. *GIScience & Remote Sensing* 57: 497-509.
- Haywood, A. & Stone, C. (2011) Using airborne laser scanning data to estimate structural attributes of natural eucalypt regrowth forests. *Australian Forestry*, 74(1), 4–12. <https://doi.org/10.1080/00049158.2011.10676340>
- Hillman, S., Hally, B., Wallace, L., Turner, D., Lucieer, A., Reinke, K., & Jones, S. (2021). High-resolution estimates of fire severity—An evaluation of UAS image and LiDAR mapping approaches on a sedgeland forest boundary in Tasmania, Australia. *Fire*, 4(1), 14
- Hillman, S., Wallace, L., Lucieer, A., et al. (2021) A comparison of terrestrial and UAS sensors for measuring fuel hazard in a dry sclerophyll forest. *International Journal of Applied Earth Observations and Geoinformation* 95: Article 102261. <http://doi.org/10.1016/j.jag.2020.102261>

- Hirschmugl, M., Lippl, F., & Sobe, C. (2023). Assessing the vertical structure of forests using airborne and spaceborne LiDAR data in the Austrian Alps. *Remote Sensing (Basel, Switzerland)*, 15(3), 664. <https://doi.org/10.3390/rs15030664>
- Hislop, S., Stone, C., Gibson, R.K. et al. (2023) Using dense Sentinel-2 time series to explore combined fire and drought impacts in eucalypt forests. *Frontiers in Forests and Global Change* 6: Article 1018936.
- Hislop, S., Stone, C., Samuel, J., Kathuria, A., Alaibakhsh, M., & Nguyen, T. H. (2024). Estimating the extent of selective timber harvesting in private native eucalypt forests with multi-temporal lidar. *Australian Forestry*, 86(3–4), 152–160. <https://doi.org/10.1080/00049158.2023.2288776>
- Jarron, L. R., Coops, N. C., MacKenzie, W. H., Tompalski, P., & Dykstra, P. (2020). Detection of sub-canopy forest structure using airborne LiDAR. *Remote Sensing of Environment*, 244, 111770. <https://doi.org/10.1016/j.rse.2020.111770>
- Jaskierniak, D., Lane, P. N. J., Robinson, A., & Lucieer, A. (2011). Extracting LiDAR indices to characterise multilayered forest structure using mixture distribution functions. *Remote Sensing of Environment*, 115(2), 573–585. <https://doi.org/10.1016/j.rse.2010.10.003>
- Jucker, T. (2022). Deciphering the fingerprint of disturbance on the three-dimensional structure of the world's forests. *New Phytologist*, 233(2), 612-617.
- Kamoske, A. G., Dahlin, K. M., Stark, S. C., & Serbin, S. P. (2019). Leaf area density from airborne LiDAR: Comparing sensors and resolutions in a temperate broadleaf forest ecosystem. *Forest Ecology and Management*, 433, 364–375. <https://doi.org/10.1016/j.foreco.2018.11.017>
- Kane, V. R., McGaughey, R. J., Bakker, J. D., Gersonde, R. F., Lutz, J. A., & Franklin, J. F. (2010). Comparisons between field- and LiDAR-based measures of stand structural complexity. *Canadian Journal of Forest Research*, 40(4), 761–773. <https://doi.org/10.1139/X10-024>
- Karna, Y. K., Penman, T. D., Aponte, C., & Bennett, L. T. (2019). Assessing legacy effects of wildfires on the crown structure of fire-tolerant eucalypt trees using airborne LiDAR Data. *Remote Sensing (Basel, Switzerland)*, 11(20), 2433. <https://doi.org/10.3390/rs11202433>
- Karna, Y. K., Penman, T. D., Aponte, C., Hinko-Najera, N., & Bennett, L. T. (2020). Persistent changes in the horizontal and vertical canopy structure of fire-tolerant forests after severe fire as quantified using multi-temporal airborne lidar data. *Forest Ecology and Management*, 472, 118255. <https://doi.org/10.1016/j.foreco.2020.118255>
- Kathuria, A. (2023) Sampling design for forest resource assessment of private native forest, Northern NSW. Technical report for NSW Local Land Services. Available at <https://dx.doi.org/10.13140/RG.2.2.17698.20166>
- Kay, H., Santoro, M., Cartus, O., Bunting, P., & Lucas, R. (2021). Exploring the relationship between forest canopy height and canopy foliage density from Spaceborne LiDAR observations. *Remote Sensing*, 13(24), 4961. <https://doi.org/10.3390/rs13244961>

- Khan, M. S., Kim, I. S., & Seo, J. (2023). A boundary and voxel-based 3D geological data management system leveraging BIM and GIS. *International Journal of Applied Earth Observation and Geoinformation*, 118, 103277.
- Knapp, N., Huth, A., & Fischer, R. (2021). Tree crowns cause border effects in area-based biomass estimations from remote sensing. *Remote Sensing (Basel, Switzerland)*, 13(8), 1592. <https://doi.org/10.3390/rs13081592>
- Krisanski, S., Taskhiri, M. S., Gonzalez Aracil, S., Herries, D., & Turner, P. (2021). Sensor agnostic semantic segmentation of structurally diverse and complex forest point clouds using deep learning. *Remote Sensing (Basel, Switzerland)*, 13(8), 1413. <https://doi.org/10.3390/rs13081413>
- Krisanski, S., Taskhiri, M. S., Gonzalez Aracil, S., Herries, D., Muneri, A., Gurung, M. B., Montgomery, J., & Turner, P. (2021). Forest Structural Complexity Tool—An open source, fully-automated tool for measuring forest point clouds. *Remote Sensing (Basel, Switzerland)*, 13(22), 4677. <https://doi.org/10.3390/rs13224677>
- LaRue, E. A., Fahey, R. T., Alvshere, B. C., Atkins, J. W., Bhatt, P., Buma, B., ... & Fei, S. (2023). A theoretical framework for the ecological role of three-dimensional structural diversity. *Frontiers in Ecology and the Environment*, 21(1), 4-13.
- Lee, Y., Woo, H., & Lee, J.-S. (2022). Forest inventory assessment using integrated light detection and ranging (LiDAR) systems: Merged point cloud of airborne and mobile laser scanning systems. *Sensors and Materials*, 34(12), 4583. <https://doi.org/10.18494/SAM4100>
- Lefsky, M. A., W. B. Cohen, G. G. Parker, and D. J. Harding. (2002). Lidar remote sensing for ecosystem studies: Lidar, an emerging remote sensing technology that directly measures the three-dimensional distribution of plant canopies, can accurately estimate vegetation structural attributes, and should be of particular interest to forest, landscape, and global ecologists. *BioScience* 52: 19–30. [https://doi.org/10.1641/0006-3568\(2002\)052%5b0019:LRSFES%5d2.0.CO;2](https://doi.org/10.1641/0006-3568(2002)052%5b0019:LRSFES%5d2.0.CO;2)
- Leiterer, R., Morsdorf, F., Torabzadeh, H., Schaepman, M. E., Mucke, W., Pfeifer, N., & Hollaus, M. (2012). A voxel-based approach for canopy structure characterization using full-waveform airborne laser scanning. 2012 IEEE International Geoscience and Remote Sensing Symposium, 3399–3402. <https://doi.org/10.1109/IGARSS.2012.6350691>
- Li, W., Hu, X., Su, Y., Tao, S., Ma, Q., & Guo, Q. (2024). A new method for voxel-based modelling of three-dimensional forest scenes with integration of terrestrial and airborne LiDAR data. *Methods in Ecology and Evolution*. <https://doi.org/10.1111/2041-210X.14290>
- Liao, Z., Van Dijk, A. I., He, B., Larraondo, P. R., & Scarth, P. F. (2020). Woody vegetation cover, height and biomass at 25-m resolution across Australia derived from multiple site, airborne and satellite observations. *International Journal of Applied Earth Observation and Geoinformation*, 93, 102209. <https://doi.org/10.1016/j.jag.2020.102209>
- Listopad, C. M. C. S., Masters, R. E., Drake, J., Weishampel, J., & Branquinho, C. (2015). Structural diversity indices based on airborne LiDAR as ecological indicators for managing highly dynamic landscapes. *Ecological Indicators*, 57, 268–279. <https://doi.org/10.1016/j.ecolind.2015.04.017>

- Liu, L., & Lim, S. (2018). A voxel-based multiscale morphological airborne lidar filtering algorithm for digital elevation models for forest regions. *Measurement : Journal of the International Measurement Confederation*, 123, 135–144. <https://doi.org/10.1016/j.measurement.2018.03.020>
- Liu, Q., Fu, L., Chen, Q., Wang, G., Luo, P., Sharma, R. P., ... & Duan, G. (2020). Analysis of the spatial differences in canopy height models from UAV LiDAR and photogrammetry. *Remote Sensing*, 12(18), 2884. <https://doi.org/10.1016/j.jag.2020.102209>
- Luo, J., Zhang, M., Zhou, X., Chen, J., & Tian, Y. (2018). Tree height and DBH growth model establishment of main tree species in Wuling Mountain small watershed. In *IOP Conference Series: Earth and Environmental Science* (Vol. 108, No. 4, p. 042003). IOP Publishing. <https://doi.org/10.1088/1755-1315/108/4/042003>
- Matasci, G., Hermosilla, T., Wulder, M. A., White, J. C., Coops, N. C., Hobart, G. W., Bolton, D. K., Tompalski, P., & Bater, C. W. (2018). Three decades of forest structural dynamics over Canada's forested ecosystems using Landsat time-series and lidar plots. *Remote Sensing of Environment*, 216, 697–714. <https://doi.org/10.1016/j.rse.2018.07.024>
- Mäyrä, J., Keski-Saari, S., Kivinen, S., Tanhuanpää, T., Hurskainen, P., Kullberg, P., Poikolainen, L., Viinikka, A., Tuominen, S., Kumpula, T., & Vihervaara, P. (2021). Tree species classification from airborne hyperspectral and LiDAR data using 3D convolutional neural networks. *Remote Sensing of Environment*, 256, 112322. <https://doi.org/10.1016/j.rse.2021.112322>
- Mazlan, S. M., Wan Mohd Jaafar, W. S., Muhmad Kamarulzaman, A. M., Saad, S. N. M., Mohd Ghazali, N., Adrah, E., ... & Mahmud, M. R. (2023). A review on the use of LiDAR remote sensing for forest landscape restoration. *Concepts and Applications of Remote Sensing in Forestry*, 49-74. <https://doi.org/10.1016/j.jag.2020.102209>
- Mielcarek, M., Stereńczak, K., & Khosravipour, A. (2018). Testing and evaluating different LiDAR-derived canopy height model generation methods for tree height estimation. *International journal of applied earth observation and geoinformation*, 71, 132-143. <https://doi.org/10.1016/j.jag.2018.05.002>
- Moran, C.J., Rowell, E.M. & Seielstad, C.A. (2018) A data-driven framework to identify and compare forest structure classes using LiDAR. *Remote Sensing of Environment* 211: 154-166. <https://doi.org/10.1016/j.rse.2018.04.005>
- Moudrý, V., Cord, A. F., Gábor, L., Laurin, G. V., Barták, V., Gdulová, K., Malavasi, M., Rocchini, D., Stereńczak, K., Prošek, J., Klápště, P., & Wild, J. (2023). Vegetation structure derived from airborne laser scanning to assess species distribution and habitat suitability: The way forward. *Diversity & Distributions*, 29(1), 39–50. <https://doi.org/10.1111/ddi.13644>
- Muddarisna, N., Yuniwati, E. D., Masrurroh, H., & Oktaviansyah, A. R. (2020). An automated approach using topographic position index (TPI) for landform mapping (case study: Gede Watershed, Malang Regency, East Java, Indonesia). In *IOP Conference Series: Earth and Environmental Science* (Vol. 412, No. 1, p. 012027). IOP Publishing. <http://dx.doi.org/10.1088/1755-1315/412/1/012027>

- Nguyen, T. H., Jones, S. D., Soto-Berelov, M., Haywood, A., & Hislop, S. (2020). Monitoring aboveground forest biomass dynamics over three decades using Landsat time-series and single-date inventory data. *International Journal of Applied Earth Observation and Geoinformation*, 84, 101952. <https://doi.org/10.1016/j.jag.2019.101952>
- Pearse, G.D., Watt, M.S., Dash, J.P., et al. (2018) Comparison of models describing forest inventory attributes using standard and voxel-based LiDAR predictors across a range of pulse densities. *International Journal of Applied Earth Observation Geoinformation* 78: 341-351 <http://doi.org/10.1016/j.jag.2018.10.008>
- Penner, M., Pitt, D. G., & Woods, M. E. (2013). Parametric vs. nonparametric LiDAR models for operational forest inventory in boreal Ontario. *Canadian Journal of Remote Sensing*, 39(5), 426-443. <http://dx.doi.org/10.5589/m13-049>
- Pérez-Carrasco, M., Karelovic, B., Molina, R., Saavedra, R., Cerulo, P., & Cabrera-Vives, G. (2022). Precision silviculture: use of UAVs and comparison of deep learning models for the identification and segmentation of tree crowns in pine crops. *International Journal of Digital Earth*, 15(1), 2223–2238. <https://doi.org/10.1080/17538947.2022.2152882>
- Petras, V., Petrasova, A., McCarter, J. B., Mitasova, H., & Meentemeyer, R. K. (2023). Point Density Variations in Airborne Lidar Point Clouds. *Sensors (Basel, Switzerland)*, 23(3), 1593. <https://doi.org/10.3390/s23031593>
- Puletti, N., Galluzzi, M., Grotti, M. & Ferrara, C. (2021) Characterizing subcanopy structure of Mediterranean forests by terrestrial laser scanning data. *Remote Sensing Applications: Society and Environment*. 24: Article 100620. <https://doi.org/10.1016/j.rsase.2021.100620>
- Puletti, N., Castronuovo, R. & Ferrara, C. (2023) Crossing 3D Forest: An R package for evaluating empty space structure in forest ecosystems. *Research & Reviews: Journal of Ecology and Environmental Sciences* 11: 001. <https://doi.org/10.1016/j.rsase.2021.100620>
- Qi, Z., Li, S., Pang, Y., Du, L., Zhang, H., & Li, Z. (2023). Monitoring Spatiotemporal Variation of Individual Tree Biomass Using Multitemporal LiDAR Data. *Remote Sensing (Basel, Switzerland)*, 15(19), 4768. <https://doi.org/10.3390/rs15194768>
- Qin, Y., Xiao, X., Wigneron, J. P., Ciais, P., Canadell, J. G., Brandt, M., ... & Moore III, B. (2022). Large loss and rapid recovery of vegetation cover and aboveground biomass over forest areas in Australia during 2019–2020. *Remote Sensing of Environment*, 278, 113087.
- Roussel, J.-R., Auty, D., Coops, N. C., Tompalski, P., Goodbody, T. R. H., Meador, A. S., Bourdon, J.-F., de Boissieu, F., & Achim, A. (2020). lidR: An R package for analysis of Airborne Laser Scanning (ALS) data. *Remote Sensing of Environment*, 251, 112061. <https://doi.org/10.1016/j.rse.2020.112061>
- Roussel, J.-R., Caspersen, J., Béland, M., Thomas, S., & Achim, A. (2017). Removing bias from LiDAR-based estimates of canopy height: Accounting for the effects of pulse density and footprint size. *Remote Sensing of Environment*, 198, 1–16. <https://doi.org/10.1016/j.rse.2017.05.032>

- Sanchez-Lopez, N., Boschetti, L., & Hudak, A. T. (2020). Reconstruction of the disturbance history of a temperate coniferous forest through stand-level analysis of airborne LiDAR data. *Forestry: An International Journal of Forest Research*, 93(1), 38-55. <https://doi.org/10.1093/forestry/cpz048>
- Senf, C., & Seidl, R. (2022). Post-disturbance canopy recovery and the resilience of Europe's forests. *Global Ecology and Biogeography*, 31(1), 25-36.
- Shang, X. & Chisholm, L.A. (2013) Classification of Australian native forest species using hyperspectral remote sensing and machine-learning classification algorithms. *IEEE Journal of Selected Topics in Applied Earth Observations and Remote Sensing* 7: 2481-2489.
- Silva, C. A., Hudak, A. T., Vierling, L. A., Valbuena, R., Cardil, A., Mohan, M., Almeida, D. R. A., Broadbent, E. N., Almeyda Zambrano, A. M., Wilkinson, B., Sharma, A., Drake, J. B., Medley, P. B., Vogel, J. G., Prata, G. A., Atkins, J. W., Hamamura, C., Johnson, D. J., & Klauberg, C. (2022). treetop: A Shiny-based application and R package for extracting forest information from LiDAR data for ecologists and conservationists. *Methods in Ecology and Evolution*, 13(6), 1164–1176. <https://doi.org/10.1111/2041-210X.13830>
- Szostak, M. (2020). Automated land cover change detection and forest succession monitoring using LiDAR Point Clouds and GIS analyses. *Geosciences*, 10(8), 321. <https://doi.org/10.3390/geosciences10080321>
- Torresan, C., Corona, P., Scrinzi, G. & Marsal, J.V. (2016) Using classification trees to predict forest structure types from LiDAR data. *Annals of Forest Research*, 59(2), 281–298. <https://doi.org/10.15287/afr.2016.423>
- Vatandaslar, C., Seki, M. & Zeybek, M. (2023) Assessing the potential of mobile laser scanning for stand-level forest inventories in near-natural forests. *Forestry: An International Journal of Forest Research*, 96(4), 448–464. <https://doi.org/10.1093/forestry/cpad016>
- Viana-Soto, A., García, M., Aguado, I., & Salas, J. (2022). Assessing post-fire forest structure recovery by combining LiDAR data and Landsat time series in Mediterranean pine forests. *International Journal of Applied Earth Observation and Geoinformation*, 108, 102754. <https://doi.org/10.1016/j.jag.2022.102754>
- Wang, C., Luo, S., Xi, X., Nie, S., Ma, D., & Huang, Y. (2020). Influence of voxel size on forest canopy height estimates using full-waveform airborne LiDAR data. *Forest Ecosystems*, 7(1), 1–12. <https://doi.org/10.1186/s40663-020-00243-2>
- Wang, H., Seaborn, T., Wang, Z., Caudill, C. C., & Link, T. E. (2021). Modeling tree canopy height using machine learning over mixed vegetation landscapes. *International Journal of Applied Earth Observation and Geoinformation*, 101, 102353. <https://doi.org/10.1016/j.jag.2021.102353>
- Watt, M. S., Dash, J. P., Bhandari, S., & Watt, P. (2015). Comparing parametric and non-parametric methods of predicting Site Index for radiata pine using combinations of data derived from environmental surfaces, satellite imagery and airborne laser scanning. *Forest Ecology and Management*, 357, 1-9. <http://dx.doi.org/10.1016/j.foreco.2015.08.001>

- Weiss, A. (2001, July). Topographic position and landforms analysis. In *Poster presentation, ESRI user conference, San Diego, CA* (Vol. 200).
- Whelan, A. W., Cannon, J. B., Bigelow, S. W., Rutledge, B. T., & Sánchez Meador, A. J. (2023). Improving generalized models of forest structure in complex forest types using area- and voxel-based approaches from lidar. *Remote Sensing of Environment*, 284, 113362. <https://doi.org/10.1016/j.rse.2022.113362>
- White, J. C., Hermosilla, T., Wulder, M. A., & Coops, N. C. (2022). Mapping, validating, and interpreting spatio-temporal trends in post-disturbance forest recovery. *Remote Sensing of Environment*, 271, 112904. <https://doi.org/10.1016/j.rse.2022.112904>
- White, J., Tompalski, P., Vastaranta, M., Wulder, M. A., Saarinen, N., Stepper, C., & Coops, N. C. (2017). A model development and application guide for generating an enhanced forest inventory using airborne laser scanning data and an area-based approach. <http://dx.doi.org/10.13140/RG.2.2.26770.96964>
- Wilkes, P., Disney, M., Armston, J., et al. (2023) TLS2trees: A scalable tree segmentation pipeline for TLS data. *Methods in Ecology and Evolution*. <http://doi.org/10.1111/2041-210X.14233>
- Windrim, L., & Bryson, M. (2020). Detection, Segmentation, and Model Fitting of Individual Tree Stems from Airborne Laser Scanning of Forests Using Deep Learning. *Remote Sensing (Basel, Switzerland)*, 12(9), 1469-. <https://doi.org/10.3390/rs12091469>
- Wulder, M. A., Bater, C. W., Coops, N. C., Hilker, T., & White, J. C. (2008). The role of LiDAR in sustainable forest management. *The forestry chronicle*, 84(6), 807-826. <http://dx.doi.org/10.5558/tfc84807-6>
- Xu, Y., Tong, X., & Stilla, U. (2021). Voxel-based representation of 3D point clouds: Methods, applications, and its potential use in the construction industry. *Automation in Construction*, 126, 103675. <https://doi.org/10.1016/j.autcon.2021.103675>
- Zhang, J., Zhao, X., Chen, Z. & Lu, Z. (2019) A review of deep learning-based semantic segmentation for point cloud. *IEEE Access* 7: 179118-179133.
- Zhang, W., He, Z., & Li, X. (2022). Voxel-based Urban Vegetation Volume Analysis with LiDAR Point Cloud. In *Proceedings of the Fábos Conference on Landscape and Greenway Planning* (Vol. 7, No. 1, p. 67). <https://doi.org/10.1016/j.autcon.2021.103675>
- Zhang, Z., Cao, L., & She, G. (2017). Estimating Forest Structural Parameters Using Canopy Metrics Derived from Airborne LiDAR Data in Subtropical Forests. *Remote Sensing (Basel, Switzerland)*, 9(9), 940. <https://doi.org/10.3390/rs9090940>
- Zhao, H., Morgenroth, J., Pearse, G., & Schindler, J. (2023). A Systematic Review of Individual Tree Crown Detection and Delineation with Convolutional Neural Networks (CNN). *Current Forestry Reports*, 9(3), 149–170. <https://doi.org/10.1007/s40725-023-00184-3>
- Zięba-Kulawik, K., Skoczylas, K., Wężyk, P., Teller, J., Mustafa, A., & Omrani, H. (2021). Monitoring of urban forests using 3D spatial indices based on LiDAR point clouds and voxel approach. *Urban Forestry & Urban Greening*, 65, 127324-. <https://doi.org/10.1016/j.ufug.2021.127324>

Appendix A: Supplementary figures for all ALS captures

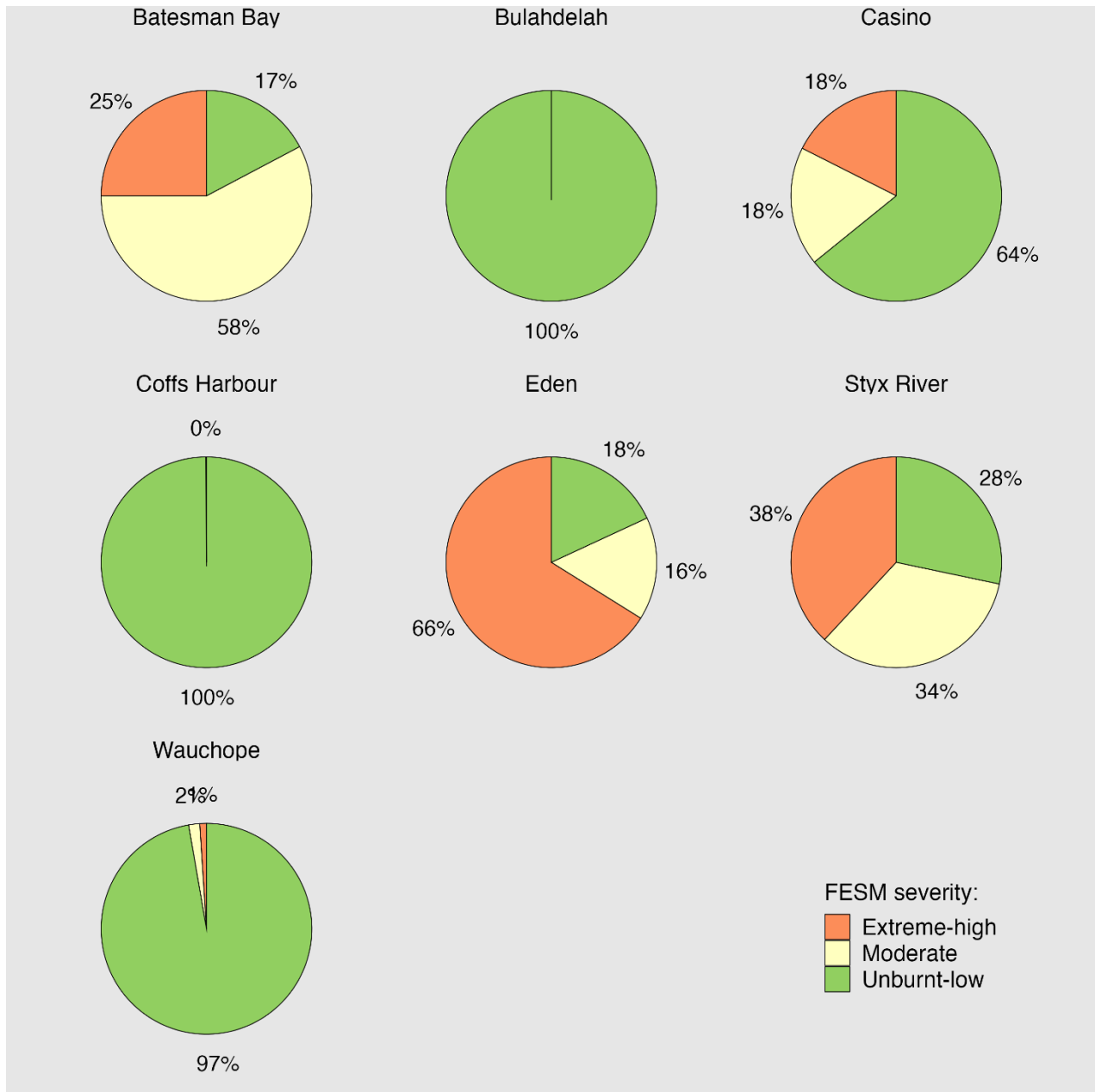


Figure A1 - Fire extent and severity mapping ratings (FESM) for all captures. Note that FESM ratings are traditionally categorised into five levels (unburnt, low severity, moderate, high, and extreme severity). For clarity, we have condensed these five levels to three where low severity is merged with unburnt, and high severity is merged with extreme.

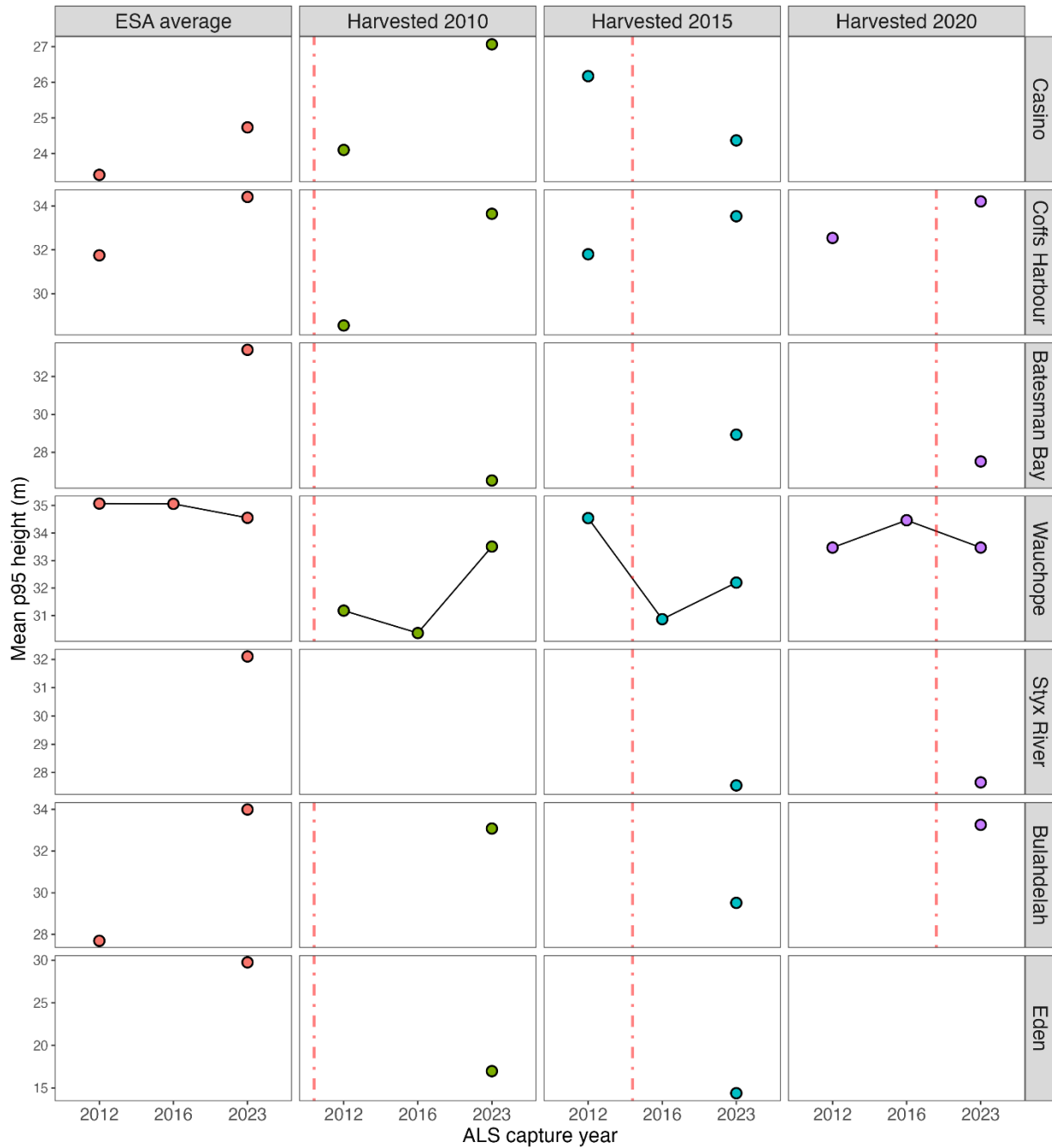


Figure A2 - Mean p95 heights across all forest capture regions (vertical panels). Across the panels, the vertical red dashed line is a visual guide of the approximate timepoint of silvicultural disturbance, noting the change in this timepoint across regions (horizontal panels).

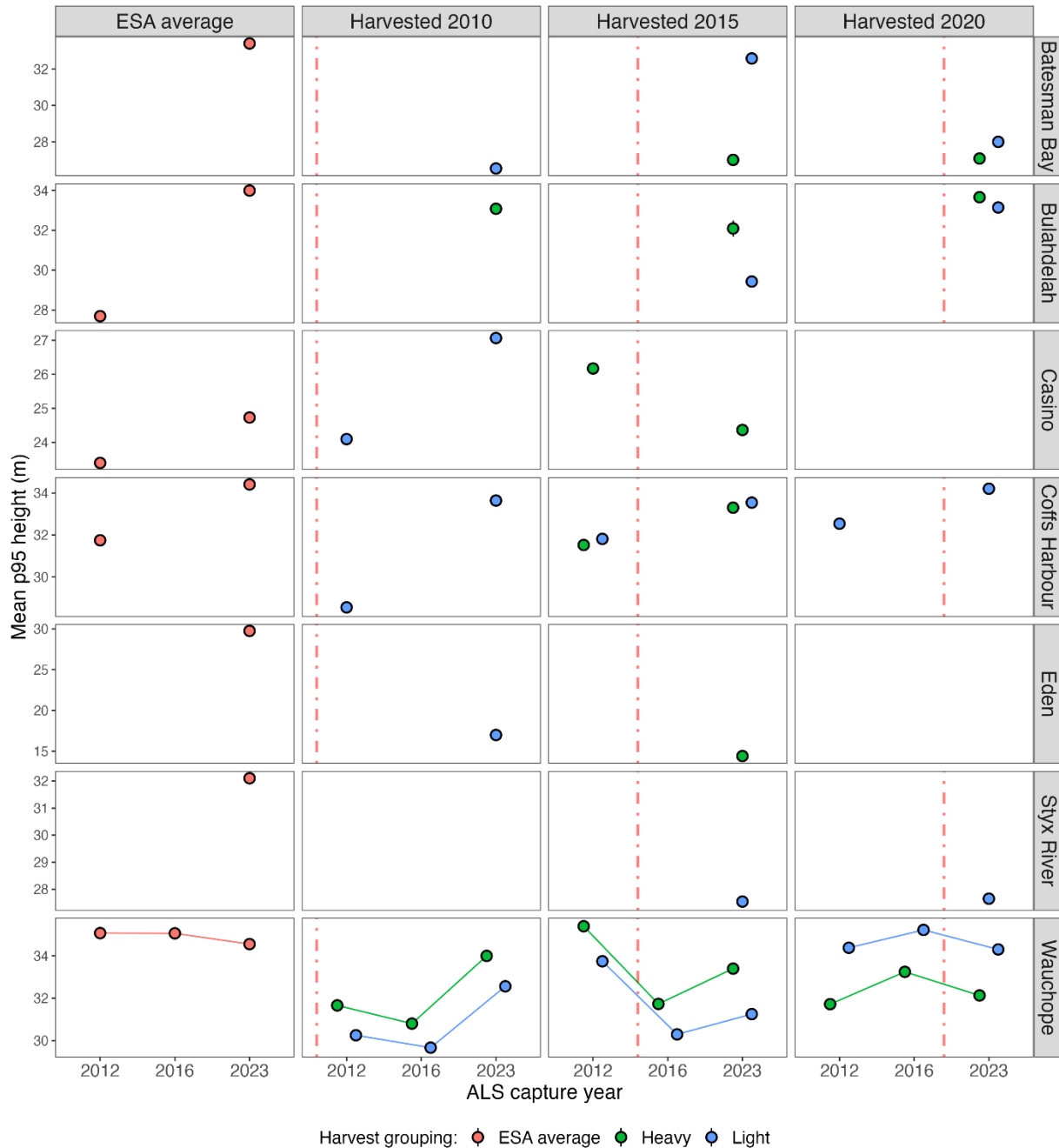


Figure A3 - Mean p95 heights across all forest capture regions (vertical panels) as a function of silvicultural practice. Across the panels, the vertical red dashed line is a visual guide of the approximate timepoint of silvicultural disturbance, noting the change in this timepoint across regions (horizontal panels). For clarity, we present only “light” (blue) and “heavy” (green) silvicultural practices in this figure, noting that other silvicultural practices, such as mixed practices or salvage harvests, are present in the data.

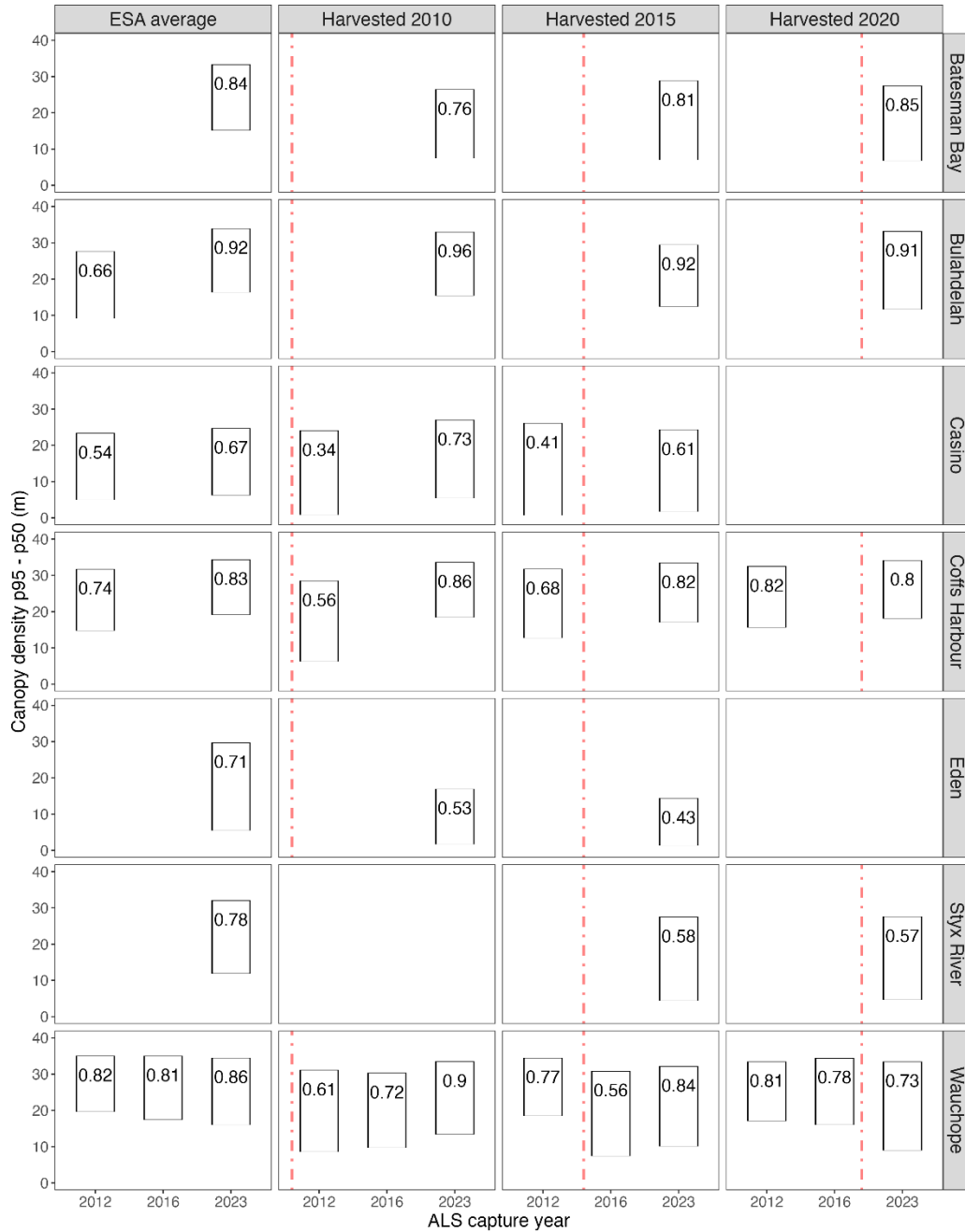


Figure A4 - Corresponding panel to Figure 22 in the main report for canopy foliage density for all regions. Three metrics, p95, p50, and canopy coverages, combined to illustrate canopy foliage density. Horizontal panels show separate spatial locations that were last harvested in 2010, 2015, or 2020. Vertical panels show different forest regions. Separate LiDAR captures shown on the x-axis as a rectangle. Canopy height metrics are displayed as a rectangle where the mean p95 return height (m) is shown by the upper edge of the rectangle, and mean p50 return height (m) is shown by the lower edge of the rectangle. Canopy coverage, as the proportion of area covered by the canopy, is displayed as a decimal within the rectangle. The harvesting time point is depicted with a red dotted line. Note that the harvesting timepoint changes across panels as each location was harvested in a different year.

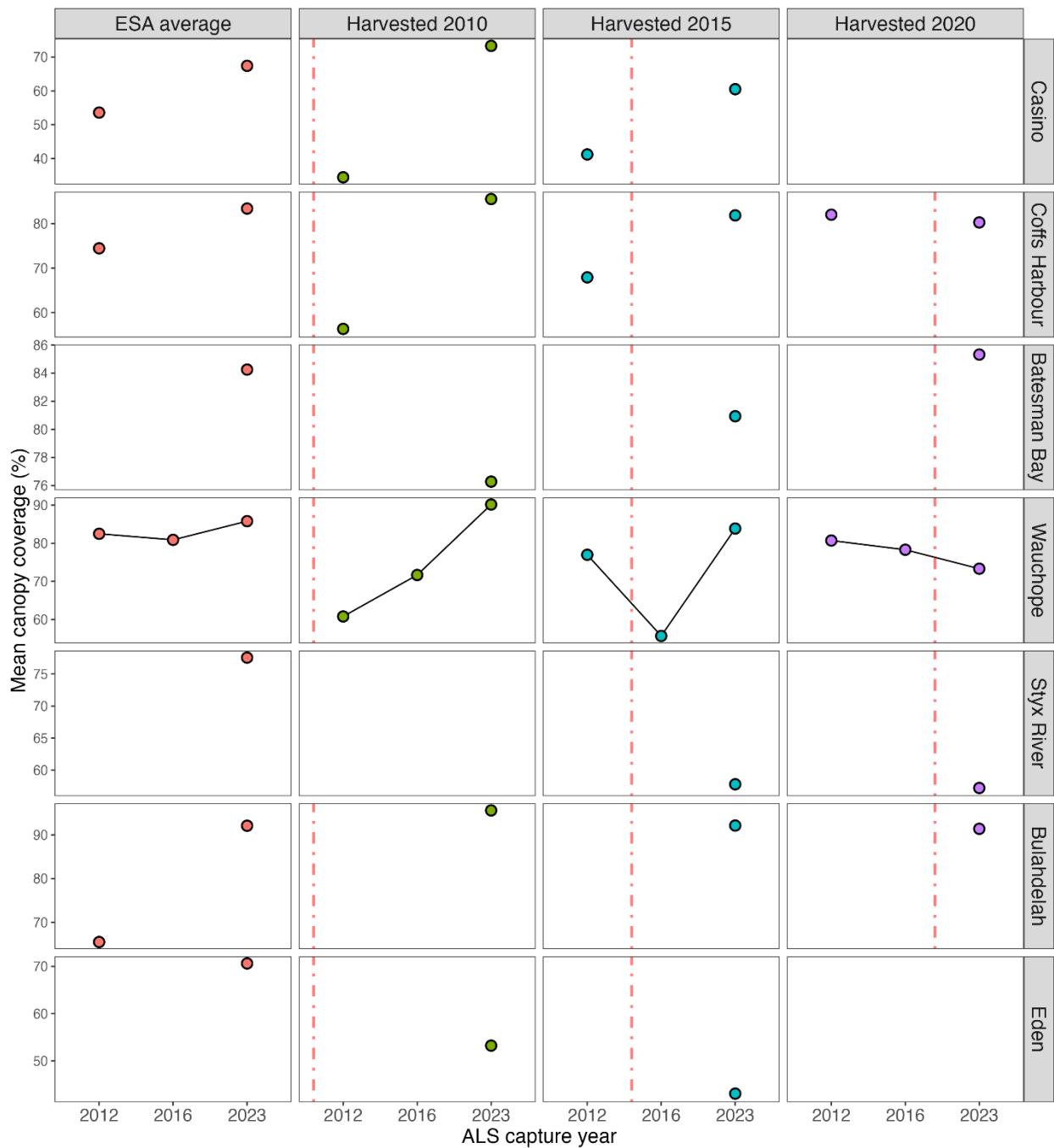


Figure A5 - Plots outlining overview of canopy coverage for multiple captures across all forest regions with separate lines indicating silvicultural method. Across the panels, the vertical red dashed line is a visual guide of the approximate timepoint of silvicultural disturbance, noting the change in this timepoint across regions (horizontal panels).

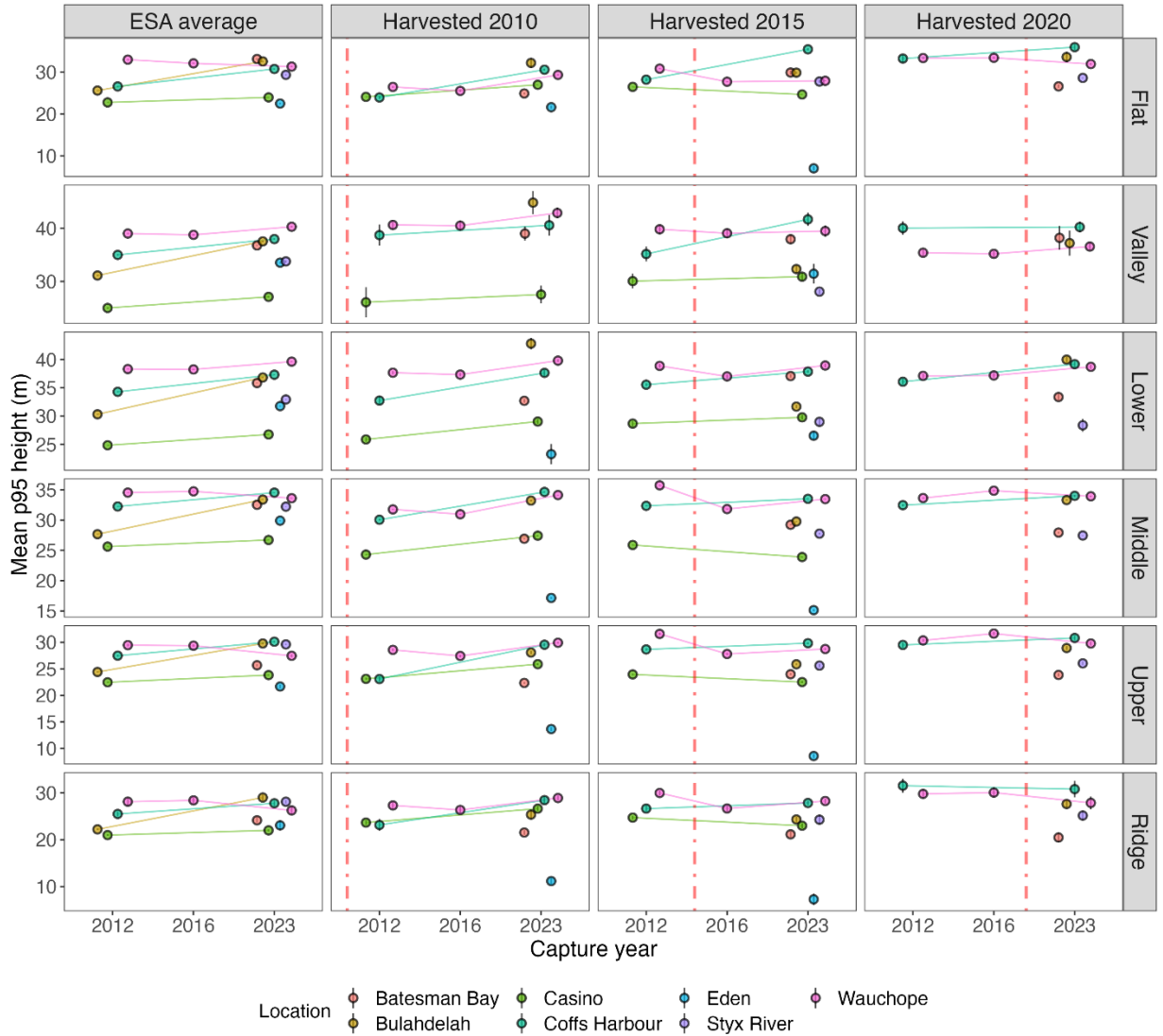
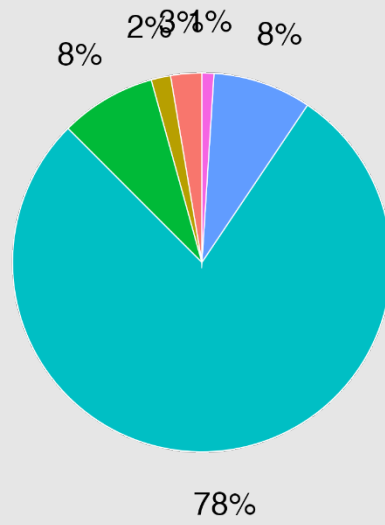


Figure A6 - Plots outlining overview of mean p95 heights for multiple captures with separate lines indicating forest capture region and vertical panels indicating slope classification. Across the panels, the vertical red dashed line is a visual guide of the approximate timepoint of silvicultural disturbance, noting the change in this timepoint across regions (horizontal panels).

Batesman Bay

Landform class:

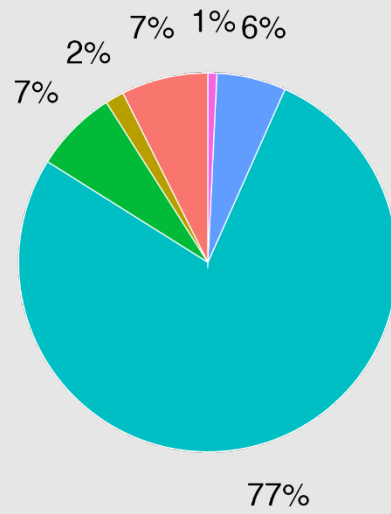
- Flat
- Valley
- Lower
- Middle
- Upper
- Ridge



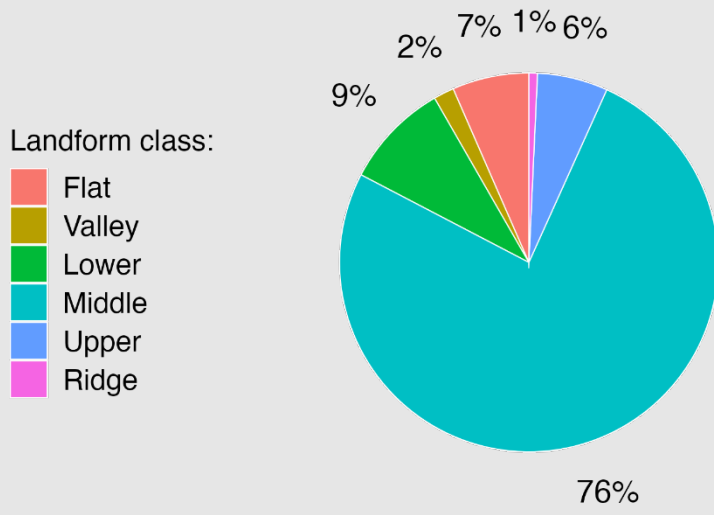
Eden

Landform class:

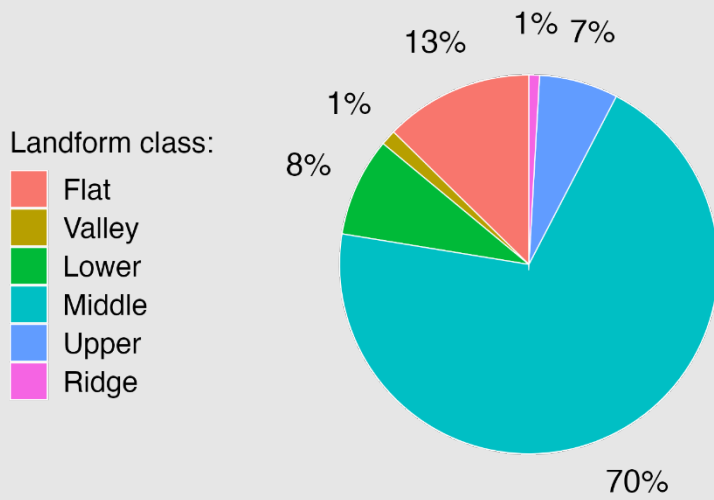
- Flat
- Valley
- Lower
- Middle
- Upper
- Ridge



Bulahdelah



Styx River



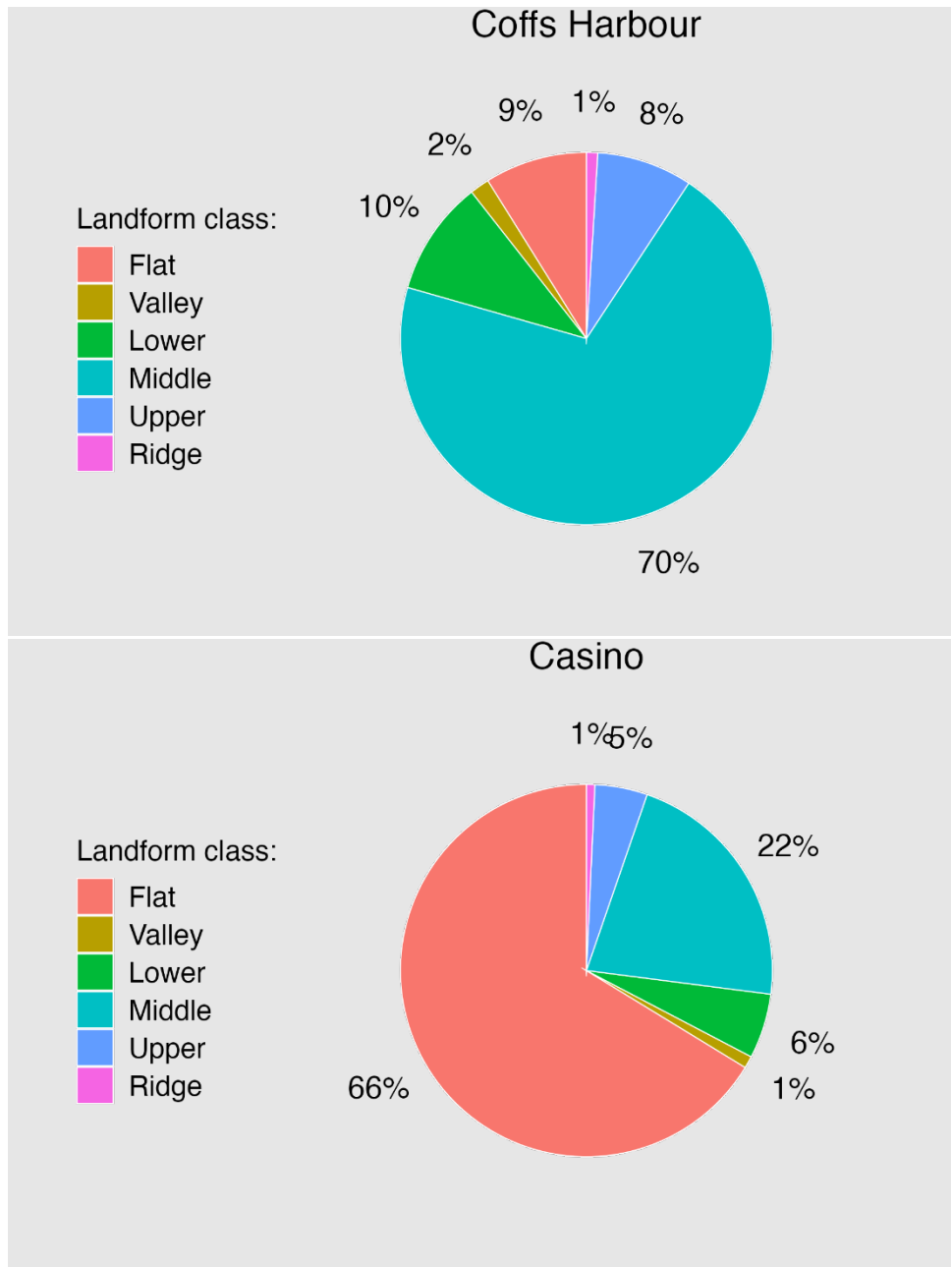


Figure A7 - Pie charts outlining percentage of slope classifications in different forest capture regions.

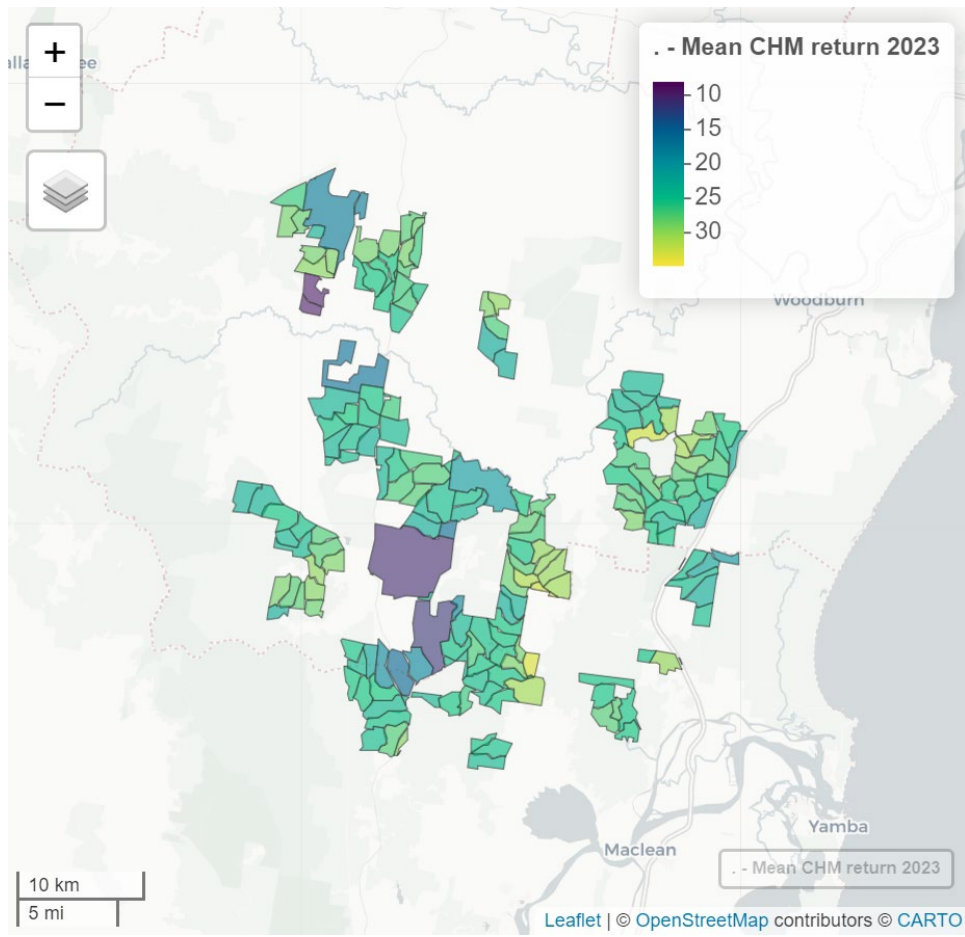


Figure A8.1 - Maps of forest capture regions, polygons grouped by LLA (Casino).

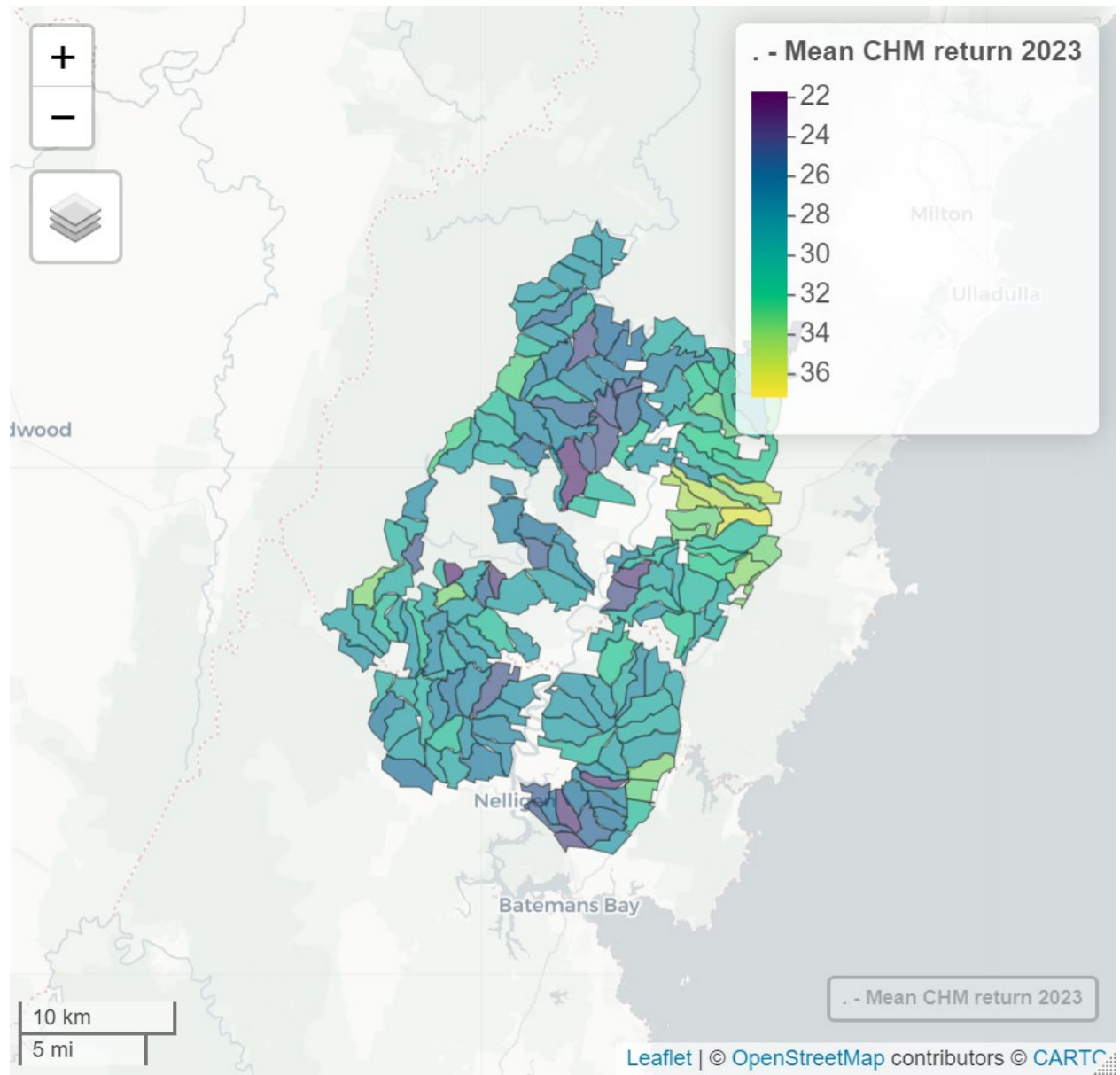


Figure A8.2 - Maps of forest capture regions, polygons grouped by LLA (Batemans Bay).

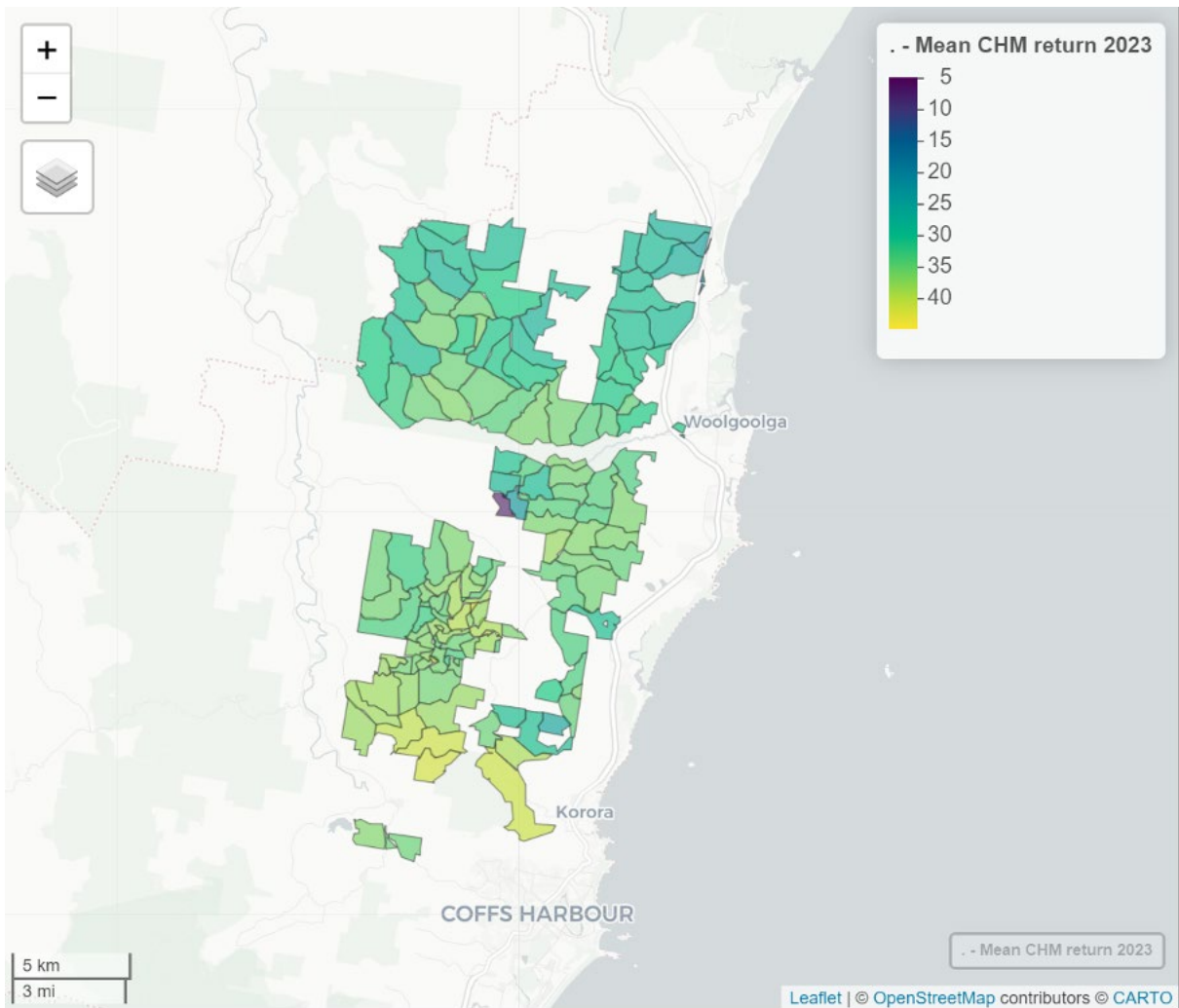


Figure A8.3 - Maps of forest capture regions, polygons grouped by LLA (Coffs Harbour).

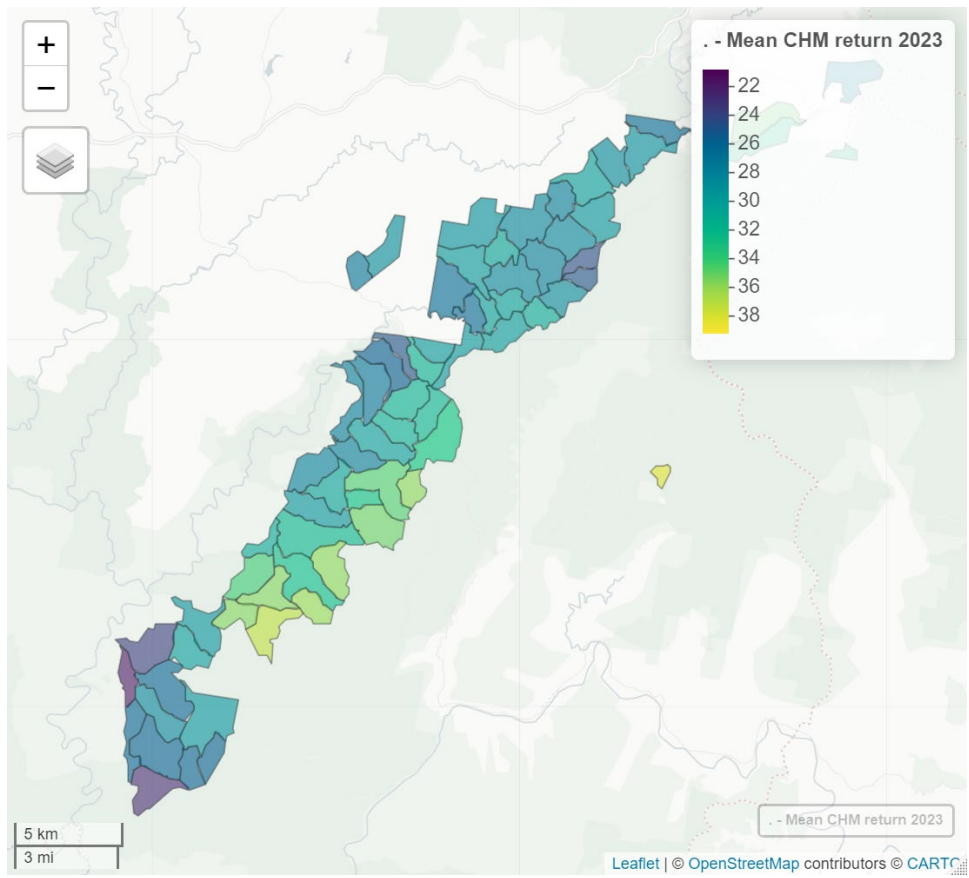


Figure A8.4 - Maps of forest capture regions, polygons grouped by LLA (Styx River).

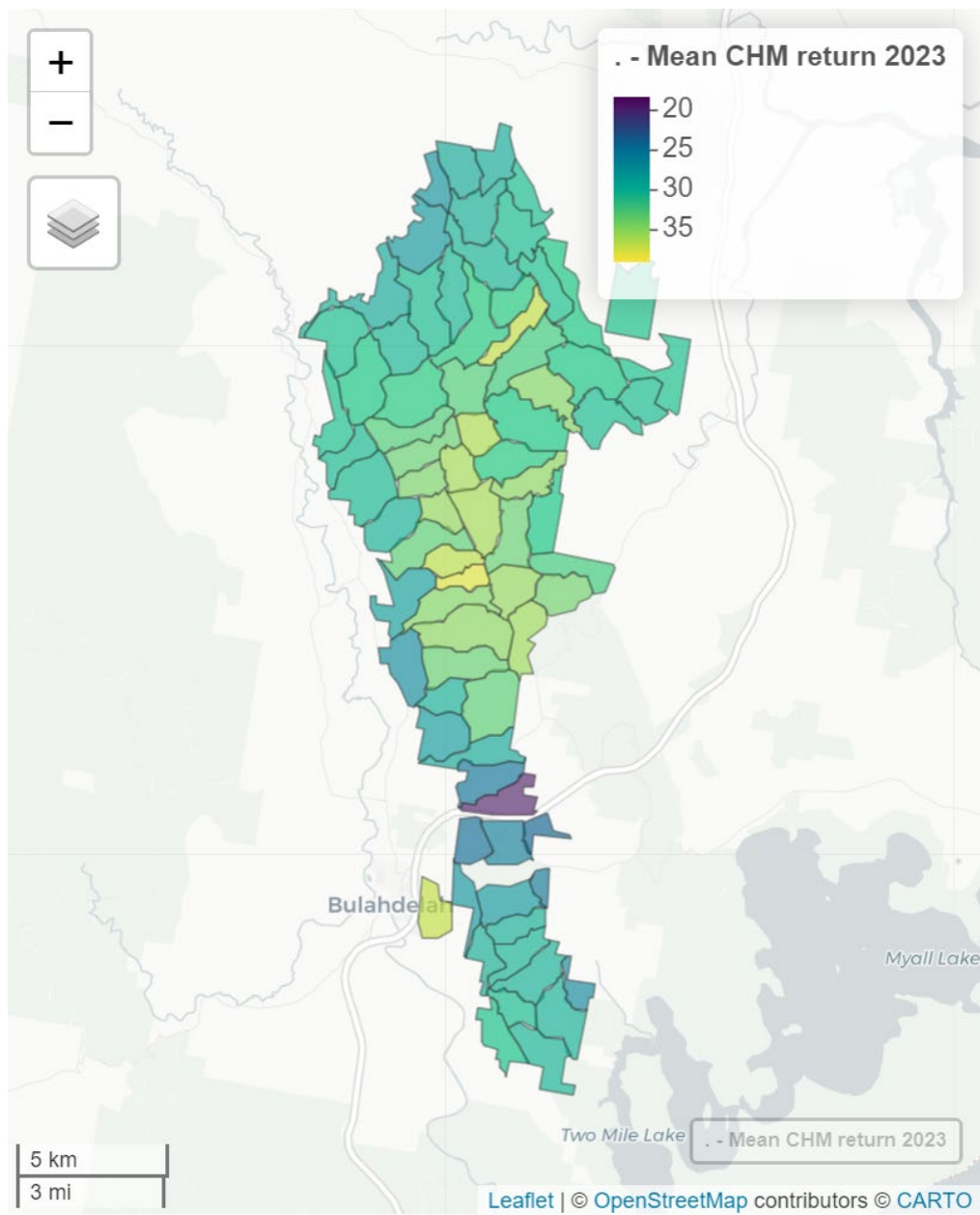


Figure A8.5 - Maps of forest capture regions, polygons grouped by LLA (Bulahdelah).

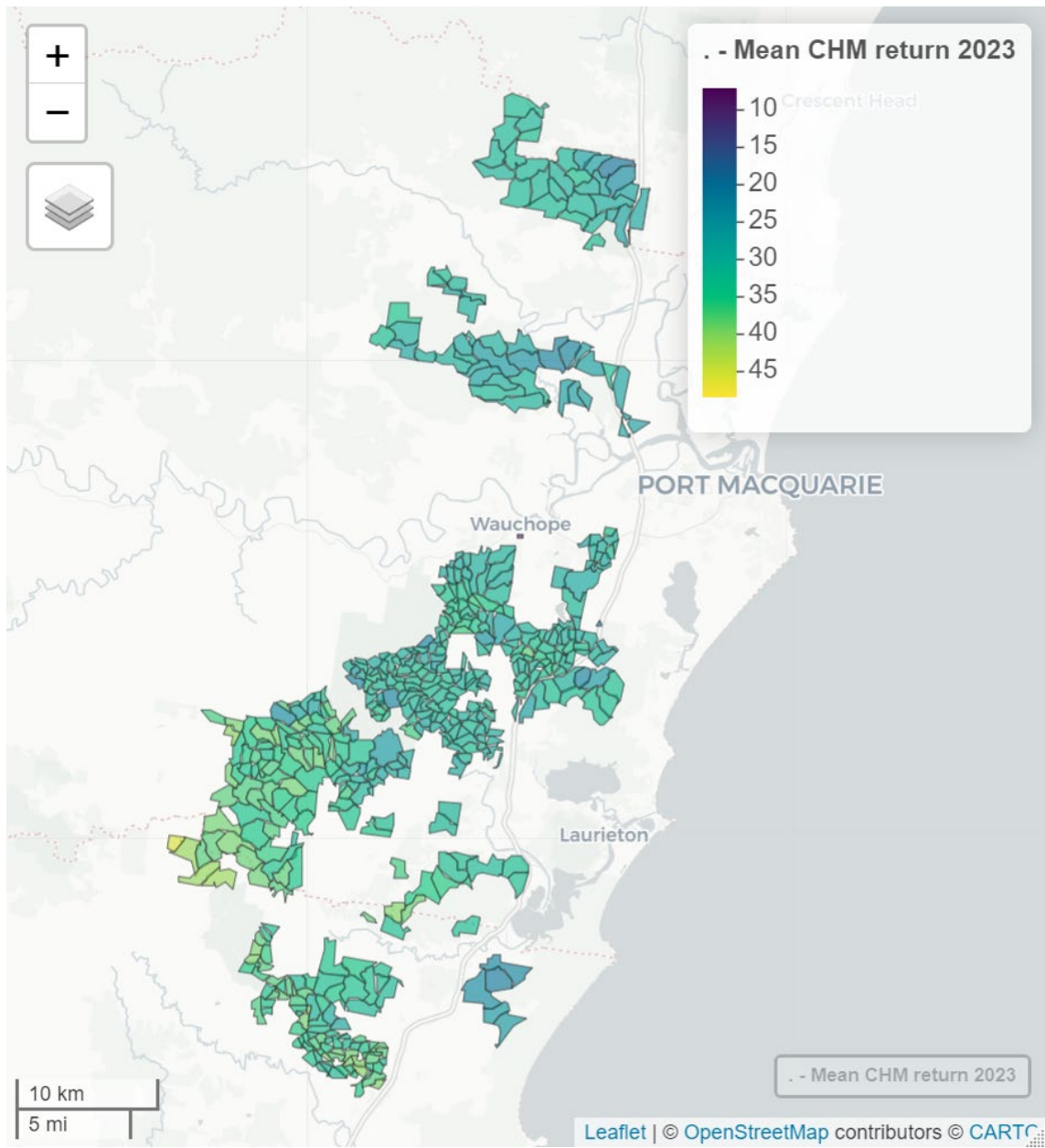


Figure A8.6 - Maps of forest capture regions, polygons grouped by LLA (Wauchope).

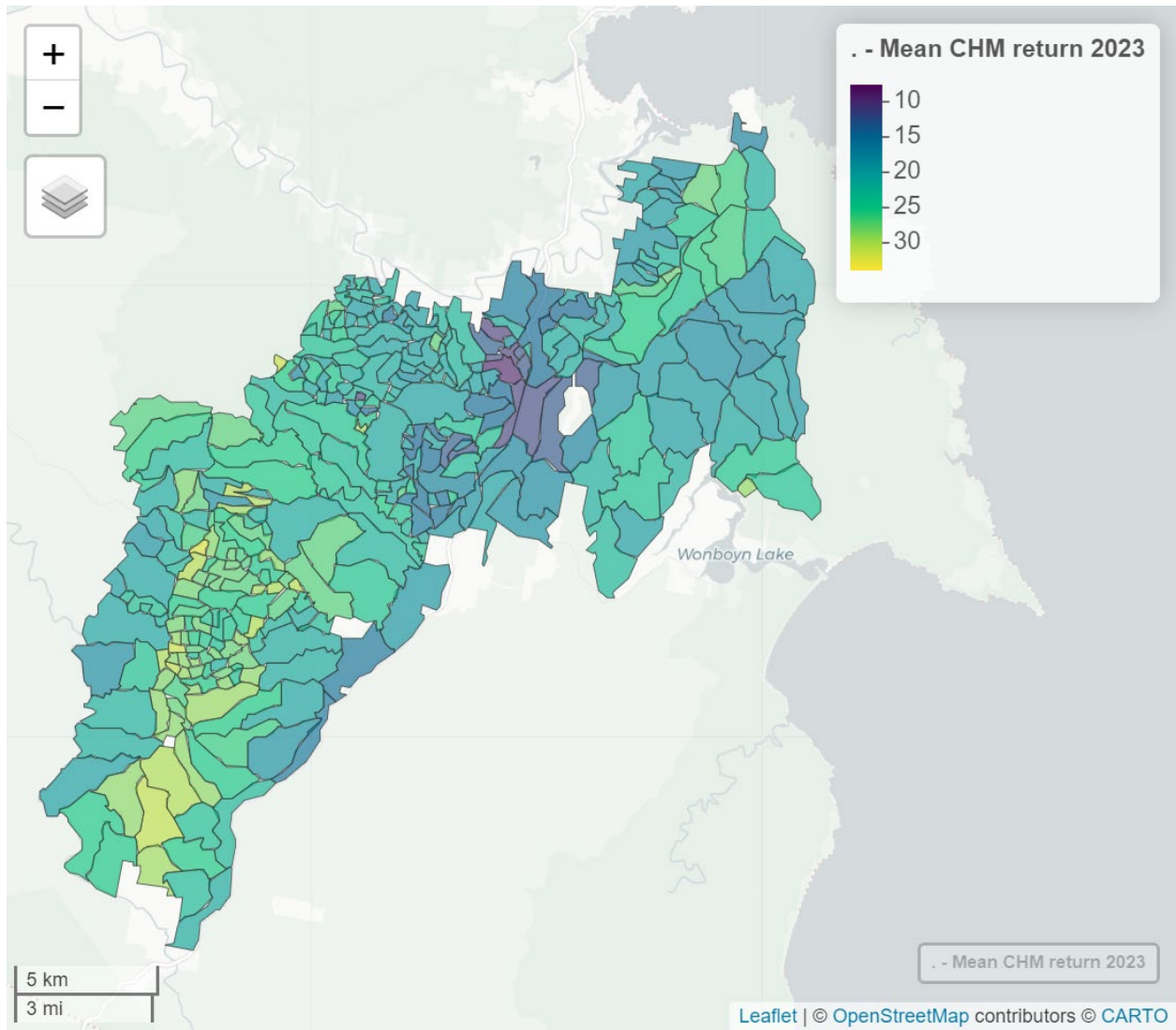


Figure A8.7 - Maps of Forest Capture Regions, polygons grouped by LLA (Eden).

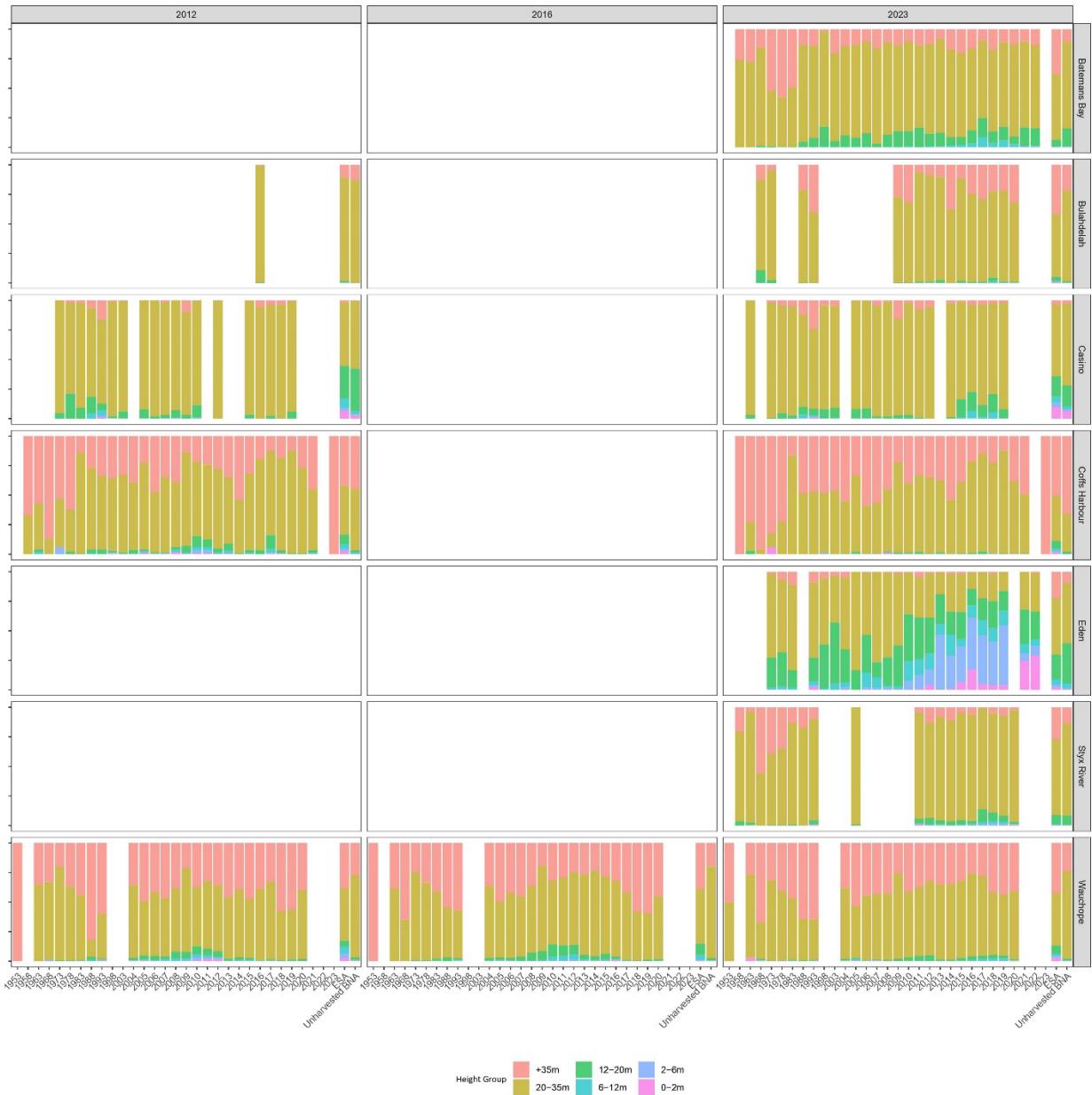


Figure A9 - Stacked plots of height classifications for multiple ALS captures with x-axis indicating year of last harvest and vertical panels indicating forest capture region.



Figure A10 – Stacked plots of height classifications for multiple ALS captures with x-axis indicating harvested, unharvested, or reason for exclusion and vertical panels indicating separate forest capture region.



Figure A11 – Stacked plots of height classifications for all 2023 ALS captures with x-axis indicating harvested, unharvested, or reason for exclusion and vertical panels indicating separate forest capture region.

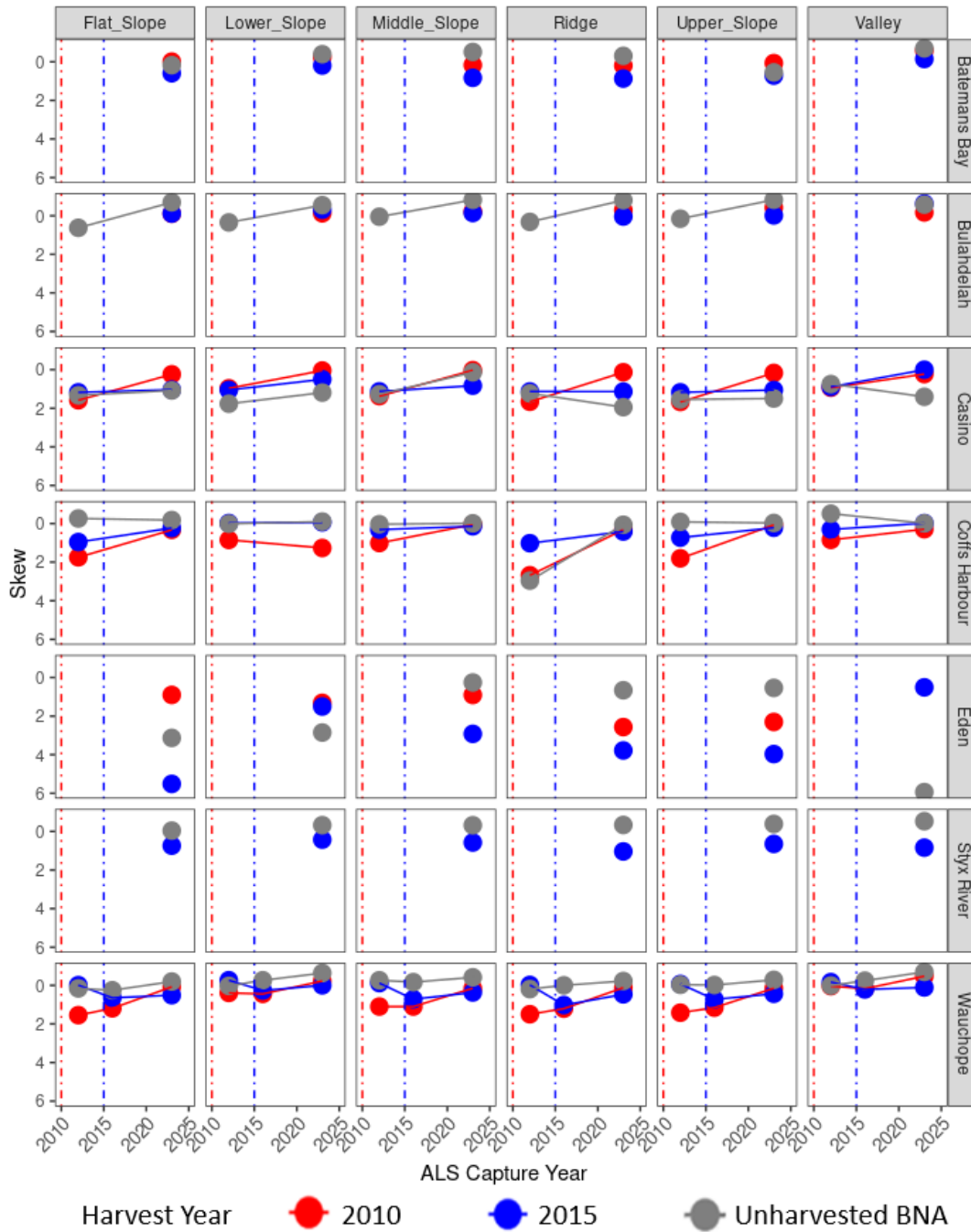


Figure A12 - Plots outlining skew of returns for multiple ALS captures and whether areas were harvested or unharvested with horizontal panels indicating different slope classifications and vertical panels indicating different forest capture regions

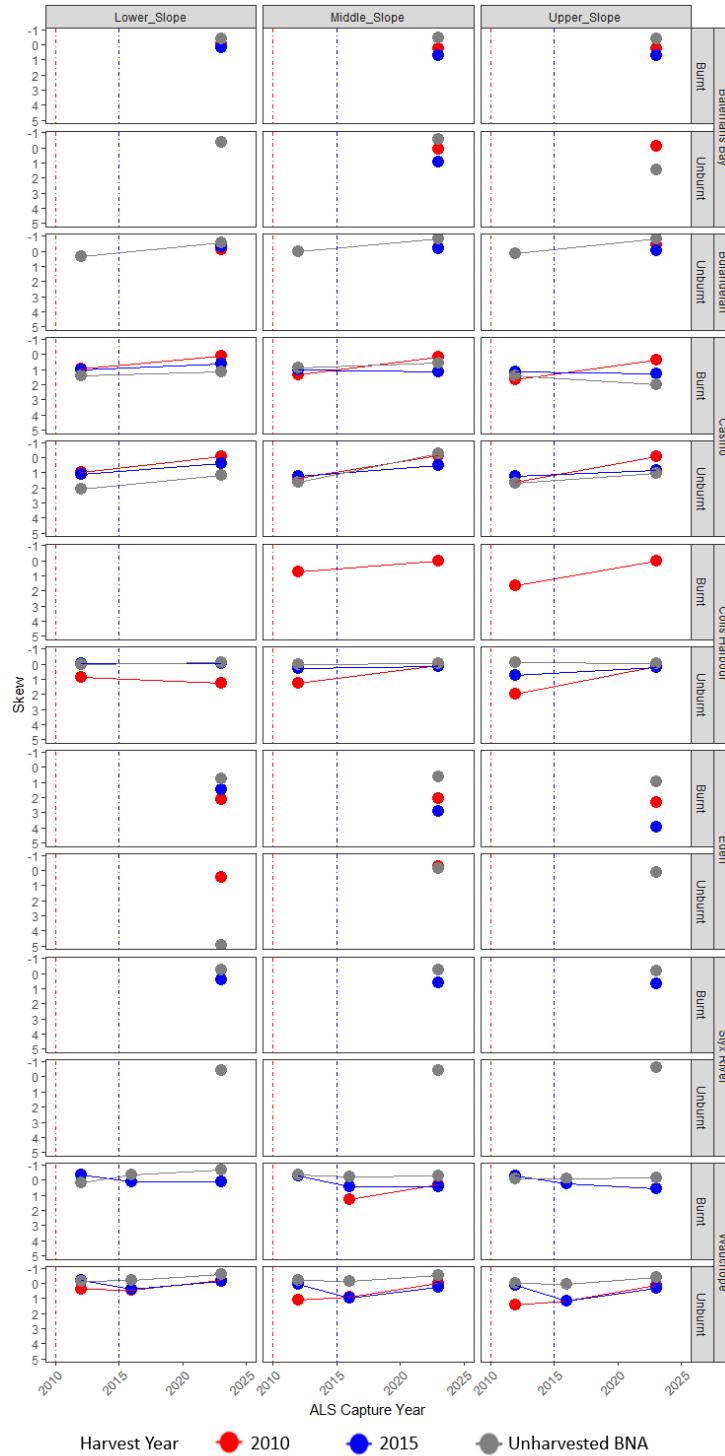


Figure A13 - Plots outlining skew of returns for multiple ALS captures and whether areas were harvested or unharvested with horizontal panels indicating different slope classifications and vertical panels indicating different forest capture regions and burn status.

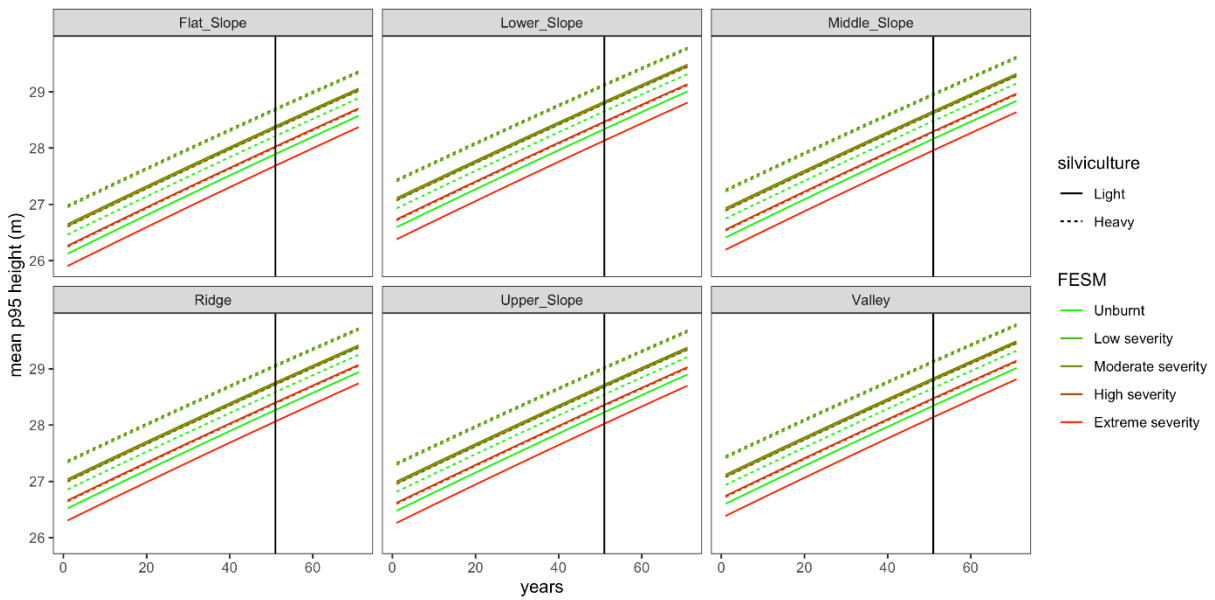


Figure A14 - This figure models canopy top height recovery for Batemans Bay across different slope types for each harvest group and FESM class. Preceding the vertical line are the model's account of data and following is the model's prediction of p95 height. Note that predictions appear linear because p95 does not converge on the asymptotic value equal to the 99th percentile of p95.

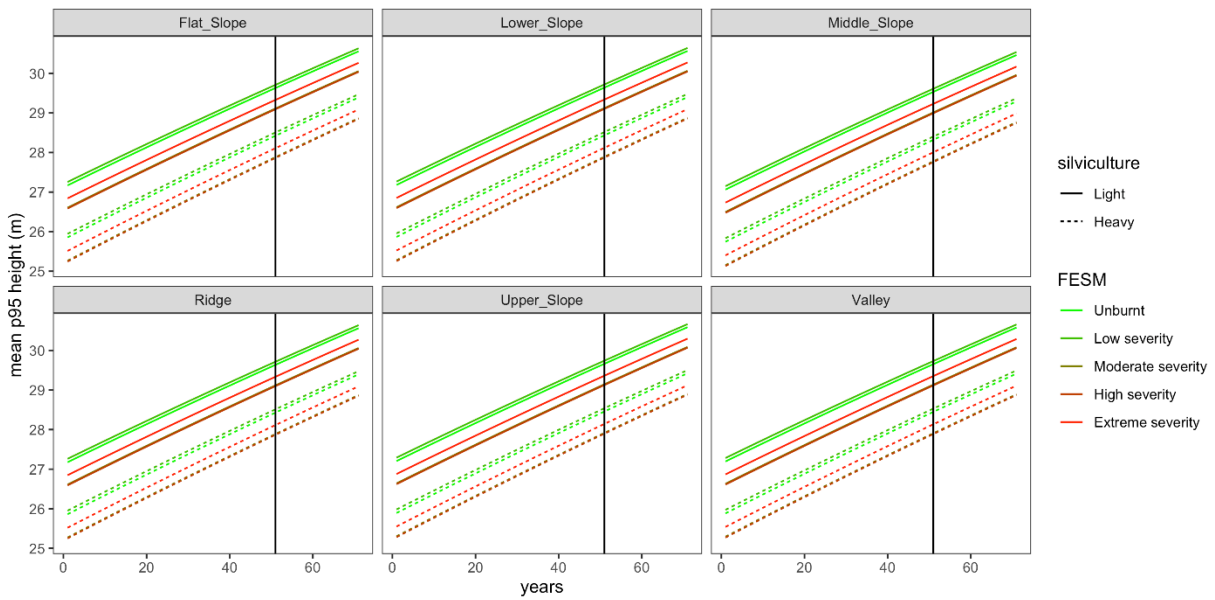


Figure A15 - Modelling of canopy top height recovery for Casino

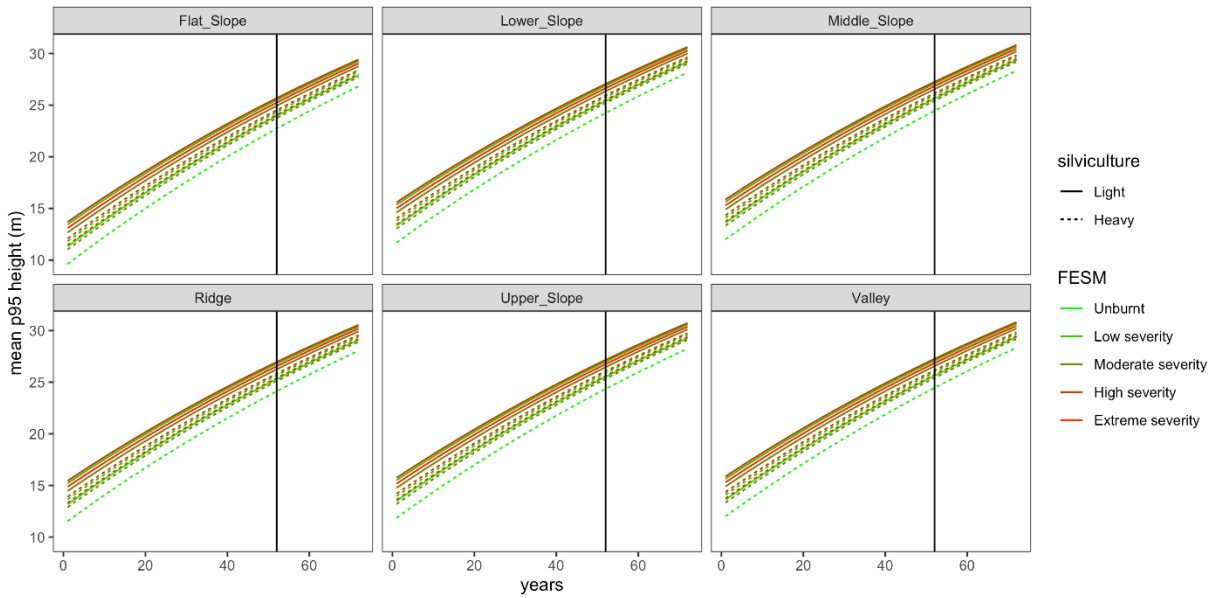


Figure A16 - Modelling of canopy top height recovery for Eden

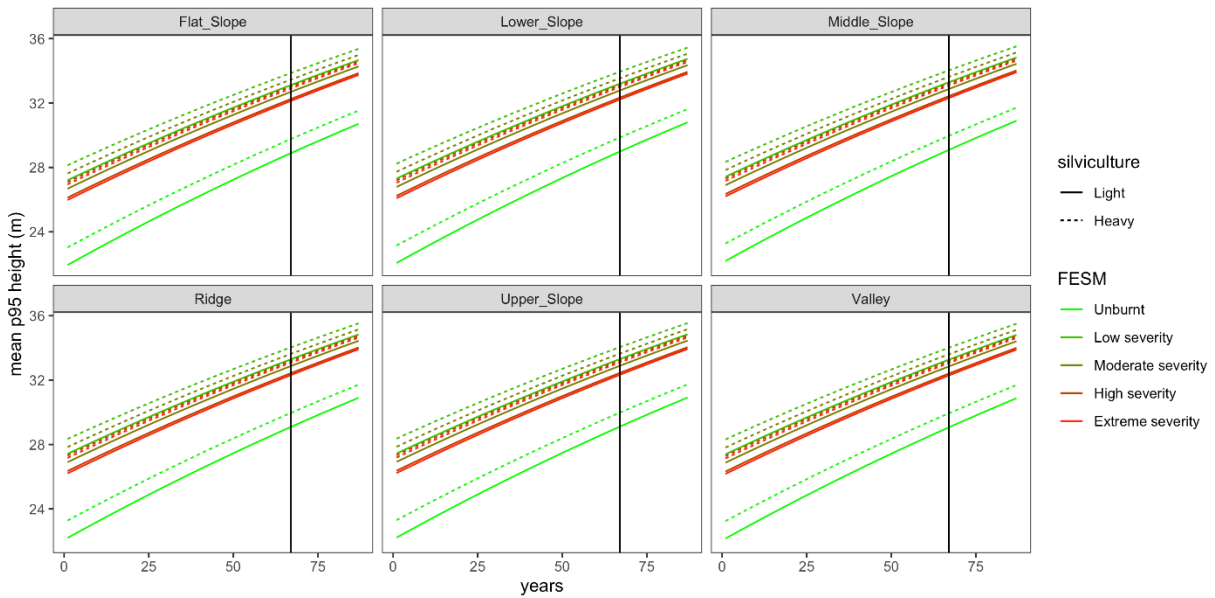


Figure A17 - Modelling of canopy top height recovery for Styx River

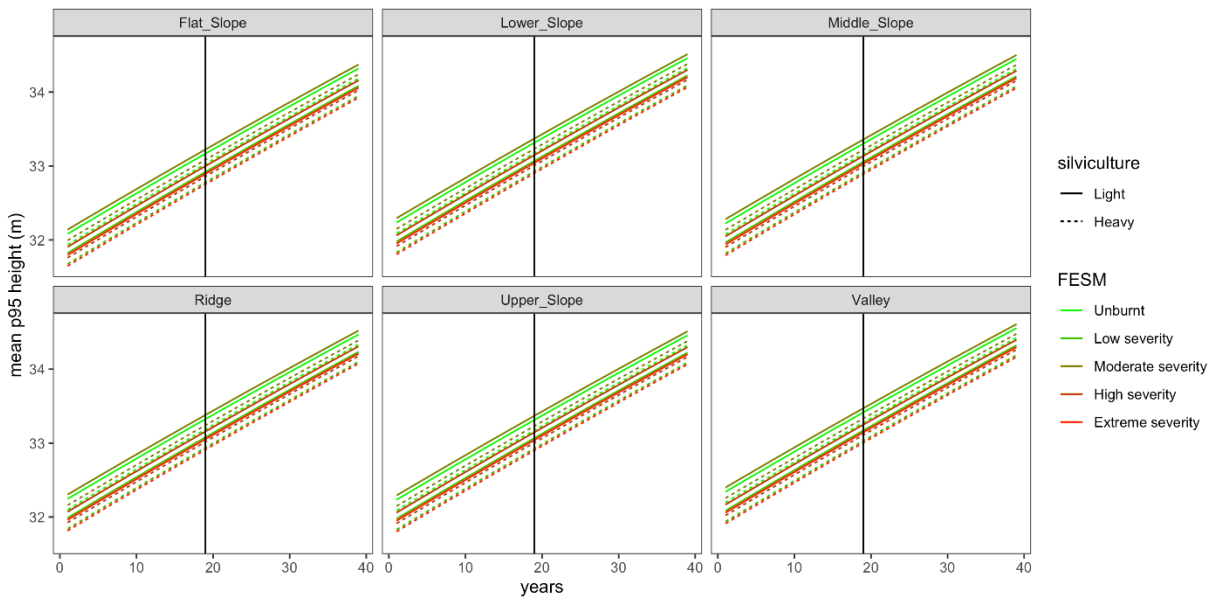


Figure A18 - Modelling of canopy top height recovery for Wauchope

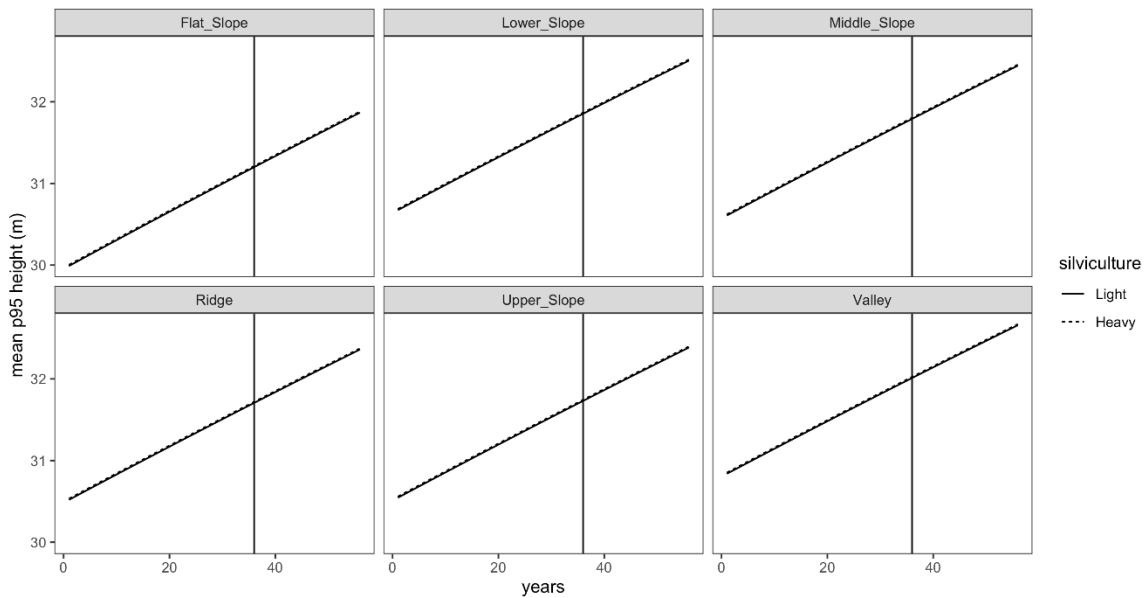
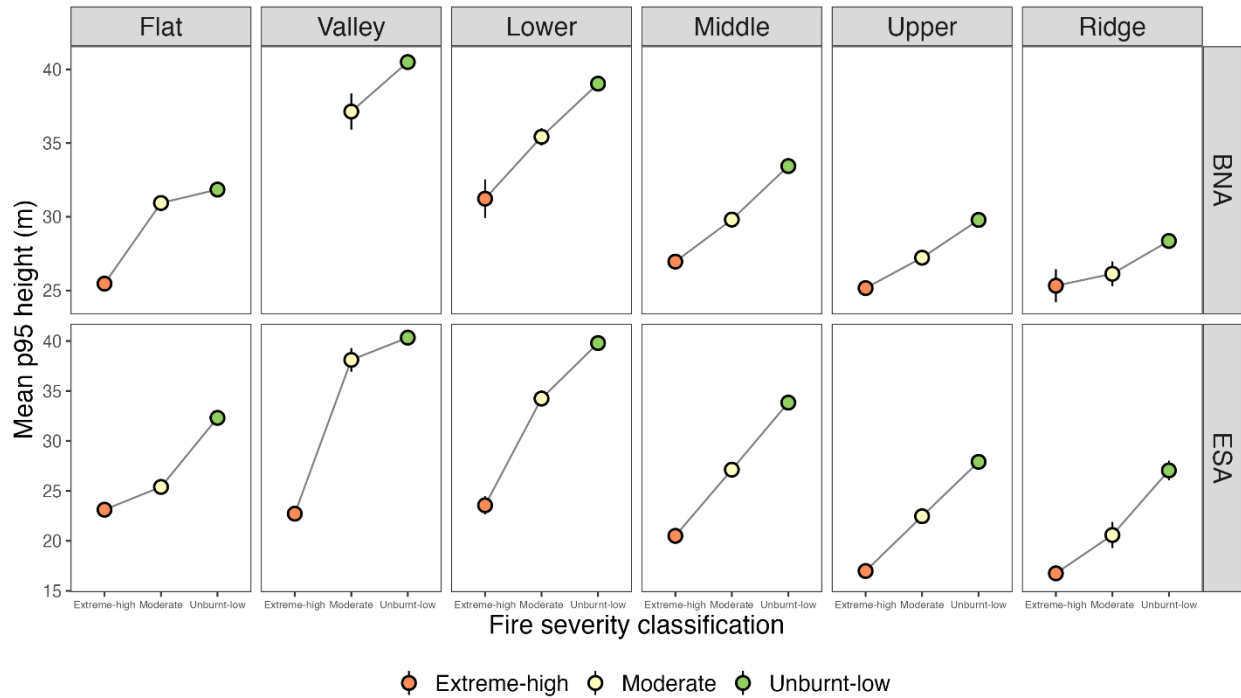
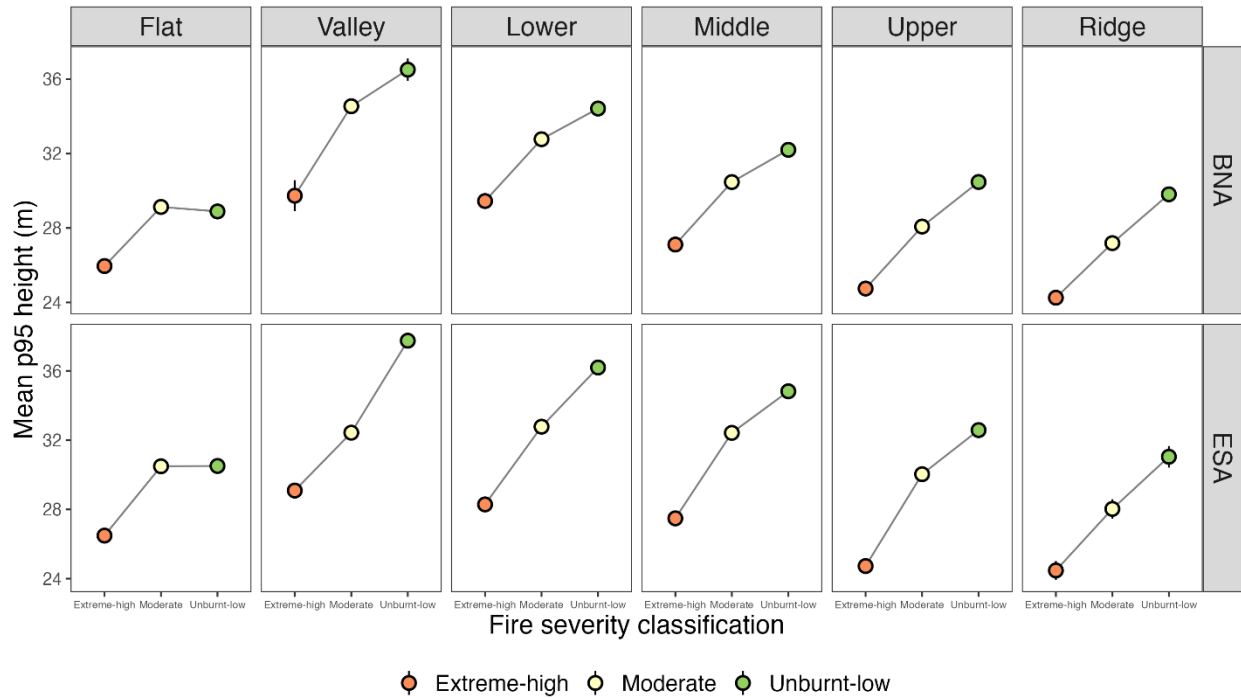


Figure A19 - Modelling of canopy top height recovery for Bulahdelah. Note that FESM class is absent in this figure because there is no FESM class data in the dataset.



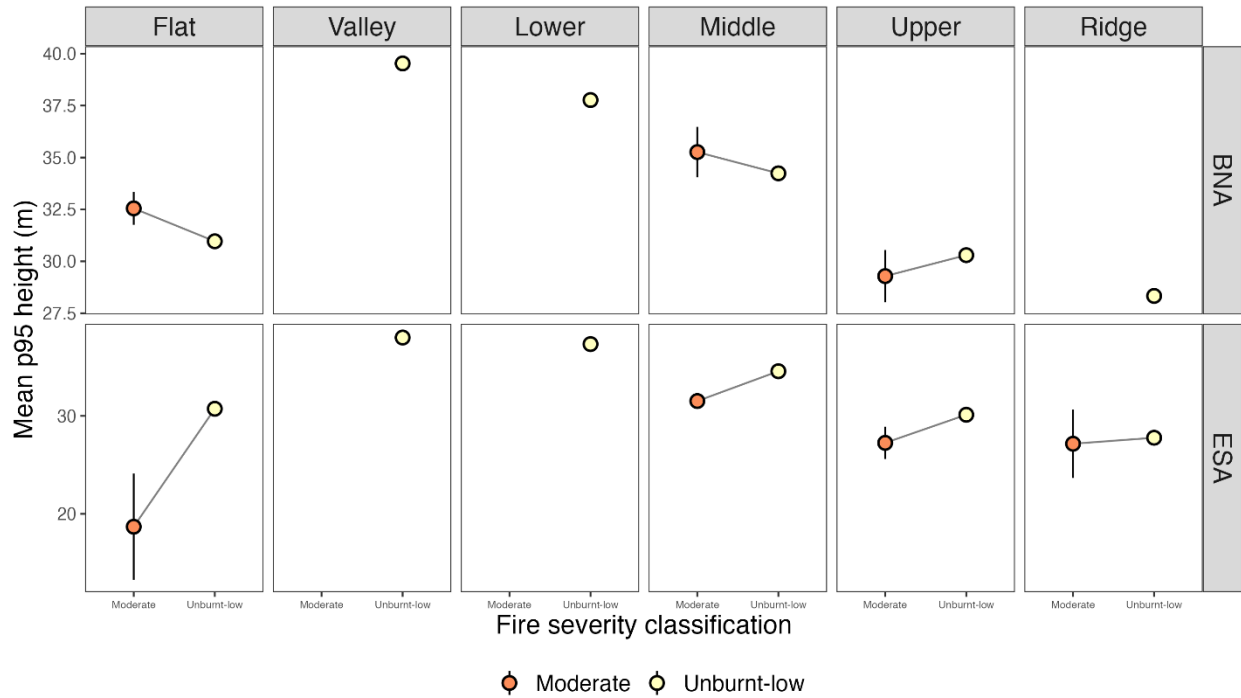
(Region: Wauchope)

Figure A20. Mean p95 height returns for the Wauchope region as measured in the 2023 ALS capture. Points represent mean values and error bars represent standard errors. Landform slope class is presented across horizontal panels and base net area (BNA) vs. environmentally significant area (ESA) status is shown on vertical panels. FESM is categorised into three categories shown in separate colours. Note that although we show the mean values, each region is composed of varying landform features (see Figure A7 for slope composition within each region) and fire severity impacts (see Figure A1 for FESM composition within each region). These data are the companion data that match the Eden data shown in Figure 11 of the main report.



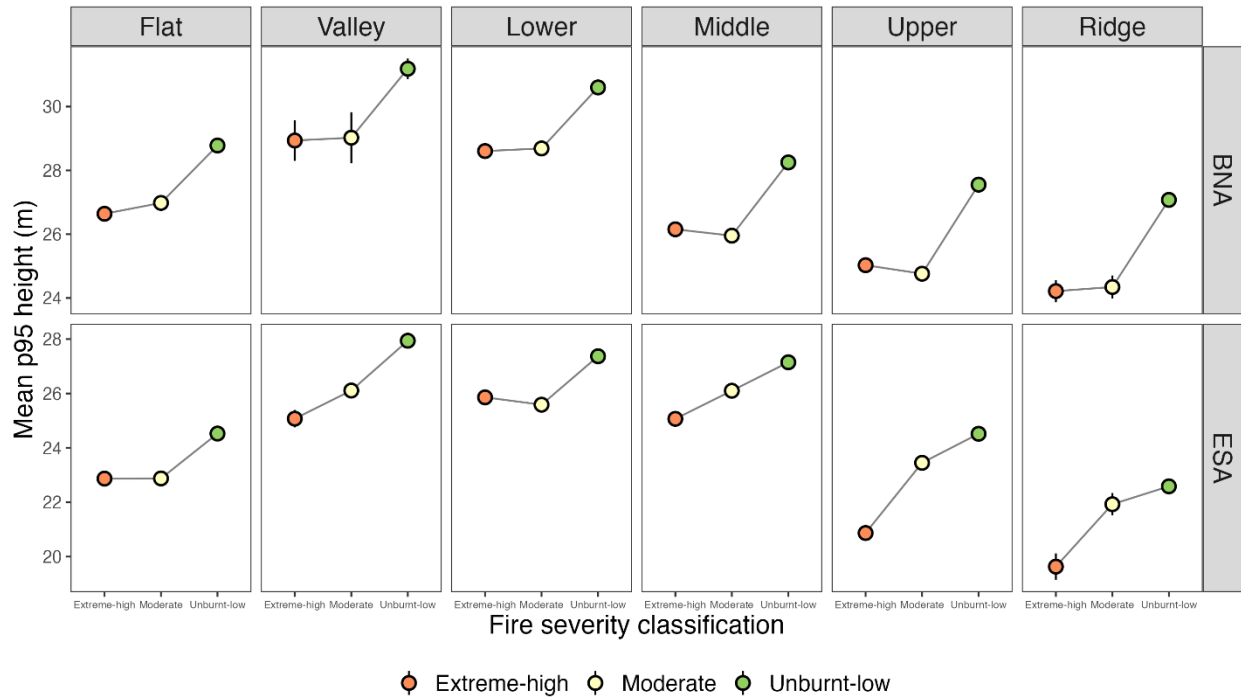
(Region: Styx River)

Figure A21. Mean p95 height returns for the Styx River region as measured in the 2023 ALS capture. Points represent mean values and error bars represent standard errors. Landform slope class is presented across horizontal panels and base net area (BNA) vs. environmentally significant area (ESA) status is shown on vertical panels. FESM is categorised into three categories shown in separate colours. Note that although we show the mean values, each region is composed of varying landform features (see Figure A7 for slope composition within each region) and fire severity impacts (see Figure A1 for FESM composition within each region). These data are the companion data that match the Eden data shown in Figure 11 of the main report.



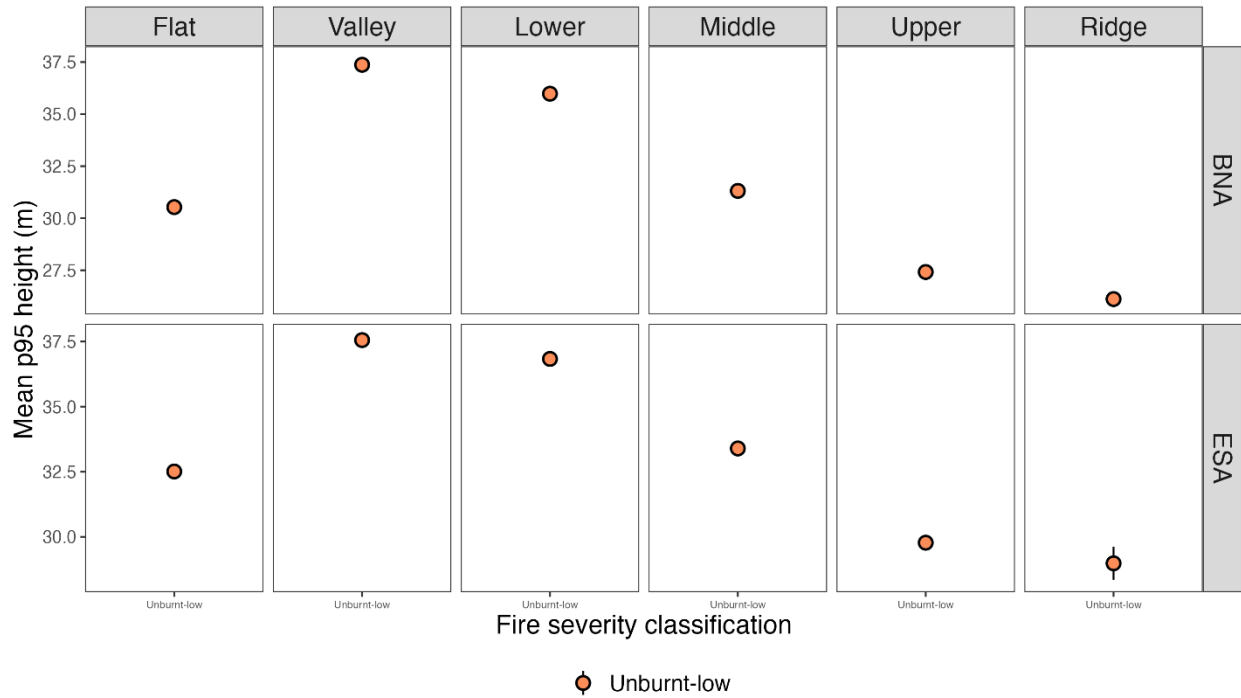
(Region: Coffs Harbour)

Figure A22. Mean p95 height returns for the Coffs Harbour region as measured in the 2023 ALS capture. Points represent mean values and error bars represent standard errors. Landform slope class is presented across horizontal panels and base net area (BNA) vs. environmentally significant area (ESA) status is shown on vertical panels. FESM is categorised into three categories shown in separate colours. Note that although we show the mean values, each region is composed of varying landform features (see Figure A7 for slope composition within each region) and fire severity impacts (see Figure A1 for FESM composition within each region). These data are the companion data that match the Eden data shown in Figure 11 of the main report.



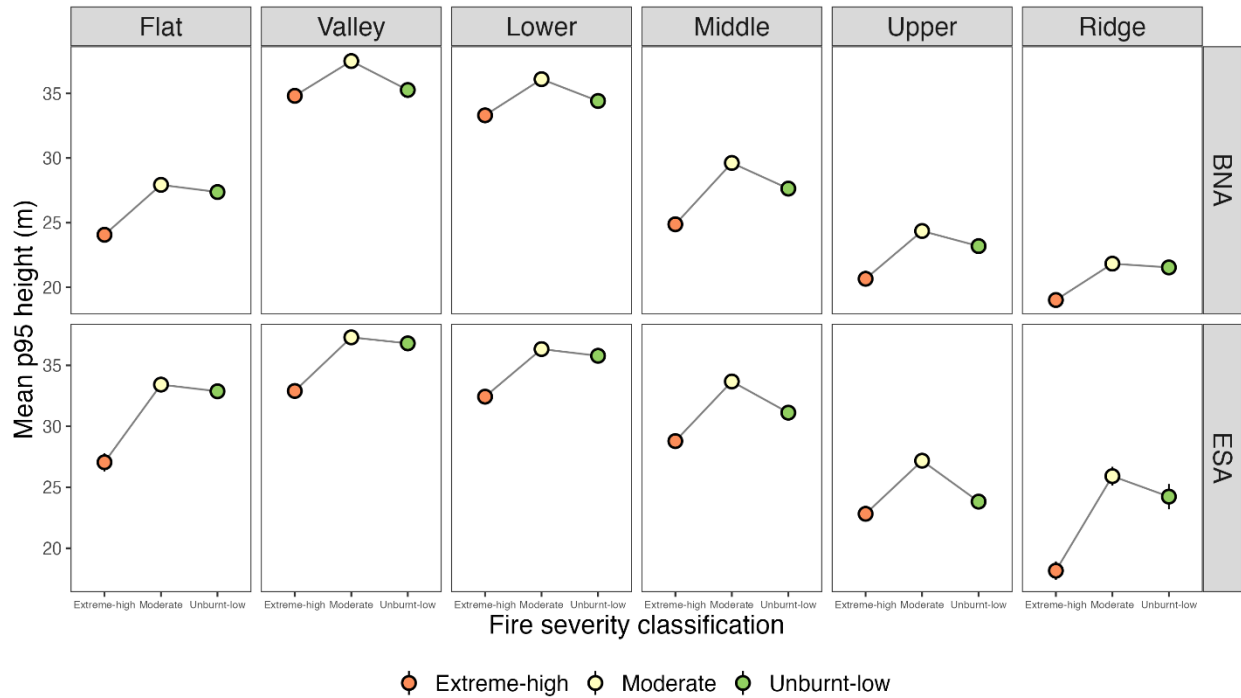
(Region: Casino)

Figure A23. Mean p95 height returns for the Casino region as measured in the 2023 ALS capture. Points represent mean values and error bars represent standard errors. Landform slope class is presented across horizontal panels and base net area (BNA) vs. environmentally significant area (ESA) status is shown on vertical panels. FESM is categorised into three categories shown in separate colours. Note that although we show the mean values, each region is composed of varying landform features (see Figure A7 for slope composition within each region) and fire severity impacts (see Figure A1 for FESM composition within each region). These data are the companion data that match the Eden data shown in Figure 11 of the main report.



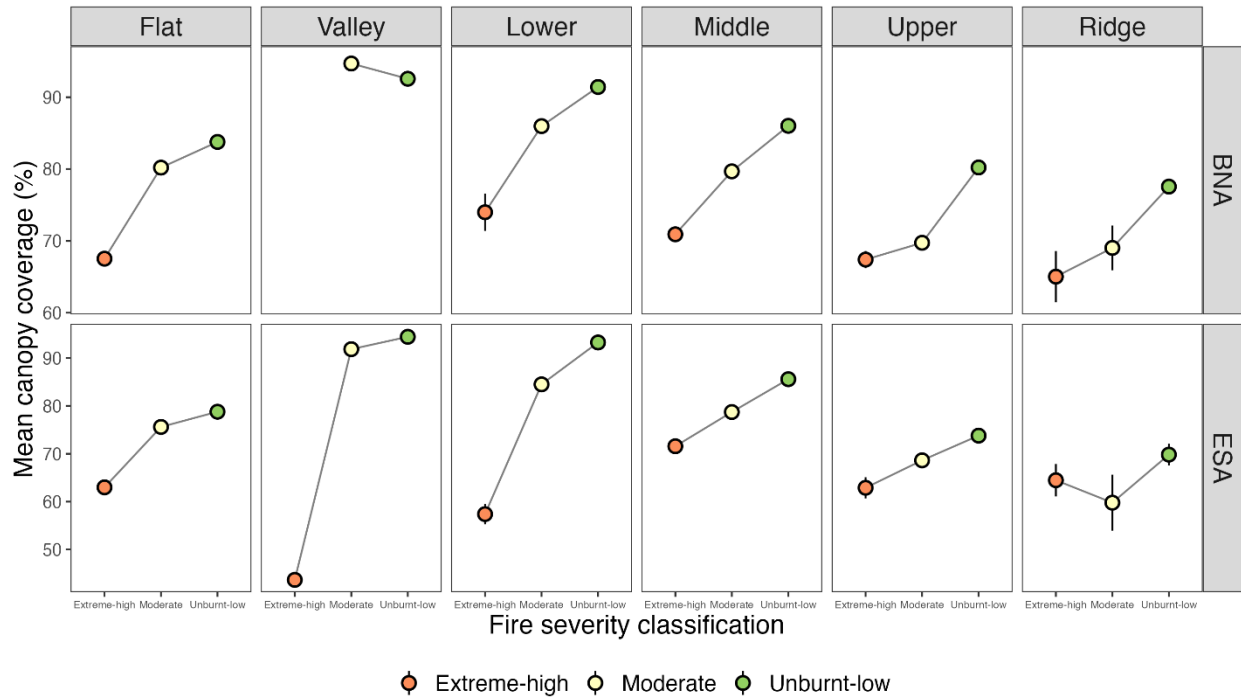
(Region: Bulahdelah)

Figure A24. Mean p95 height returns for the Bulahdelah region as measured in the 2023 ALS capture. Points represent mean values and error bars represent standard errors. Landform slope class is presented across horizontal panels and base net area (BNA) vs. environmentally significant area (ESA) status is shown on vertical panels. FESM is categorised into three categories shown in separate colours. Note that although we show the mean values, each region is composed of varying landform features (see Figure A7 for slope composition within each region) and fire severity impacts (see Figure A1 for FESM composition within each region). These data are the companion data that match the Eden data shown in Figure 11 of the main report.



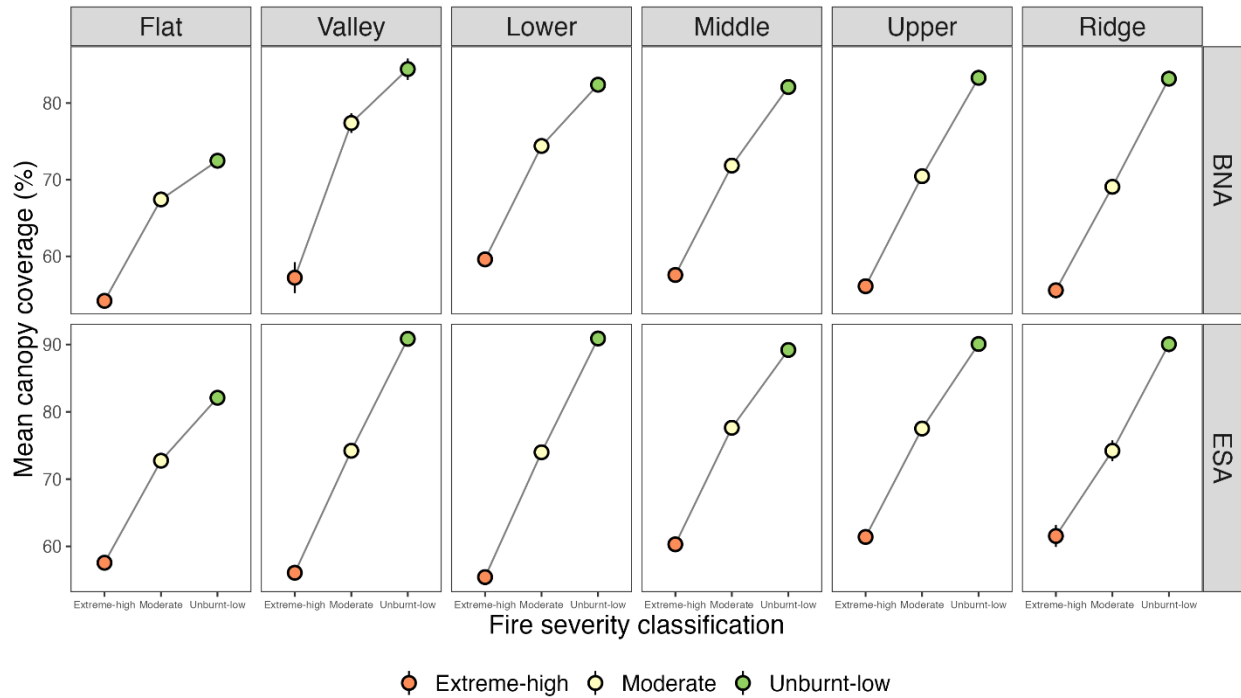
(Region: Batesman Bay)

Figure A25. Mean p95 height returns for the Batemans Bay region as measured in the 2023 ALS capture. Points represent mean values and error bars represent standard errors. Landform slope class is presented across horizontal panels and base net area (BNA) vs. environmentally significant area (ESA) status is shown on vertical panels. FESM is categorised into three categories shown in separate colours. Note that although we show the mean values, each region is composed of varying landform features (see Figure A7 for slope composition within each region) and fire severity impacts (see Figure A1 for FESM composition within each region). These data are the companion data that match the Eden data shown in Figure 11 of the main report.



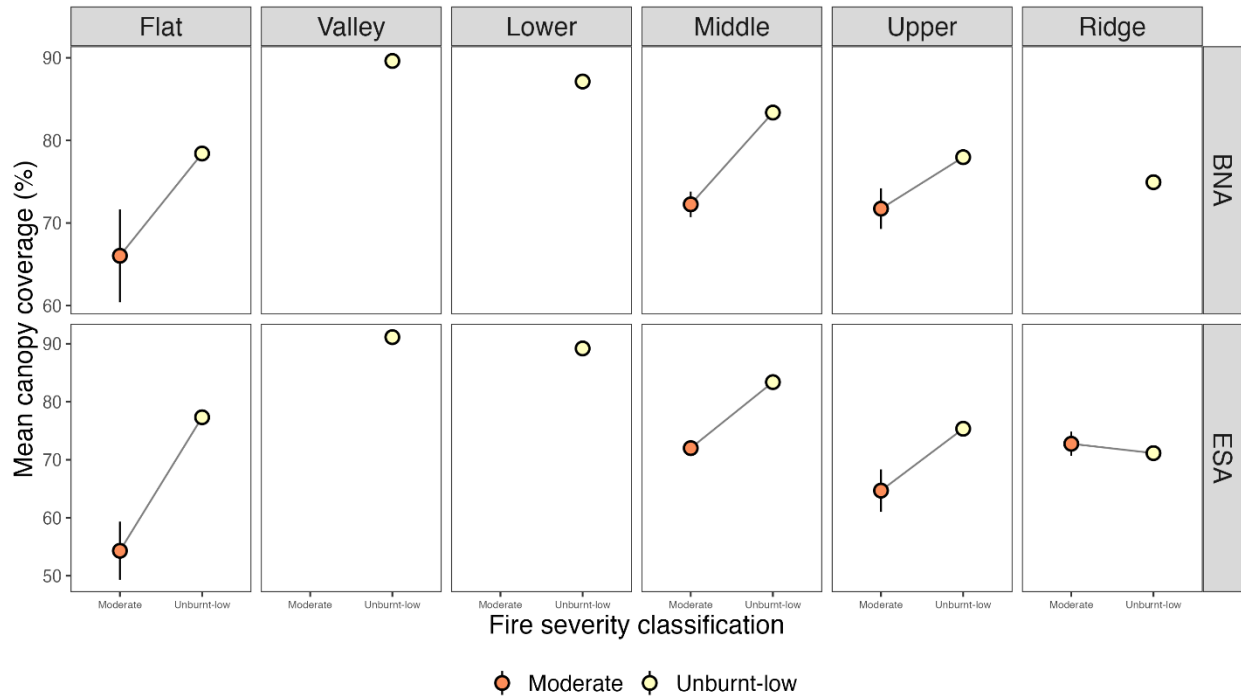
(Region: Wauchope)

Figure A26. Mean canopy coverage for the Wauchope region as measured in the 2023 ALS capture. Points represent mean values and error bars represent standard errors. Landform slope class is presented across horizontal panels and base net area (BNA) vs. environmentally significant area (ESA) status is shown on vertical panels. FESM is categorised into three categories shown in separate colours. Note that although we show the mean values, each region is composed of varying landform features (see Figure A7 for slope composition within each region) and fire severity impacts (see Figure A1 for FESM composition within each region). These data are the companion data that match the Eden data shown in Figure 20 of the main report.



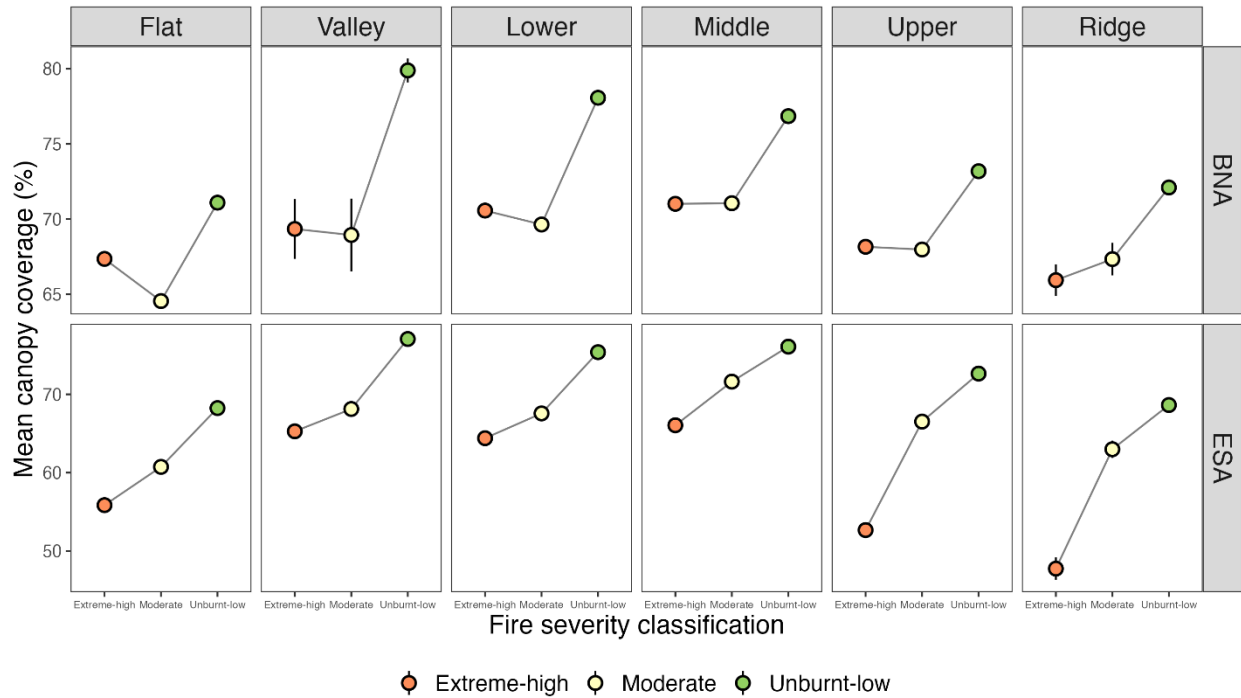
(Region: Styx River)

Figure A27. Mean canopy coverage for the Styx River region as measured in the 2023 ALS capture. Points represent mean values and error bars represent standard errors. Landform slope class is presented across horizontal panels and base net area (BNA) vs. environmentally significant area (ESA) status is shown on vertical panels. FESM is categorised into three categories shown in separate colours. Note that although we show the mean values, each region is composed of varying landform features (see Figure A7 for slope composition within each region) and fire severity impacts (see Figure A1 for FESM composition within each region). These data are the companion data that match the Eden data shown in Figure 20 of the main report.



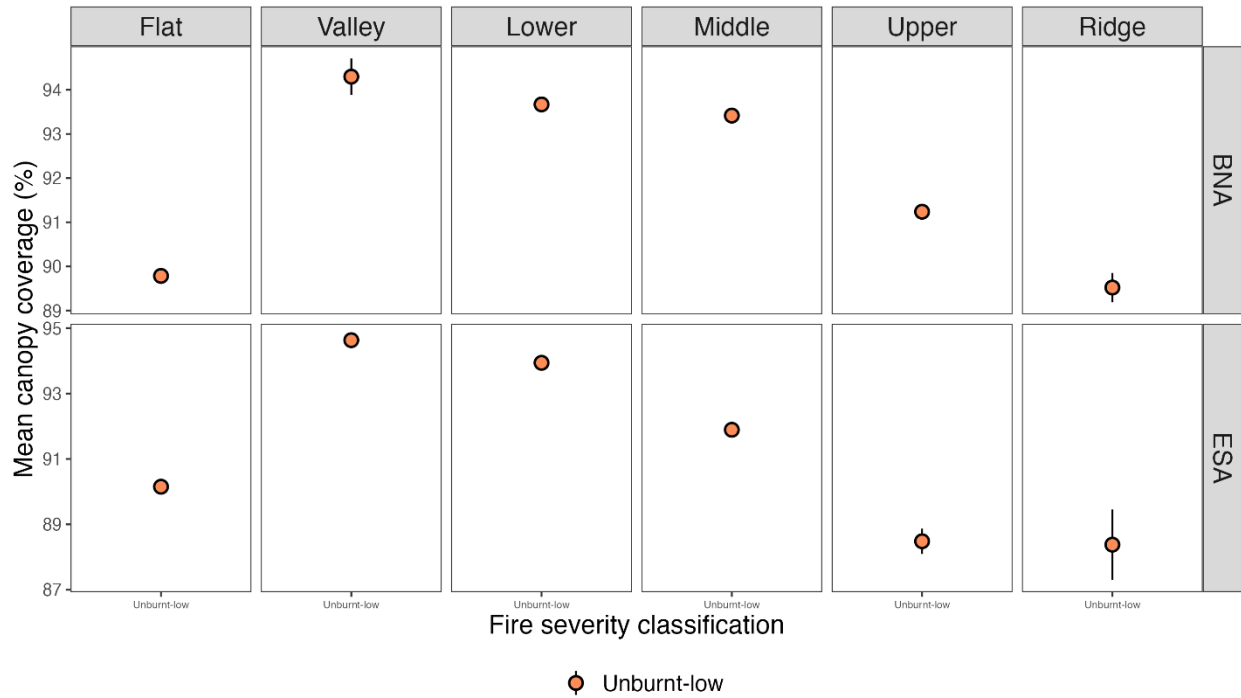
(Region: Coffs Harbour)

Figure A28. Mean canopy coverage for the Coffs Harbour region as measured in the 2023 ALS capture. Points represent mean values and error bars represent standard errors. Landform slope class is presented across horizontal panels and base net area (BNA) vs. environmentally significant area (ESA) status is shown on vertical panels. FESM is categorised into three categories shown in separate colours. Note that although we show the mean values, each region is composed of varying landform features (see Figure A7 for slope composition within each region) and fire severity impacts (see Figure A1 for FESM composition within each region). These data are the companion data that match the Eden data shown in Figure 20 of the main report.



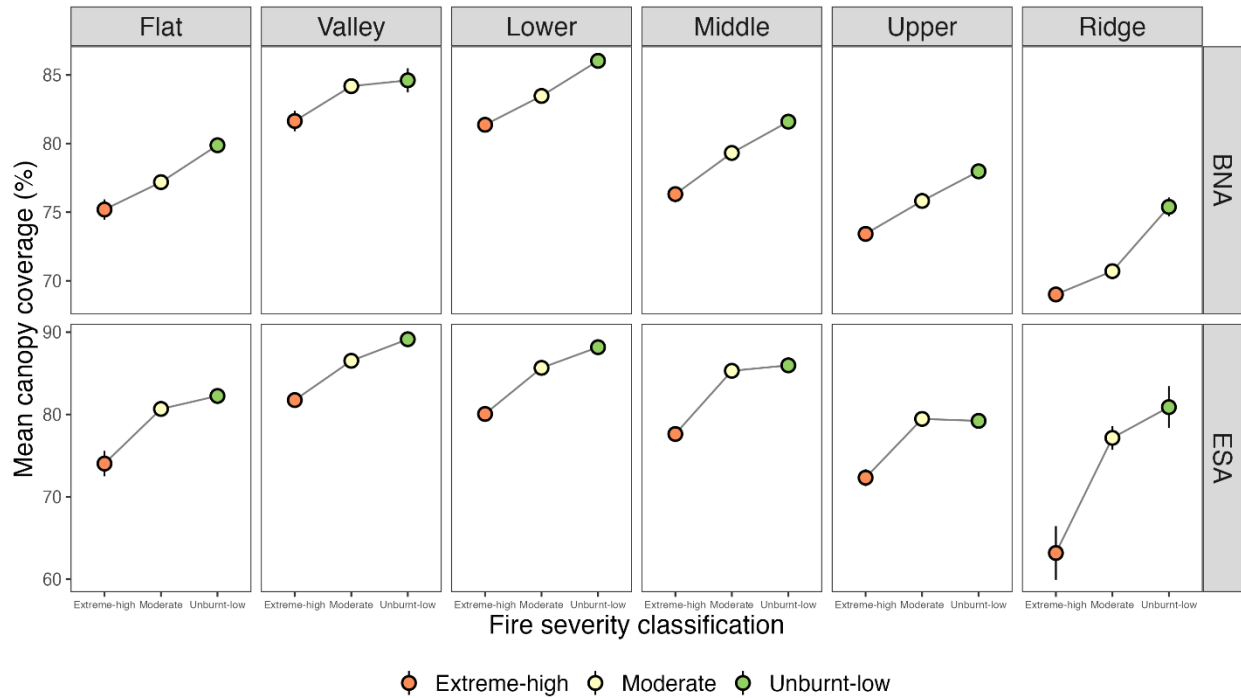
(Region: Casino)

Figure A29. Mean canopy coverage for the Casino region as measured in the 2023 ALS capture. Points represent mean values and error bars represent standard errors. Landform slope class is presented across horizontal panels and base net area (BNA) vs. environmentally significant area (ESA) status is shown on vertical panels. FESM is categorised into three categories shown in separate colours. Note that although we show the mean values, each region is composed of varying landform features (see Figure A7 for slope composition within each region) and fire severity impacts (see Figure A1 for FESM composition within each region). These data are the companion data that match the Eden data shown in Figure 20 of the main report. These data are the companion data that match the Eden data shown in Figure 20 of the main report.



(Region: Bulahdelah)

Figure A30. Mean canopy coverage for the Bulahdelah region as measured in the 2023 ALS capture. Points represent mean values and error bars represent standard errors. Landform slope class is presented across horizontal panels and base net area (BNA) vs. environmentally significant area (ESA) status is shown on vertical panels. FESM is categorised into three categories shown in separate colours. Note that although we show the mean values, each region is composed of varying landform features (see Figure A7 for slope composition within each region) and fire severity impacts (see Figure A1 for FESM composition within each region). These data are the companion data that match the Eden data shown in Figure 20 of the main report.



(Region: Batesman Bay)

Figure A31. Mean canopy coverage for the Batemans Bay region as measured in the 2023 ALS capture. Points represent mean values and error bars represent standard errors. Landform slope class is presented across horizontal panels and base net area (BNA) vs. environmentally significant area (ESA) status is shown on vertical panels. FESM is categorised into three categories shown in separate colours. Note that although we show the mean values, each region is composed of varying landform features (see Figure A7 for slope composition within each region) and fire severity impacts (see Figure A1 for FESM composition within each region). These data are the companion data that match the Eden data shown in Figure 20 of the main report.

Appendix B: LiDAR in forestry research: a literature review

1. Introduction

LiDAR (Light Detection and Ranging) is a remote sensing technology that has greatly improved our ability to measure forest structure and dynamics at the level of individual trees and over large areas (Atkins et al., 2023; Estrada et al., 2023; Lefsky et al., 2002; Matasci et al., 2018; Whelan et al., 2023; White et al., 2017; Wulder et al., 2008). Due to technological and theoretical breakthroughs, airborne LiDAR (ALS) and terrestrial LiDAR (TLS) technologies are being implemented in various and novel ways in ecological research, and much of the literature explores the effectiveness of LiDAR alongside aerial imagery and traditional field-based methods of collecting forest data (Bouvier et al., 2015; Coops et al., 2021; Haywood & Stone, 2011).

It is also well-documented that although LiDAR can provide accurate information about forest dynamics, it comes with the high cost of enormous data size and bears the difficulties associated with sharing and working with data this immense (Atkins et al., 2023). Currently, there is a vigorous effort in the field to navigate this issue so that appropriate ecological decisions can be made promptly considering climate change and restoration efforts (Almeida et al., 2019; Bartels et al., 2016; Bolton et al., 2015; Estrada et al., 2023; Hislop & Stone, 2023; Mazlan et al., 2023).

In the context of New South Wales state forests, using ALS to analyse structural changes following disturbances has garnered significant attention due to its implications for forest management, ecological stability, biodiversity conservation, and species richness. Understanding the methodologies employed in mapping ALS metrics onto forest structure attributes is crucial for analysing ALS data accurately and efficiently.

This literature review aims to explore the existing literature on LiDAR applications in forestry research. The primary objectives include identifying key concepts used in forestry research, mapping the research objectives of studies investigating LiDAR's use in forestry, identifying common methodologies for estimating forest structural diversity, understanding the types of ancillary data used in conjunction with LiDAR, and exploring computational models and statistical analyses applied to LiDAR and ancillary data. By achieving these goals, this review seeks to provide a broad understanding of the current state of knowledge surrounding LiDAR's use in forest research and management.

2. Methods

2.1 Search and inclusion strategies

Published findings about the use of LiDAR in forestry applications were collected by searching Google Scholar. Keywords used included terms concerning LiDAR, forest structure, forest recovery dynamics, and data analysis approaches.

Table B1. Search terms used to access publications about LiDAR in forestry applications

Database	Search Terms
Google Scholar	AND/OR(LiDAR, airborne LiDAR, ALS, terrestrial LiDAR, TLS), OR(canopy, canopy height, canopy height model, forest structure, forest structural complexity, forest structural diversity, leaf area density, vegetation density), OR(area-based approach, voxel-based approach, voxel, voxelisation), OR(forest recovery, forest regeneration, fire disturbance, post-fire recovery, silvicultural disturbance), OR(parametric, non-parametric, deep learning, machine learning, random forest), OR(fire risk, fire severity, fuel load, wildfire, wildfire risk), OR(Australia, NSW, eucalypt forest)

The searches produced a collection of 99 peer reviewed articles (including 84 research articles, 5 application articles, and 10 review articles), 2 technical reports, 1 conference paper, and 1 book chapter. Search terms were qualitatively screened based on titles, abstracts, keywords, and study approaches. Studies that involved forestry research but did not specifically include the use LiDAR technology were excluded. For example, studies that only evaluated the use of other remote sensing technologies, such as Landsat and remote imaging in forestry applications, were excluded. Studies that focused on tree species classification rather than forest structural attributes were also excluded, along with studies that investigated forest recovery trends without using LiDAR. The qualitative screening reduced the number of studies to 83.

3. Results

















3.1 Forest sites


The included articles used data from various forest sites around the world: USA (16 studies); Australia (12 studies); Brazil (9 studies); China and Finland (5 studies); Italy (4 studies); Germany, Poland, Spain, and New Zealand (2 studies); and Austria, Chile, France, Norway, Panama, South Korea, and Switzerland (1 study). Most of the included articles investigated only one forest site. However, four articles used point clouds from multiple sites, and nine articles did not examine any forest site on account of exploring LiDAR from a theoretical viewpoint or through technical applications.

3.2 Thematic analysis

One of the first tasks was classifying the broad themes in LiDAR and forestry research. LiDAR is a versatile technology used to answer various questions concerning trees, forests, and ecological management, so articles often involve multiple topics corresponding to their specific research questions. For example, some articles compare the effectiveness of airborne LiDAR to other point clouds (Arkin et al., 2023; Ferrara et al., 2023), and others estimate forest structure using a combination of LiDAR and aerial imagery (Arkin et al., 2023; Blackman & Yuan, 2020; Matasci et al., 2018; Viana-Soto et al., 2022; White et al., 2022). Table B2 shows the themes compiled from reading the articles' introduction, methods, and results sections. The themes were represented by emoji graphics to facilitate the ease of organising the literature. Figure B1 shows the frequency of themes in this review.

Table B2. Theme legend and topics

Graphic	Theme(s)	Examples of topics and keywords within theme
	Forest structure	Forest structural diversity (FSD), canopy structural complexity, canopy height model, canopy layers, understory structural complexity, understory vegetation density, species richness, height metrics, distribution metrics, leaf area index (LAI), leaf area density (LAD), volume, edge effects, stand age distribution, size class distribution, stand basal area, skewness, standard deviation, coefficient of variation
	Individual tree attributes	Tree detection methods, tree crown delineation, height metrics, diameter metrics, position metrics, shape metrics, volume estimation, biomass estimation, species classification, individual tree mapping, basal area
	Urban forests	Urban canopy coverage, urban development, urban vegetation, vegetation indicators, object-based image analysis
	Forest regrowth / Tree regeneration	Forest landscape restoration, growth indicators, recovery rates, recovery dynamics
	Aerial imagery	RGB imagery, hyperspectral imagery, Sentinel-2 satellite imagery, Landsat time series, GIS
	Airborne LiDAR	High-density ALS, low-density ALS, ALS point clouds
	Terrestrial LiDAR	High-density TLS, low-density TLS, TLS point clouds
	Point clouds	LiDAR point clouds, photogrammetry point clouds, 2D point clouds, 3D point clouds
	Multitemporal analysis	Multitemporal LiDAR, Landsat time series
	Topography	Digital terrain model, digital elevation model
	Fire	Fire disturbance, fire severity, fuel estimation, fuel load, wildfire risk, canopy fuel, surface fuel, recovery time, recovery dynamics, stand-replacing disturbance, snag detection, burn ratio
	Harvest	Silvicultural disturbance, harvest events, timber harvest, recovery time, recovery dynamics
	Climate	Drought, drought recovery, climate change
	Australia	Australian forest, eucalypt forest, eucalypt regeneration, 'Black Summer' wildfires
	Fauna	Species richness
	Analysis methods	Parametric, non-parametric, machine learning, deep learning, random forest, support vector machines, k-nearest neighbour, convolutional neural network, effective number of layers, regression, ordinary least squares regression (OLS), seemingly unrelated regression (SUR), partial least squares regression, Wilcoxon test
	Voxel-based analysis	Voxelisation, volume voxelisation, 3D point cloud, 3D volume, smoothing

	Construction	Construction industry, urban environments
---	--------------	---

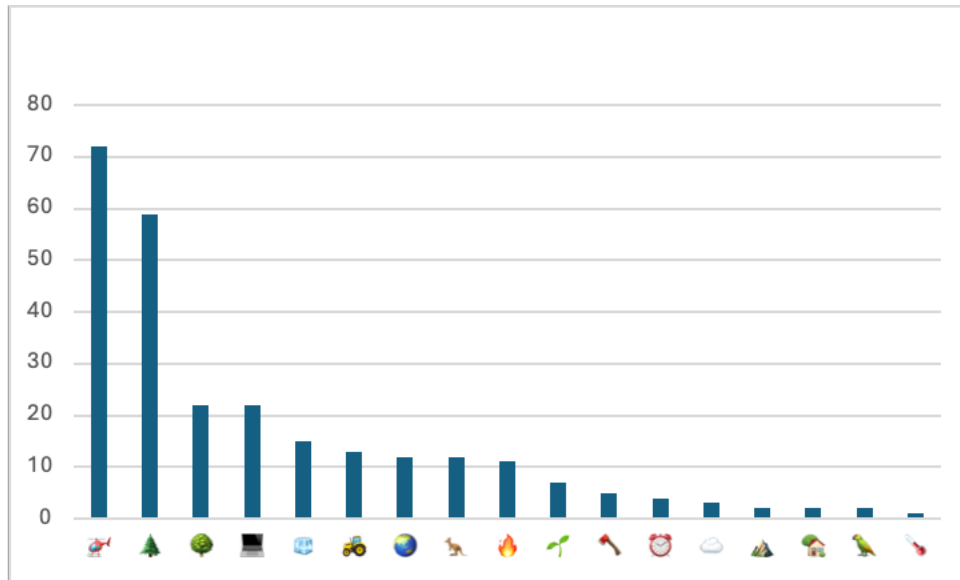


Figure B1 - Frequency of themes in articles. See Table B2 for graphics legend.

3.3 Primary methodologies







A key distinction extracted from this review is that LiDAR is used in three primary ways to analyse forest structure. First, the area-based approach (ABA) (see Table B3) aims to create a predictive model connecting ALS variables with a specific inventory attribute at chosen sample plot areas (White et al., 2017). The models derived from the ABA are typically based on metrics obtained from summarisations of individual LiDAR returns over these areas (Moran, 2018; Whelan et al., 2023). In this review, the ABA was found to be the most frequently used approach for utilising LiDAR in forestry research.













By contrast, the voxel-based approach (VBA) (see Table B4) uses metrics based on summarisation by volumetric pixel (Whelan et al., 2023). Although the VBA is also used to analyse forest structural diversity over large areas, it is not as widely known. Some evidence suggests that compared to the ABA, the VBA is more sensitive to horizontal and vertical forest structural complexity because the data is not limited to the first LiDAR returns (Whelan et al., 2023). For this reason, it captures the heterogeneity of sub-canopy vegetation relatively well. Other evidence suggests that a mixture of both approaches yields the best outcome (Blackburn, 2021).











The third approach, known as individual tree segmentation (ITS) or individual tree detection (ITD) (see Table B5), involves using LiDAR metrics to derive attributes of individual trees. This approach has applications in classifying tree species, identifying snags, measuring biomass, delineating tree crowns, and estimating crown structure, among others (Brolly et al., 2021; Casas et al., 2016; Chen et al., 2006; Karna et al., 2019; Mielcarek et al., 2018; Wilkes et al., 2023). While the literature refers to ITS as a separate LiDAR methodology, it is sometimes used alongside the ABA (Silva et al., 2022; Torrensan et al., 2016) and VBA (Knapp et al., 2021; Leiterer et al., 2012; Li et al., 2024; Pearse et al., 2018), depending on the research question under evaluation.












Patterns in analyses were identified across all three primary methodologies, and it was found that a significant variety of statistical approaches are used to correlate LiDAR data with field samples and forest inventory data. Parametric regression analyses such as linear regression, polynomial regression, ordinary least squares (OLS), partial least squares (PLS), and seemingly unrelated regression (SUR) were used in all three methodologies. Non-parametric machine learning (ML) methods were also used commonly, but the type of ML analyses varied based on approach. The ITS approach primarily uses support vector machines, artificial neural networks, and deep learning. Whereas the ABA approach relies more heavily on random forest algorithms, k-nearest neighbour, and convolutional neural networks (Estrada et al., 2023). Some studies also used a simple comparison of summary statistics such as mean height, skewness, and standard deviation, to calculate height parameters of forest areas (Bolten et al., 2015; Hillman et al., 2021 Szostak, 2020).

Table B3. Studies using an area-based (ABA) methodology

Author(s)	Year	Article type	Themes	Study area	Research objective	Primary methodology	Data types	Analysis methods
Adhikari, Montes & Peduzzi https://doi.org/10.3390/rs15051284	2023	Research		Chile	Forest structural diversity (FSD)	Area-based	ALS Inventory	Least Squares Regression Adaptive Least Absolute Shrinkage and Selection Operator (ALASSO) Generalised Additive Modeling Selection (GAMSEL) Random forest (RF)
Almeida et al. https://doi.org/10.1016/j.foreco.2019.02.002	2019	Research		Brazil	FSD	Area-based	Inventory TLS	RF
Arkin et al. https://doi.org/10.1093/forestry/cpad020	2023	Research		Canada	Fuel estimation	Area-based	ALS DAP Field MLS	Linear regression
Atkins et al. https://doi.org/10.1002/ecs2.4633	2023(a)	Review		—	FSD	Area-based	—	—
Atkins et al. https://doi.org/10.1111/2041-210x.14040	2023(b)	Research		USA	FSD	Area-based	ALS Inventory	Shannon–Weiner diversity function MacArthur–Horn algorithm
Atkins et al. https://doi.org/10.1111/2041-210x.13061	2018	Application		—	FSD	Area-based	—	—

Blackman & Yuan https://doi.org/10.3390/rs12111820	2020	Research		USA	FSD	Area-based	Aerial images ALS	Watershed segmentation algorithm
Bolton, Coops, & Wulder https://doi.org/10.1016/j.rse.2015.03.004	2015	Research		Canada	FSD	Area-based	ALS Landsat	Summary statistics
Bouvier et al. https://doi.org/10.1016/j.rse.2014.10.004	2015	Research		France	FSD	Area-based	ALS Field	Linear regression
Campbell et al. https://doi.org/10.1016/j.rse.2018.06.023	2018	Research		USA	FSD	Area-based	ALS Field	Linear regression
Coops et al. https://doi.org/10.1016/j.rse.2021.112477	2021	Review		—	FSD	Area-based	Mixed	Regression Imputation Machine learning
Cosenza et al. https://doi.org/10.1093/forestry/cpaa034	2021	Research		Brazil Finland Norway USA	FSD	Area-based	ALS Field	OLS kNN RF
Fisher et al. https://doi.org/10.1016/j.rse.2019.111520	2020	Research		Australia	FSD	Area-based	ALS Field	Regression Multiple-output regression
Francis, Lutz, & Farris https://doi.org/10.1016/j.foreco.2023.121035	2023	Research		USA	FSD	Area-based	ALS Field	Perfect plasticity approximation (PPA) model
Gelabert et al. https://www.tandfonline.com/doi/pdf/10.1080/15481603.2020.1738060	2020	Research		Spain	FSD	Area-based	ALS	kNN SVM RF
Haywood & Stone https://doi.org/10.1080/00049158.2011.10676340	2011	Research		Australia	FSD	Area-based	ALS Field	Regression
Hillman et al. https://doi.org/10.3390/fire4010014	2021	Research		Australia	FSD Fire severity	Area-based	ALS SfM	RF
Hirschmugl, Lippel & Sobe	2023	Research		Austria	FSD	Area-based	ALS GEDl	Break-detection algorithm (BDA) Expert-based

https://doi.org/10.3390/rs15030664								assessment (EBA)
Hislop et al. https://doi.org/10.1080/00049158.2023.2288776	2013	Research		Australia	FSD	Area-based	ALS RGB imagery	CHM (Canopy Height Model) difference maps Convolution filter
Jarron et al. https://doi.org/10.1016/j.rse.2020.111770	2011	Research		Canada	FSD	Area-based	ALS Field	Linear regression Forward-stepwise regression 10-fold cross-validation Two-sample t-test
Kane et al. https://doi.org/10.1139/X10-024	2010	Research		USA	FSD	Area-based	ALS Field	Linear regression
Karna et al. https://doi.org/10.1016/j.foreco.2020.118255	2020	Research		Australia	FSD	Area-based	ALS Field	Two-way ANOVA RF
Kay et al. https://doi.org/10.3390/rs13244961	2021	Research		Multiple	FSD	Area-based	Ice, Cloud and Elevation Satellite (ICESat) Geoscience Laser Altimeter System (GLAS) LiDAR	Least squares regression
Krisanski et al. https://doi.org/10.3390/rs13081413	2021(a)	Research		Mixed	FSD	Area-based	ALS MLS TLS UAS-AP	Deep learning
Lefsky et al. https://doi.org/10.1641/0006-3568(2002)052[0019:LRSFES]2.0.CO;2	2002	Review		—	FSD	Area-based	—	—
Liao et al. https://doi.org/10.1016/j.iag.2020.102209	2020	Research		Australia	FSD	Area-based	ALS Field Landsat	RF
Listopad et al. https://doi.org/10.1016/j.ecolind.2015.04.017	2015	Research		USA	FSD Fire severity	Area-based	ALS Field	One-way ANOVA Linear regression Principal Components Analysis (PCA)
Liu et al.	2020	Research		China	FSD	Area-based	ALS UAV-AP	Ordinary neighbor (ON)

https://doi.org/10.3390/rs12182884								Constrained neighbor (CN)
Matasci et al. https://doi.org/10.1016/j.rse.2018.07.024	2018	Research		Canada	FSD	Area-based	ALS Landsat	RF
Mazlan et al. https://doi.org/10.1007/978-981-19-4200-6_3	2023	Book chapter		—	FSD Forest landscape restoration	Area-based	ALS Field	—
Moran, Rowell & Seielstad https://doi.org/10.1016/j.rse.2018.04.005	2018	Research		USA	FSD	Area-based	ALS Field	Random forest Hierarchical clustering
Nguyen et al. https://doi.org/10.1016/j.iag.2019.101952	2020	Research		Australia	FSD	Area-based	ALS Disturbance data Inventory Landsat	kNN RF
Roussel et al. https://doi.org/10.1016/j.rse.2020.112061	2020	Review		—	—	Area-based	—	—
Roussel et al. https://doi.org/10.1016/j.rse.2017.05.032	2017	Research		Canada	FSD	Area-based	ALS	Probabilistic models
Sanchez-Lopez, Boschetti & Hudak https://doi.org/10.1093/forestry/cpz048	2020	Research		USA	FSD	Area-based	ALS Disturbance data	RF
Szostak https://doi.org/10.3390/geosciences10080321	2020	Research		Poland	FSD	Area-based	ALS Cadastral data Orthophoto maps,	Summary statistics
Viana-Soto et al. https://doi.org/10.1016/j.iag.2022.102754	2022	Research		Spain	FSD Post-fire recovery	Area-based	ALS Landsat	SVR
Wang et al. https://doi.org/10.1016/j.iag.2021.102353	2021	Research		USA	FSD	Area-based	ALS Landsat	RF
Watt et al. http://dx.doi.org/10.1016/j.foreco.2015.08.001	2015	Research		New Zealand	Site Index	Area-based	ALS Field RapidEye imagery	Multiple regression models kNN















White et al. https://doi.org/10.1016/j.rse.2022.112904	2022	Research		Canada	FSD Recovery trends	Area-based	AL Landsat	Getis statistic
White et al. http://dx.doi.org/10.13140/RG.2.2.26770.96964	2017(a)	Technical report		Multiple	FSD	Area-based	ALS Field	Mixed
Wulder et al. http://dx.doi.org/10.5558/tfc84807-6	2008	Mixed		—	FSD	Area-based	ALS	—

Table B4. Studies using a voxel-based (VBA) methodology

Author(s)	Year	Article type	Themes	Study area	Research objective	Primary methodology	Data types	Analysis methods
Aalto et al. https://doi.org/10.1016/j.foreco.2023.120885	2023	Research		Finland	FSD	Voxel-based	TLS	Random forest (RF) Wilcoxon test
Almeida et al. https://doi.org/10.3390/rs11010092	2019 (b)	Research		Brazil	FSD	Voxel-based	ALS	MacArthur-Horn equation
Carrasco et al. https://doi.org/10.3390/rs11070743	2019	Research		USA	FSD	Voxel-based	ALS, Field	Linear regression RF
Ehbrecht et al. https://doi.org/10.1016/j.foreco.2016.09.003	2016	Research		Germany	FSD	Voxel-based	Field, TLS	Linear regression
Ferrara et al. https://doi.org/10.3390/s23010511	2023	Research		Italy	FSD	Voxel-based	ALS, Field, TLS	Linear regression
Hillman et al. http://doi.org/10.1016/j.iag.2020.102261	2021	Research		Australia	FSD, Fuel hazard	Voxel-based	ALS, TLS	Summary statistics
Jaskierniak et al. https://doi.org/10.1016/j.rse.2010.10.003	2022	Research		Australia	FSD	Voxel-based	ALS, Field	Generalised Additive Models for Location, Scale and Shape (GAMLSS)
Kamoske et al. https://doi.org/10.1016/j.foreco.2018.11.017	2010	Research		USA	FSD	Voxel-based	ALS, Field	Linear regression
Puletti et al. https://doi.org/10.1016/j.rsase.2021.100620	2021	Research		Italy	FSD	Voxel-based	Field, TLS	Hierarchical clustering analysis Principal Component Analysis Spearman correlation coefficient Wilcoxon test
Puletti, Castronuovo & Ferra https://www.biorxiv.org/content/10.1101/2023.02.01.526548.full	2023	Research		Italy	FSD	Voxel-based	Field, TLS	crossing3dforest
Wang et al.	2020	Research		China	FSD	Voxel-based	ALS, Field	RF














https://doi.org/10.1186/s40663-020-00243-2								
Xu, Tong & Stilla https://doi.org/10.1016/j.autcon.2021.103675	2021	Review		NA	Construction	Voxel-based	Multiple point clouds	Deep learning
Zhang, He & Li https://doi.org/10.7275/t8fk-8w94	2022	Conference paper		China	Urban vegetation attributes	Voxel-based	ALS	PointCNN
Zhang, Cao & She https://doi.org/10.3390/rs9090940	2017	Research		China	FSD	Voxel-based	ALS, Field	Multiple regression
Zięba-Kulawik et al. https://doi.org/10.1016/j.ufug.2021.127324	2021	Research		Luxembourg	Urban vegetation attributes	Voxel-based	ALS, Cadastral shapefiles	Linear regression

Table B5. Studies using an individual tree segmentation (ITS) methodology

Author(s)	Year	Article type	Themes	Study area	Research objective	Primary methodology	Data types	Analysis methods
Brolly et al. https://doi.org/10.3390/rs13040542	2021	Research		Finland	Individual tree attributes	Individual tree segmentation	TLS	Linear regression
Bryson, Wang, & Allworth https://doi.org/10.3390/rs15092380	2023	Application		Australia, New Zealand	Individual tree attributes	Individual tree segmentation	ALS, TLS	Deep learning
Casas et al. https://doi.org/10.1016/j.rse.2015.12.044	2016	Research		USA	Burned forest characterization	Individual tree segmentation	Field, ALS	Watershed Segmentation algorithm Snag/live classification model Conifer/hardwood snag classification model Gaussian process regression model
Chang et al. https://ieeexplore.ieee.org/stamp/stamp.jsp?arnumber=9913319	2022	Research		Finland	Individual tree attributes	Individual tree segmentation	Field, TLS	Hierarchical clustering
Chen et al. https://www.ingentaconnect.com/content/asprs/pers/2006/00000072/00000008/art00003?crawler=true&mimetype=application/pdf	2006	Research		USA	Individual tree attributes	Individual tree segmentation	ALS	Canopy maxima model
Estrada et al. https://doi.org/10.3389/fpls.2023.1139232	2023	Review		NA	FSD Forest health	Individual tree segmentation	Mixed remote sensing devices	Linear regression Deep learning RF k-nearest neighbour (kNN)
Karna et al. https://doi.org/10.3390/rs11202433	2019	Research		Australia	Individual tree attributes	Individual tree segmentation	Field, ALS	Generalised linear mixed effects models (LMEM)
Krisanski et al. https://doi.org/10.3390/rs13224677	2021(b)	Research		Mixed	Individual tree attributes	Individual tree segmentation	Field, TLS	Forest Structural Complexity Tool (FSCT)
Lee, Woo & Lee https://doi.org/10.18494/SAM4100	2022	Research		South Korea	Individual tree attributes	Individual tree segmentation	ALS, MLS	Circular fitting algorithms
















Mäyrä et al. https://doi.org/10.1016/j.rse.2021.112322	2021	Research		Finland	Individual tree attributes	Individual tree segmentation	ALS, Hyperspectral imagery	3D convolutional neural network (CNN)
Mielcarek, Stereńczak & Khosravipour https://doi.org/10.1016/j.jag.2018.05.002	2018	Research		Belarus Poland	Individual tree attributes	Individual tree segmentation	Field, ALS	Linear regression
Penner, Pitt & Woods http://dx.doi.org/10.5589/m13-049	2013	Research		Canada	Individual tree attributes	Individual tree segmentation	Field, ALS	Seamingly unrelated regression (SUR) RF kNN
Qi et al. https://doi.org/10.3390/rs15194768	2023	Research		China	Individual tree attributes	Individual tree segmentation	Field, multitemporal ALS	Individual tree segmentation algorithms Linear regression 10-fold cross-validation
Wilkes et al. http://doi.org/10.1111/2041-210X.14233	2023	Research		Multiple	Individual tree attributes	Individual tree segmentation	TLS	TLS2trees
Windrim & Bryson https://doi.org/10.3390/rs12091469	2020	Research		Australia	Individual tree attributes	Individual tree segmentation	ALS	Deep learning
Zhao et al. https://doi.org/10.1007/s40725-023-00184-3	2023	Systematic review		NA	Individual tree attributes	Individual tree segmentation	Mixed	CNN

Table B6 - Studies using mixed methodologies

Author(s)	Year	Article type	Themes	Study area	Research objective	Primary methodology	Data types	Analysis methods
Blackburn, Buscaglia, & Meador https://doi.org/10.1139/cjfr-2020-0506	2021	Research		USA	FSD	Area-based Voxel-based	ALS	Watershed segmentation algorithm
Knapp, Huth, & Fischer https://doi.org/10.3390/rs13081592	2021	Research		Panama	FSD, Individual tree attributes	Voxel-based Individual tree segmentation	Inventory , ALS simulations	Power law regression models
Leiterer et al. https://doi.org/10.1109/IGARSS.2012.6350691	2012	Research		Switzerland	FSD, Individual tree attributes	Voxel-based Individual tree segmentation	Field, TLS	Hierarchical multi-dimensional fuzzy clustering approach
Li et al. https://doi.org/10.1111/2041-210X.14290	2024	Research		Germany	FSD, Individual tree attributes	Voxel-based Individual tree segmentation	ALS, TLS	Physically based ray tracer (PBRT) Voxel-based radiative transfer (VBRT)
Pearse et al. http://doi.org/10.1016/j.jag.2018.10.008	2018	Research		Australia	Individual tree attributes	Voxel-based Individual tree segmentation	Field, ALS	RF
Silva et al. https://doi.org/10.1111/2041-210X.13830	2022	Application		Brazil	FSD, Individual tree attributes	Area-based Individual tree segmentation	ALS	Treetop application
Torresan et al. https://doi.org/10.15287/afr.2016.423	2016	Research		Italy	FSD, Individual tree attributes	Area-based Individual tree segmentation	Field, ALS	Pearson correlation test Hierarchical clustering algorithm Kruskall-Wallis test
Whelan et al. https://doi.org/10.1016/j.rse.2022.113362	2023	Research		USA	FSD	Area-based Voxel-based	Inventory, ALS	Simulated annealing Multiplicative power model

4. Discussion

Our literature review provides a broad overview of how LiDAR technology is used in forestry research. In particular, it focuses on how LiDAR can help to gain accurate insights about forest structural complexity and dynamics. Several key themes, methodologies and statistical analysis approaches emerged from the literature, shedding light on the current state of knowledge and practices in the field. One of the primary findings from this review is the widespread use of LiDAR in forestry research across different geographical regions, including but not limited to the USA, Australia, Brazil, Canada, China, and Finland. The diverse range of forest sites studied demonstrates the global applicability of LiDAR technology in assessing forest structure.

The themes identified in the literature span a wide spectrum, encompassing comparisons of different LiDAR technologies, integration of LiDAR with aerial imagery, demonstration of various statistical analyses, and applications of LiDAR in estimating forest structure, post-disturbance recovery trends, and fauna biodiversity assessments. Furthermore, this review provides valuable insights into the distinctions between the ABA, VBA, and ITS approaches, shedding light on the potential advantages of each method. One limitation of this review is that it does not explore how multitemporal LiDAR analysis is employed in forestry research, which could be a promising avenue for future investigation. Multitemporal LiDAR analysis was not frequently encountered in our search, potentially due to the challenges posed by the substantial data load and the limited resources available for computation.

Overall, this literature review contributes to our understanding of the breadth and depth of LiDAR applications in forestry research. By synthesising key concepts, methodologies, and trends, this review is a valuable resource for researchers, practitioners, and policymakers involved in forest management, conservation, and ecosystem monitoring. Future research directions may focus on exploring advanced LiDAR data processing techniques, improving integration with other remote sensing technologies, and addressing challenges related to data management and accessibility in large-scale LiDAR applications for forestry and environmental studies.

5. Conclusions

LiDAR has been used in forestry applications for over two decades and is rapidly evolving as technology and computational methods continue to improve. While LiDAR can provide accurate measurements of individual trees, stands, and heterogeneous forests, significant challenges remain in the realm of data storage, processing, and management. Furthermore, a standardised and efficient methodology for aligning LiDAR metrics with forest structural attributes remains to be found. This literature review demonstrates a widespread effort to advance this technology and find ways to use LiDAR to understand forest structural dynamics more precisely. So far, the ABA has been the most widespread methodology for assessing forest structure over large areas. However, the VBA shows promise for measuring the horizontal and vertical complexity of heterogeneous forests with a higher sensitivity than the ABA. On the other hand, the ITS is a well-known method for analysing the structure of individual trees. The range of statistical and modelling approaches used to analyse LiDAR data demonstrates the energetic effort of foresters, ecologists, and researchers alike to find fruitful ways of plumbing such rich and immense information.